UNIVERSITY OF OKLAHOMA

GRADUATE COLLEGE

STUDY OF SILICA SOL-GEL MATERIALS FOR SENSOR DEVELOPMENT

A DISSERTATION

SUBMITTED TO THE GRADUATE FACULTY

in partial fulfillment of the requirements for the

Degree of

DOCTOR OF PHILOSOPHY

By

QIONG LEI
Norman, Oklahoma
2010

STUDY OF SILICA SOL-GEL MATERIALS FOR SENSOR DEVELOPMENT

A DISSERTATION APPROVED FOR THE
DEPARTMENT OF CHEMISTRY AND BIOCHEMISTRY

BY

_____
Dr. Wai Tak Yip, Chair

_____
Dr. LeRoy C.Blank

_____
Dr. Richard W. Taylor

_____
Dr. Robert L. White

_____
Dr. Lloyd A. Bumm

I dedicate this dissertation to my parents and my in-laws for their endless love and support.

ACKNOWLEDGEMENTS

It would not have been possible for me to complete my Ph.D work and this dissertation without the help and support of many people.

First and foremost, I am heartily thankful to my major advisor, Dr. Wai Tak Yip, who introduced me to the magical world of single molecule and the important material science field of silica sol-gel. His abroad knowledge, great patience and continuous support helped me overcome many difficulties and develop an understanding of my projects, which leads to the completion of this dissertation.

I also want to thank all my graduate committee members, Dr. LeRoy C. Blank, Dr. Richard W. Taylor, Dr. Robert L. White, and Dr. Lloyd A. Bumm, for their advice and help throughout my graduate study. From them, I also learned how to be a good teacher.

My special thanks to Dr. Matt B. Johnson in the department of physics and astronomy, for his financial support and guidance of the silica hydrogel-like thin film project. I am also grateful for the help from those people in his group, especially to Dr. Joel C. Keay and Ernest Sanchez.

Two heads are better than one. I feel fortunate to have all the lab members to work with. I would never forget their kind help, discussion and friendship as well. These people are: Dr. James W. Gilliland, Yongyao Zhou, Dr. Tami A. Martyn, Lucas Fontenelle, Tim Dowd, and Yan Xiong. There are still many other friends in this department I also want to thank without listing their names here.

I want to thank all the professors and staff in the department of chemistry and biochemistry who helped me during my PhD study.

I must thank my husband, Dr. Xiaoxu Jiang, my parents, my in-laws and my sister. They always love me, understand me, support me and help me going through all those hard times.

Last, but not least, I want to thank my daughter, Ruiyi Alice Jiang. “You are my sunshine, my only sunshine. You make me happy when skies are gray.”

TABLE OF CONTENTS

LIST OF TABLES

LIST OF FIGURES

ABSTRACT

Silica sol-gel is a transparent, highly porous silicon oxide glass made at room temperature by sol-gel process. The name of silica sol-gel comes from the observable physical phase transition from liquid sol to solid gel during its preparation. Silica sol-gel is chemically inert, thermally stable, and photostable, it can be fabricated into different desired shapes during or after gelation, and its porous structure allows encapsulation of guest molecules either before or after gelation while still retaining their functions and sensitivities to surrounding environments. All those distinctive features make silica sol-gel ideal for sensor development. Study of guest-host interactions in silica sol-gel is important for silica-based sensor development, because it helps to tailor local environments inside sol-gel matrix so that higher guest loading, longer shelf-life, higher sensitivity and faster response of silica gel based sensors could be achieved.

We focused on pore surface modification of two different types of silica sol-gel by post-grafting method, and construction of stable silica hydrogel-like thin films for sensor development. By monitoring the mobility and photostability of rhodamine 6G (R6G) molecules in silica alcogel thin films through single molecule spectroscopy (SMS), the guest-host interactions altered by post-synthesis grafting were examined. While physical confinement remains the major factor that controls mobility in modified alcogels, both R6G mobility and photostability register discernable changes after surface charges are respectively reversed and neutralized by aminopropyltriethoxysilane (APTS) and methyltriethoxysilane (MTES) grafting. The change in R6G photostability

was found to be more sensitive to surface grafting than that of mobility. In addition, silica film modification by 0.4% APTS is as efficient as that by pure MTES in lowering R6G photostability, which suggests that surface charge reversal is more effective than charge neutralization in disrupting R6G/silica attraction.

Similar post-grafting method was applied to highly hydrated silica hydrogel monoliths. Rhodamine 6G (R6G) and fluorescein (Fl) molecules were used as probes to monitor the surface modification inside silica hydrogel by measuring anisotropy values of doped dyes. Due to the larger pore sizes, pore surface modification inside hydrogel was more effective than in alcogel. Surface modification by chemical reactions of 3-Aminopropyltrimethoxysilane (APTS) and methyltriethoxysilane (MTES) showed dramatic effect on guest molecule mobility, whereas surface modification by physical method, that is to increase ionic strength by using 1.0 M sodium chloride or to neutralize pore surfaces by adding pH 2.0 hydrochloric acid, barely showed any effect. Charge-reversal by APTS is a more effective way to modify pore surfaces in hydrogel than hydrophobic capping from MTES. The ease of tracking surface modification inside hydrogel by simply locating R6G dye band, and the negligible pore fluid effect on R6G in modified hydrogel makes R6G a better probe than Fl to monitor the pore surface modification process in silica hydrogel monoliths.

During the study of post-grafting on silica alcogel thin film, a new approach to produce stable silica hydrogel-like thin films was discovered. Homogeneous thin film hydrogel-like samples with thickness between 100 nm and 300 nm were produced, and they showed a very hydrophilic surface, high dye loading capacity, and the support of molecular diffusion. The reactive stage of starting silica gel matrix was elongated by

increasing environmental humidity, the reproducibility of sample preparation was greatly improved by controlling environmental humidity, and the dye loading capacity of samples was improved more than ten times by using phosphate buffer solutions (PBS). The concentration of R6G trapped inside hydrogel-like thin film could reach as high as 900 times of its saturated aqueous solution. Dye encapsulation can simply be accomplished by dipping a chemically reactive alcogel thin film into a dye-doped buffer solution. Since alcohol exposure can be kept to a minimum during dye encapsulation, this new silica film makes a promising candidate for biomolecule encapsulation and thus biosensor development. A prototype silica hydrogel-like thin film pH sensor was also constructed and tested, and it showed faster response than the corresponding alcogel thin film sensor.

CHAPTER 1 INTRODUCTION

1.1 SOL-GEL PROCESS

1.1.1 Sol-gel Reactions

Sol-gel process is a popular approach to synthesize inorganic oxide materials using inorganic metal salts or organic metal alkoxides as precursors.[1-2] Usually, sol-gel process is carried out at room temperature and is realized by a two-step reaction. Since this dissertation focuses on studies of silica sol-gel (or referred as sol-gel silicate) material, we'll use silicate gels as examples to illustrate this process.

Tetralkyl orthosilicates, such as tetraethyl orthosilicate (TEOS) and tetramethyl orthosilicate (TMOS), are the most widely used precursors to make sol-gel silicates. As illustrated in Figure 1.1, three reactions perfectly describe the sol-gel process. Briefly, with the presence of acid or base as a catalyst, silicon alkoxide reacts with water and undergoes a hydrolysis process to produce silanols, and then those partially hydrolyzed silanols are involved in condensation reactions to form a porous, three-dimensional

Hydrolysis

$$\equiv Si - OR + H_2O \longrightarrow \equiv Si - OH + ROH$$

Condensations

$$\equiv Si - OR + HO - Si \equiv \longrightarrow \equiv Si - O - Si \equiv + ROH$$

$$\equiv Si - OH + HO - Si \equiv \longrightarrow \equiv Si - O - Si \equiv + H_2O$$

Figure 1.1 Reactions in sol-gel process. R represents alkyl group.

framework of silicon oxide. The name of silica sol-gel comes from the observable physical phase transition from liquid sol to solid gel during its preparation. In short, once silica alkoxide molecules hydrolyze and start condensation, depending on the reaction conditions, they turn into clusters of either dense oxide particles or branched macromolecules and suspend in the liquid, which is sol ("a colloidal suspension of solid particles in a liquid")[1]; With the growth of clusters by aggregation of particles or condensation of macromolecules, the moment when clusters collide and the last link is formed between them, the sol solution suddenly loses its fluidity and turns into an elastic solid, that is a gel. This sudden physical phase change is called gelation, and the time it takes from sol to gel is gelation time or gel time.

1.1.2 Sol-gel Mechanisms

The hydrolysis and condensation rates are affected by many factors, such as the precursor type and concentration, the molar ratio of H_2O : Si, the catalyst type and concentration, the solvent, temperature, pressure and the existence of electrolytes.[1, 3-5] Although there are many mechanisms of sol-gel process proposed by different research groups, it is generally agreed that hydrolysis follows "a bimolecular displacement mechanism",[1, 4, 6] and condensation involves bimolecular nucleophilic substitution reaction with a penta- or hexacoordinate transition intermediate or state.[1, 6] In an acid-catalyzed hydrolysis, an alkoxide group is first rapidly protonated and then subjected to attack by water to form a pentacoordinate intermediate or transition state, which decays by the displacement/generation of an alcohol. Under basic condition, hydrolysis proceeds by the rapid dissociation of water into a nucleophilic hydroxyl anion first, followed by its attack to silicon atom to form a pentacoordinated

intermediate or state, which decays by the displacement/generation of an alkoxide anion. In a condensation reaction, if it is acid-catalyzed, a silanol is rapidly protonated first and turns electrophilic, which make it susceptible to nucleophilic attack from a neutral silanol, finally the reaction ends with formation of siloxane bond and by-product of protonated water; while if it's base-catalyzed, condensation proceeds by the rapid deprotonation of silanol first, followed by its attack to a neutral silanol to form a stable penta- or hexacoordinate transition intermediate or state, which decays by the displacement/generation of an alkoxide anion or hydroxyl.

1.1.3 Sol-gel Structures

By adjusting the reaction conditions to control the relative rates of hydrolysis and condensation, we can obtain silica gels with different structures and properties. The pore size of silica gel could vary from as small as 1 nm in diameter to as large as more than 200nm in diameter.[7-11] First of all, as the mechanisms suggest, hydrolysis and condensation reaction rates are pH dependent. Figure 1.2 illustrates different structures of silica sol-gel prepared under different pH conditions.[4] Generally, under low pH conditions (pH $\leq$ 2), the hydrolysis rate is far higher than the rate of condensation, resulting in silica sol-gel with weakly-branched polymer network. Under high pH conditions (pH > 8), for example the conditions used by Stöber (the molar ratio of H_2O : Si is between 7.5 and 50 or even higher, and the concentration of catalyst NH_3 is 1 ~ 7 M),[12] condensation was much faster than hydrolysis, and uniform spherical particles with sizes ranged from 50 nm to 2000 nm in diameter were obtained. Under intermediate pH conditions (pH = 3 ~ 8), depending on the pH and the molar ratio of H_2O : Si, silica sol-gel with structures from weakly-branched to uniformly porous, to

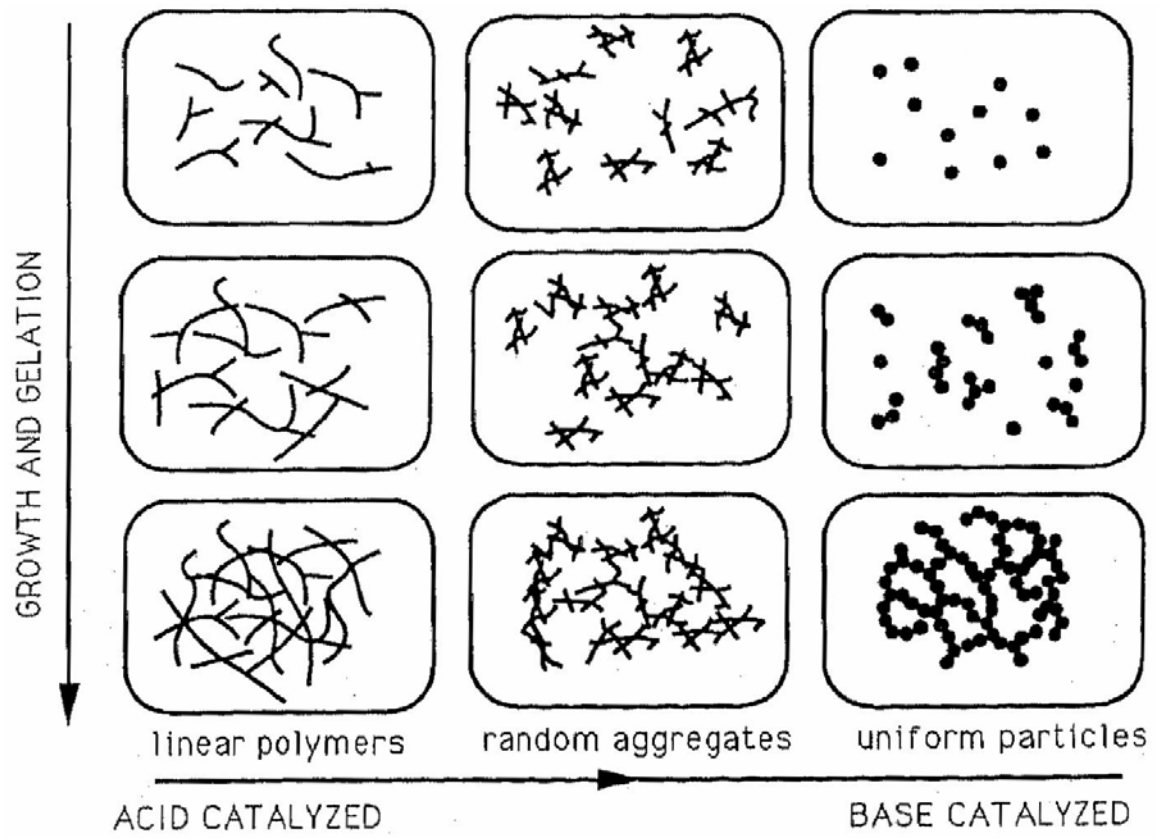

Figure 1.2 Schematic of silica sol-gel structure affected by pH. Reproduced with permission from ref. 4. Copyright 1989 the Swiss Chemical Society (SCS) and its Divisions.

surface fractals, to mass fractals, to even smooth monosized silica spheres are all able to be obtained.[1, 4, 13] The structure and properties of silica sol-gel can also be tuned by varying the molar ratio of starting materials,[12, 14-15] by introducing reactive additives such as organically modified silanes,[16-17] other metal alkoxides,[18-19] and polymers[20-22] to initial sol preparation to make hybrid sol-gel, or by mixing surfactants,[23-26] organic dye molecules[24, 27-29] or enzymes[20-21, 30] during gelation to template the pore sizes and shapes. In addition, the solvent, temperature, pressure and the existence of electrolytes during sol-gel preparation were all observed to affect the hydrolysis or condensation rate so that resulting in differently structured silica gel.[1, 3].

Hydrolysis and condensation reactions don't stop at the gelation point, but continue for weeks or even months during aging.[1] New –Si-O-Si– bonds are created by the continued poly-condensation reactions, which not only help strengthening and stiffening the gel network, but also result in the shrinkage of gel. When gel shrinking and solvent evaporation happen simultaneously during aging, pores collapse. It is very obvious that the structure and properties of silica gel keeps changing during aging. Scherer *et al* did extensive studies to report how silica sol-gel structure evolves during aging, and factors that could affect the gel structure, such as aging time, temperature, pore fluids and pH, were explored.[7-8, 31-37]

There are two types of silica sol-gel investigated in this dissertation: silica alcogel and silica hydrogel. The difference between alcogel and hydrogel is the dispersion medium, with the former is alcohol and the latter is water. Traditionally, alcohol such as ethanol or methanol was always mixed with silane precursors and water to initialize the sol-gel process, because water and most alkoxysilanes are immiscible, alcohol can work as a homogenizing agent.[1] Silica sol-gel which is produced in an alcohol-water system throughout the whole sol-gel process is generally categorized as alcogel. In 1987, Avnir and Kaufman first successfully synthesized silica sol-gel without adding alcohol as a mutual solvent, and they explained that since alcohol is a by-product of hydrolysis and the initial release of alcohol is sufficient to homogenize the reaction system.[38] Today, alcohol-free route becomes very common for making biocompatible silica hydrogel. One of the most popular procedures to make silica hydrogel is a two-step sol-gel process, which involves an acid-catalyzed hydrolysis step, and then a neutral condensation-gelation step.[14, 39-40] TMOS is a more preferable precursor than TEOS

since the by-product methanol is less toxic to biological molecules than ethanol.[21] Alcohol generated in hydrolysis step is usually removed before the condensation-gelation step by natural evaporation or rotary evaporation,[41] or could be removed by rinsing after gelation.[42] After the homogeneous sol is generated in the first step, usually buffer solution or growth media of cells is mixed with sol to conduct the condensation-gelation in the second step. By adjusting the volume ratio of sol and the buffer solution, silica hydrogel with different pore sizes could be achieved. The higher the portion of buffer solution, the longer the gel time, and the larger the pore size will be obtained. Hydrogel usually contains up to 99% of water. Compared to hydrogel, alcogel has a denser internal structure.[43]

It is worth to point out that there are another three terms often used to describe dried silica sol-gel materials. They are xerogel, aerogel and ambigel. If a wet gel (regardless hydrogel or alcogel) undergoes natural evaporation, a xerogel is obtained; if the wet gel is dried by a supercritical drying process, an aerogel is produced; if the wet gel contains high portions of hydrophobic groups in the matrix or on the pore surfaces, after evaporation, it turns into ambigel.[10, 20]

1.2 GUEST - HOST INTERACTIONS IN SILICA SOL-GEL

Ever since the pioneer work of Avnir et al. on the entrapment of an organic dye in silica gel (composites) in 1984,[44] and the subsequent discovery that trapped molecules in sol-gel matrix were sensitive to the surrounding solvent environment,[45-46] intense interest has been focused on the construction of silica gel based sensors. Since then, a

lot of silica gel based chemical sensors and biosensors have been developed, such as pH sensors, ion sensors, glucose sensors.[11, 21-22, 30, 47-51]

The investigation of guest-host interactions inside silica sol-gel is important for sensor development, because understanding the interactions helps to manipulate the properties of silica gel materials so that gaining control over sensor development. Local environment of the guest molecule inside silica gel greatly affects how guest-host interacts. Generally, there are four different regions in sol-gel matrix: liquid region in pores, pore wall, the interface between pore wall and pore liquid, and constraining region between pore walls with similar dimension as trapped molecules.[5] Molecules located in liquid region of pores behave similar as those in bulk solution, the interactions between guest molecules and solvent molecules dominate, as a result the properties of the solvent, such as composition,[45-46, 52-53] pH,[53-54] polarity[55-56] and viscosity,[57-58] greatly affect the characters and motions of them. However, the influence from the pore size or pore surfaces also can't be neglected, especially when the pore sizes are getting smaller and smaller during aging, interactions between guest molecules and pore surfaces become stronger. Hydrogen-bonding[56, 59] or electrostatic interactions[28, 54, 60] are believed to contribute to the attachment of molecules to the pore surfaces. Molecules in the interface region between pore wall and pore liquid usually show significantly different properties from those molecules in bulk solution.[44, 61] Because of the existence of electric double layer on pore surface and the adsorption-desorption equilibrium of guest molecules on pore surfaces, the interactions between guest molecules and sol-gel matrix get more complicated. Zheng and coworkers studied the fluorescence properties of Rhodamine 6G (R6G) at the silica/water interface, they found

that R6G showed totally different responses to pH and ionic strength when at the interface and in bulk solution; [62-63] in another related study by Chen et al, [61] 5 nm red-shift was observed from the fluorescence spectra of R6G at the interface compared to that in bulk solution, and the rotational movement of R6G molecules was distinctly restricted at the interface. When molecules are trapped in the constraining region, they cannot move around. Physical confinement is usually used to describe this situation.

1.3 PORE SURFACE MODIFICATION OF SILICA SOL-GEL

Introducing organic groups to silica gel to make an inorganic-organic hybrid material is on one hand replacing the brittleness with rubber elasticity, and on the other hand improving its biocompatibility. Since H. Schmidt in 1985 first successfully synthesized the inorganic-organic hybrid silica gel (ormosils),[64] sol-gel research has experienced an explosion of development, and it also marks the second important period of sol-gel process.[65-66] Currently, there are two well-developed approaches to synthesize organically modified silica gel: one-pot synthesis and stepwise post-grafting.[17, 67-68]

H. Schmidt initiated the one-pot approach, which is by mixing all precursors (including the organosilanes) and solvents in one pot for the sol-gel process. Since those organosilanes are directly involved in the sol-gel reactions, organic functional groups turn into part of the sol-gel matrix, and the distribution of them is homogeneous. High loading of the organic functional groups can be easily achieved by increasing the relative amount of organosilanes at the beginning of sol-gel process. Additionally, the preparation time is short. It is now still the traditional method used to make inorganic-organic hybrid silica materials. As its name indicates, post-grafting method

involves more than one step, which is the major reason why it received less attention than the one-pot method. Generally, the silica gel has been prepared by tetraalkoxysilane precursors in the first step, and then organosilanes are mixed with the gel for a second-step reaction to introduce organic functional groups. Since organosilanes are introduced after gelation, the loading of organic functional groups is limited, and the surface coverage of organic groups is not uniform. However, post-grafting can overcome the weakened mechanical strength of hybrid material made by one-pot approach,[69] whereas introduce almost any functionality without changing the framework and distorting porosity.[70] In addition, post-grafting provides better defined silica structure, better hydrothermal stability, and more accessible functional groups than one-pot method does even with the same organosilane modifying reagent.[17, 67]

1.4 ADVANTAGES AND APPLICATIONS OF SILICA SOL-GEL MATERIALS

Silica sol-gel framework has many distinguishing advantages. It is non-toxic, non-volatile, non-flammable, optically transparent, structure-tunable, chemically inert, thermally and mechanically stable.[1, 27, 49-50, 71] There are some features of silica sol-gel deserving more discussion.

First of all, low temperature preparation process. The low temperature sol-gel process not only saves energy, minimizes evaporation losses and air pollution and so on, it also makes the encapsulation of biological molecules possible while still retaining their bioactivity.[21, 72-73] This possibility opened a new area of silica gel based biomaterials, which are suitable for many applications, such as biosensors,[22, 30, 50, 74]

biocatalysts,[11, 20, 72, 75-76] stationary phases for affinity columns,[10-11, 77] bioreactors.[10, 21, 78] In recent years, progress has been made in drug release systems[79-80] and bioactive materials[11, 21, 81].

Secondly, transparency of silica sol-gel matrix. Optical transparency down to 250 nm makes silica gel suitable for different types of quantitative spectrometric tests, such as absorption and fluorescence. It is also essential for optical sensor development.

Thirdly, mechanical workability. Silica gel can be made into all kinds of desired shapes before or during gelation. Powders and spheres,[12, 82] fiber coatings,[83-84] bulk gels including monoliths[39-40, 85-87] and thin films[88-92] are all the common configurations. If the smallest dimension of the gel is greater than a few millimeters, the object is generally called a monolith; if it is less than one micrometer in thickness, it is usually called a thin film.[1] Thin film is the most special configuration of sol-gel, because it overcomes most of the disadvantages of sol-gel processing.[1] Prepared by dipcoating[24, 68, 93-94] or spincoating,[95] thin film only requires few raw materials, which greatly lowers the material cost. Its preparation process is fast and allows multiple-layer configuration. Most importantly, thin films experience less cracking than bulk gels during drying or upon liquid exposure. Due to these extraordinary features of thin film, it becomes to the most popular form for silica gel based sensor developing.[96-98]

Fourthly, porous structure. The highly porous structure of silica gel provides the possibilities of trapping guest functional molecules either before or after the gelation, while encapsulated molecules still retain most of their functional characteristics[21, 72-73] and even exhibit enhanced stability.[44, 71, 99] The sensitivity of trapped molecules to their

surrounding solvent environment triggered the development of silica gel for sensor applications.[45-46]

Besides those applications of silica sol-gel mentioned above, silica sol-gel has also been applied to make optical materials such as non-doped[100-101] and doped glasses,[102-103] contact lenses,[64] to make scratch resistant coatings,[1-2, 64] conductive coatings,[104] antireflection coatings,[105] biocompatible coatings,[106] and to make membranes for filtration or separation.[107-108]

1.5 RESEARCH FOCUS AND SIGNIFICANCE

As a widely-explored subject for numerous applications, silica sol-gel has attracted the attention of our group for sensor development. This study focused on pore surface modification of two different types of silica sol-gel by post-grafting method, and construction of stable silica hydrogel-like thin films. By monitoring the mobility and photostability of rhodamine 6G (R6G) molecules in silica alcogel thin films through single molecule spectroscopy (SMS), the guest-host interactions altered by post-synthesis grafting were examined. Similar post-grafting method was then applied to highly hydrated silica hydrogel monoliths; more efficient surface modification was expected, because larger pore sizes in hydrogel provide higher accessibility of organosilane reagents. During the study of post-grafting on alcogel thin film, a new approach to produce stable silica hydrogel-like thin films was discovered. A lot of effort has been made to improve the reproducibility of sample preparation, and the guest loading capacity of silica hydrogel-like thin films. A prototype silica hydrogel-like thin film pH sensor was also constructed and tested.

Understanding how guest-host interactions can be affected by silane modifications is critical to sensor development. It helps tailoring the local environments inside silica sol-gel matrix, so that higher guest loading, longer shelf-life, higher sensitivity and faster response of silica gel based sensors could be achieved. Stable silica hydrogel-like thin film with a thickness only around 200 nm, which to the best of our knowledge has never been accomplished before, is expected to be a better substrate for sensing devices that demand faster response than thick monoliths.

1.6 CHAPTER 1 REFERENCES

1. Brinker, C. J.; Scherer, G. W., *Sol-Gel Science: the physics and chemistry of sol-gel processing*. Academic press: San Diego, 1990.

2. Wright, J. D.; Sommerdijk, N. A. J. M., *Sol-gel materials: chemistry and applications*. Gordon and Breach Science Publishers: Amsterdam, 2001; Vol. 4.

3. Iler, R. K., *The Chemistry of Silica* John Wiley & Sons, Inc.: New York, 1979.

4. Gallagher, D.; Ring, T. A., *Chimia* **1989,** *43* (10), 298-304.

5. Dunn, B.; Zink, J. I., *Chemistry of Materials* **1997,** *9* (11), 2280-2291.

6. Pohl, E. R.; Osterholtz, F. D., *Molecular Charaterization of Composite Interfaces*. Plenum: New York, 1985.

7. Davis, P. J.; Jeffrey Brinker, C.; Smith, D. M., *J Non-Cryst Solids* **1992,** *142*, 189-196.

8. Deshpande, R.; Hua, D.-W.; Smith, D. M.; Brinker, C. J., *J Non-Cryst Solids* **1992,** *144*, 32-44.

9. Davis, P. J.; Deshpande, R.; Smith, D. M.; Brinker, C. J.; Assink, R. A., *J Non-Cryst Solids* **1994,** *167* (3), 295-306.

10. Kato, M.; Sakai-Kato, K.; Toyo'oka, T., *Journal of Separation Science* **2005,** *28* (15), 1893-1908.

11. Jin, W.; Brennan, J. D., *Anal Chim Acta* **2002,** *461* (1), 1-36.

12. Stöber, W.; Fink, A.; Bohn, E., *J Colloid Interf Sci* **1968,** *26* (1), 62-69.

13. SCHAEFER, D. W., *Science* **1989,** *243* (4894), 1023-1027.

14. Conroy, J. F. T.; Power, M. E.; Martin, J.; Earp, B.; Hosticka, B.; Daitch, C. E.; Norris, P. M., *Journal of Sol-Gel Science and Technology* **2000,** *18* (3), 269-283.

15. Debsikdar, J. C., *Advanced Ceramic Materials* **1986,** *1* (1).

16. Sanchez, C.; Boissière, C.; Grosso, D.; Laberty, C.; Nicole, L., *Chemistry of Materials* **2008,** *20* (3), 682-737.

17. Calvo, A.; Joselevich, M.; Soler-Illia, G. J. A. A.; Williams, F. J., *Micropor Mesopor Mat* **2009,** *121* (1-3), 67-72.

18. Almeida, R. M.; Orignac, X.; Barbier, D., *Journal of Sol-Gel Science and Technology* **1994,** *2* (1), 465-467.

19. Lin, J.; Siddiqui, J. A.; Ottenbrite, R. M., *Polym Advan Technol* **2001,** *12* (5), 285-292.

20. Pierre, A. C., *Biocatal Biotransfor* **2004,** *22* (3), 145-170.

21. Avnir, D.; Coradin, T.; Lev, O.; Livage, J., *J Mater Chem* **2006,** *16* (11), 1013-1030.

22. Kato, M.; Shoda, N.; Yamamoto, T.; Shiratori, R.; Toyooka, T., *Analyst* **2009,** *134* (3), 577-581.

23. Goloub, T. P.; Koopal, L. K.; Bijsterbosch, B. H.; Sidorova, M. P., *Langmuir* **1996,** *12* (13), 3188-3194.

24. Minoofar, P.; Hernandez, R.; Franville, A. C.; Chia, S. Y.; Dunn, B.; Zink, J. I., *Journal of Sol-Gel Science and Technology* **2003,** *26* (1-3), 571-575.

25. Ye, F.; Higgins, D. A.; Collinson, M. M., *The Journal of Physical Chemistry C* **2007,** *111* (18), 6772-6780.

26. Huang, M. H.; Kartono, F.; Dunn, B.; Zink, J. I., *Chemistry of Materials* **2002,** *14* (12), 5153-5162.

27. Viteri, C. R.; Gilliland, J. W.; Yip, W. T., *Journal of the American Chemical Society* **2003,** *125* (7), 1980-1987.

28. Zhou, Y. Y.; Yip, W. T., *J Phys Chem B* **2009,** *113* (17), 5720-5727.

29. Minoofar, P. N.; Hernandez, R.; Chia, S.; Dunn, B.; Zink, J. I.; Franville, A. C., *Journal of the American Chemical Society* **2002,** *124* (48), 14388-14396.

30. Gupta, R.; Chaudhury, N. K., *Biosensors and Bioelectronics* **2007,** *22* (11), 2387-2399.

31. Scherer, G. W., *J Non-Cryst Solids* **1988,** *100* (1-3), 77-92.

32. Scherer, G. W.; Pardenek, S. A.; Swiatek, R. M., *J Non-Cryst Solids* **1988,** *107* (1), 14-22.

33. Glaves, C. L.; Brinker, C. J.; Smith, D. M.; Davis, P. J., *Chemistry of Materials* **1989,** *1* (1), 34-40.

34. Scherer, G. W., *J Non-Cryst Solids* **1989,** *109* (2-3), 183-190.

35. Scherer, G. W., *J Non-Cryst Solids* **1989,** *108* (1), 18-27.

36. Scherer, G. W., *J Non-Cryst Solids* **1989,** *108* (1), 28-36.

37. Davis, P. J.; Jeffrey Brinker, C.; Smith, D. M.; Assink, R. A., *J Non-Cryst Solids* **1992,** *142*, 197-207.

38. Avnir, D.; Kaufman, V. R., *J Non-Cryst Solids* **1987,** *92* (1), 180-182.

39. Ellerby, L. M.; Nishida, C. R.; Nishida, F.; Yamanaka, S. A.; Dunn, B.; Valentine, J. S.; Zink, J. I., *Science* **1992,** *255* (5048), 1113-1115.

40. Yu, D.; Volponi, J.; Chhabra, S.; Brinker, C. J.; Mulchandani, A.; Singh, A. K., *Biosensors and Bioelectronics* **2005,** *20* (7), 1433-1437.

41. Ferrer, M. L.; del Monte, F.; Levy, D., *Chemistry of Materials* **2002,** *14* (9), 3619-3621.

42. Premkumar, J. R.; Lev, O.; Rosen, R.; Belkin, S., *Advanced Materials* **2001,** *13* (23), 1773-1775.

43. Forest, L.; Gibiat, V.; Woignier, T., *Journal of Sol-Gel Science and Technology* **1998,** *13* (1), 329-333.

44. Avnir, D.; Levy, D.; Reisfeld, R., *The Journal of Physical Chemistry* **1984,** *88* (24), 5956-5959.

45. Kaufman, V. R.; Avnir, D.; Pines-Rojanski, D.; Huppert, D., *J Non-Cryst Solids* **1988,** *99* (2-3), 379-386.

46. Pouxviel, J. C.; Dunn, B.; Zink, J. I., *The Journal of Physical Chemistry* **1989,** *93* (5), 2134-2139.

47. Simon, D. N.; Czolk, R.; Ache, H. J., *Thin Solid Films* **1995,** *260* (1), 107-110.

48. Cerqua, K. A.; Hayden, J. E.; LaCourse, W. C., *J Non-Cryst Solids* **1988,** *100* (1-3), 471-478.

49. Zusman, R.; Rottman, C.; Ottolenghi, M.; Avnir, D., *J Non-Cryst Solids* **1990,** *122* (1), 107-109.

50. Jerónimo, P. C. A.; Araújo, A. N.; Conceição B.S.M. Montenegro, M., *Talanta* **2007,** *72* (1), 13-27.

51. Narang, U.; Prasad, P. N.; Bright, F. V.; Ramanathan, K.; Kumar, N. D.; Malhotra, B. D.; Kamalasanan, M. N.; Chandra, S., *Analytical Chemistry* **1994,** *66* (19), 3139-3144.

52. Nishida, F.; McKiernan, J. M.; Dunn, B.; Zink, J. I.; Brinker, C. J.; Hurd, A. J., *J Am Ceram Soc* **1995,** *78* (6), 1640-1648.

53. Dunn, B.; Zink, J. I., *J Mater Chem* **1991,** *1* (6), 903-913.

54. Gilliland, J. W.; Yokoyama, K.; Yip, W. T., *Chemistry of Materials* **2004,** *16* (20), 3949-3954.

55. Rottman, C.; Grader, G. S.; De Hazan, Y.; Avnir, D., *Langmuir* **1996,** *12* (23), 5505-5508.

56. Gilliland, J. W.; Yokoyama, K.; Yip, W. T., *Chemistry of Materials* **2005,** *17* (26), 6702-6712.

57. Narang, U.; Jordan, J. D.; Bright, F. V.; Prasad, P. N., *The Journal of Physical Chemistry* **1994,** *98* (33), 8101-8107.

58. Narang, U.; Wang, R.; Prasad, P. N.; Bright, F. V., *The Journal of Physical Chemistry* **1994,** *98* (1), 17-22.

59. Tleugabulova, D.; Sui, J.; Ayers, P. W.; Brennan, J. D., *The Journal of Physical Chemistry B* **2005,** *109* (16), 7850-7858.

60. Gilliland, J. W.; Yokoyama, K.; Yip, W. T., *J Phys Chem B* **2005,** *109* (11), 4816-4823.

61. Chen, Z.; Tang, Y.-J.; Xie, T.-T.; Chen, Y.; Li, Y.-Q., *Journal of Fluorescence* **2008,** *18* (1), 93-100.

62. Zheng, X.-Y.; Harata, A.; Ogawa, T., *Spectrochimica Acta Part A: Molecular and Biomolecular Spectroscopy* **2001,** *57* (2), 315-322.

63. Zheng, X.-Y.; Wachi, M.; Harata, A.; Hatano, Y., *Spectrochimica Acta Part A: Molecular and Biomolecular Spectroscopy* **2004,** *60* (5), 1085-1090.

64. Schmidt, H., *J Non-Cryst Solids* **1985,** *73* (1-3), 681-691.

65. Mackenzie, J. D., *Journal of Sol-Gel Science and Technology* **2003,** *26* (1), 23-27.

66. Dimitriev, Y.; Ivanova, Y.; Iordanova, R., *Journal of University of Chemical technology and Metallurgy* **2008,** *43* (2), 181-192.

67. Lim, M. H.; Stein, A., *Chemistry of Materials* **1999,** *11* (11), 3285-3295.

68. Nicole, L.; Boissiere, C.; Grosso, D.; Quach, A.; Sanchez, C., *J Mater Chem* **2005,** *15* (35-36), 3598-3627.

69. Mackenzie, J. D.; Huang, Q.; Iwamoto, T., *Journal of Sol-Gel Science and Technology* **1996,** *7* (3), 151-161.

70. Angelomé, P. C.; Soler-Illia, G. J. d. A. A., *Chemistry of Materials* **2005,** *17* (2), 322-331.

71. Casalboni, M.; De Matteis, F.; Francini, R.; Prosposito, P.; Senesi, R.; Grassano, U. M.; Pizzoferrato, R.; Gnappi, G.; Montenero, A., *J Lumin* **1997,** *72-74*, 475-477.

72. Carturan, G.; Campostrini, R.; Diré, S.; Scardi, V.; De Alteriis, E., *J Mol Catal* **1989,** *57* (1), L13-L16.

73. Braun, S.; Rappoport, S.; Zusman, R.; Avnir, D.; Ottolenghi, M., *Materials Letters* **1990,** *10* (1-2), 1-5.

74. Dave, B. C.; Dunn, B.; Valentine, J. S.; Zink, J. I., *Analytical Chemistry* **1994,** *66* (22), 1120A-1127A.

75. Reetz, M. T., *Advanced Materials* **1997,** *9* (12), 943-954.

76. Gill, I.; Ballesteros, A., *Trends Biotechnol* **2000,** *18* (7), 282-296.

77. Schedl, M.; Wilharm, G.; Achatz, S.; Kettrup, A.; Niessner, R.; Knopp, D., *Analytical Chemistry* **2001,** *73* (23), 5669-5676.

78. Kato, M.; Inuzuka, K.; Sakai-Kato, K.; Toyo'oka, T., *Analytical Chemistry* **2005,** *77* (6), 1813-1818.

79. Xue, J. M.; Shi, M., *Journal of Controlled Release* **2004,** *98* (2), 209-217.

80. Kortesuo, P.; Ahola, M.; Kangas, M.; Jokinen, M.; Leino, T.; Vuorilehto, L.; Laakso, S.; Kiesvaara, J.; Yli-Urpo, A.; Marvola, M., *Biomaterials* **2002,** *23* (13), 2795-2801.

81. Vallet-Regí, M.; Salinas, A. J.; Ramírez-Castellanos, J.; González-Calbet, J. M., *Chemistry of Materials* **2005,** *17* (7), 1874-1879.

82. Wu, X.; Choi, M. M. F.; Xiao, D., *Analyst* **2000,** *125* (1), 157-162.

83. Brinker, C. J., Sol?Gel Processing of Silica. In *The Colloid Chemistry of Silica*, American Chemical Society: 1994; Vol. 234, pp 361-401.

84. Premkumar, J. R.; Lev, O.; Marks, R. S.; Polyak, B.; Rosen, R.; Belkin, S., *Talanta* **2001,** *55* (5), 1029-1038.

85. Nogami, M.; Moriya, Y., *J Non-Cryst Solids* **1980,** *37* (2), 191-201.

86. Brinker, C. J.; Keefer, K. D.; Schaefer, D. W.; Ashley, C. S., *J Non-Cryst Solids* **1982,** *48* (1), 47-64.

87. Krupa, I.; Nedelčev, T.; Račko, D.; Lacík, I., *Journal of Sol-Gel Science and Technology* **2010,** *53* (1), 107-114.

88. Sakka, S.; Kamiya, K.; Makita, K.; Yamamoto, Y., *J Non-Cryst Solids* **1984,** *63* (1-2), 223-235.

89. Huang, M. H.; Soyez, H. M.; Dunn, B. S.; Zink, J. I.; Sellinger, A.; Brinker, C. J., *Journal of Sol-Gel Science and Technology* **2008,** *47* (3), 300-310.

90. Huang, M. H.; Dunn, B. S.; Zink, J. I., *Journal of the American Chemical Society* **2000,** *122* (15), 3739-3745.

91. Wang, H.; Bardo, A. M.; Collinson, M. M.; Higgins, D. A., *The Journal of Physical Chemistry B* **1998,** *102* (37), 7231-7237.

92. Mei, E.; Bardo, A. M.; Collinson, M. M.; Higgins, D. A., *The Journal of Physical Chemistry B* **2000,** *104* (43), 9973-9980.

93. Lu, Y. F.; Ganguli, R.; Drewien, C. A.; Anderson, M. T.; Brinker, C. J.; Gong, W. L.; Guo, Y. X.; Soyez, H.; Dunn, B.; Huang, M. H.; Zink, J. I., *Nature* **1997,** *389* (6649), 364-368.

94. Huang, M. H.; Soyez, H. M.; Dunn, B. S.; Zink, J. I., *Chemistry of Materials* **2000,** *12* (1), 231-235.

95. Meyerhofer, D., *Journal of Applied Physics* **1978,** *49* (7), 3993-3997.

96. Craith, B.; Donagh, C.; McEvoy, A.; Butler, T.; O'Keeffe, G.; Murphy, V., *Journal of Sol-Gel Science and Technology* **1997,** *8* (1), 1053-1061.

97. Livage, J.; et al., *Journal of Physics: Condensed Matter* **2001,** *13* (33), R673.

98. Wolfbeis, O. S.; Oehme, I.; Papkovskaya, N.; Klimant, I., *Biosensors and Bioelectronics* **2000,** *15* (1-2), 69-76.

99. English, D. S.; Furube, A.; Barbara, P. F., *Chemical Physics Letters* **2000,** *324* (1-3), 15-19.

100. Toki, M.; Miyashita, S.; Takeuchi, T.; Kanbe, S.; Kochi, A., *J Non-Cryst Solids* **1988,** *100* (1-3), 479-482.

101. Nogami, M.; Suzuki, S.; Nagasaka, K., *J Non-Cryst Solids* **1991,** *135* (2-3), 182-188.

102. Avnir, D.; Kaufman, V. R.; Reisfeld, R., *J Non-Cryst Solids* **1985,** *74* (2-3), 395-406.

103. Gvishi, R.; Reisfeld, R., *J Non-Cryst Solids* **1991,** *128* (1), 69-76.

104. Gonzalez-Oliver, C. J. R.; Kato, I., *J Non-Cryst Solids* **1986,** *82* (1-3), 400-410.

105. Hara, K.; Inazumi, T.; Izumitani, T., *J Non-Cryst Solids* **1988,** *100* (1-3), 490-493.

106. Gerritsen, M.; Kros, A.; Sprakel, V.; Lutterman, J. A.; Nolte, R. J. M.; Jansen, J. A., *Biomaterials* **2000,** *21* (1), 71-78.

107. Uhlhorn, R. J. R.; Keizer, K.; Burggraaf, A. J., *Journal of Membrane Science* **1992,** *66* (2-3), 271-287.

108. Nakanishi, K.; Minakuchi, H.; Soga, N.; Tanaka, N., *Journal of Sol-Gel Science and Technology* **1997,** *8* (1), 547-552.

CHAPTER 2 EXPERIMENTAL: SAMPLE PREPARATION, INSTRUMENTATION, AND DATA ANALYSIS

2.1 ABSTRACT

This chapter provides details of the experimental processes, brief background information about the techniques, and methods of data analysis which have been used in the subsequent research work. Procedures for preparation of silica alcogel thin films and the following surface modification of alcogel thin film by post-grafting method, preparation of silica hydrogel monoliths and the pore surface modification, as well as the novel protocol to produce stable silica hydrogel-like thin films are presented. Different instrumental methods such as single molecule spectroscopy (SMS), contact angle measurements, thermogravimetric analysis (TGA), steady-state fluorescence anisotropy measurements, absorption spectra, fluorescence recovery after photobleaching (FRAP), profile thickness measurements, atomic force microscope (AFM), and scanning electron microscope (SEM) have been applied during the investigations.

2.2 INTRODUCTION

Based on the two-step sol-gel process, typical procedures to produce silica gel materials, such as powders,[1-2] bulk gels[3-7] or thin films,[8-12] have been developed by a lot of research groups. By adjusting the H_2O : Si ratio and the concentration of catalysts (acids or bases), silica gels with different structures and properties can be produced.[13]

Our protocols to prepare silica alcogel thin films and silica hydrogel monoliths were based on their previous work, mainly the work from Higgins' group[11] and Zink's group[5] respectively, and were finalized after some modifications by several group members. Procedures for the pore surface modification in alcogel thin film and hydrogel monolith were developed and optimized by myself. During the study of surface modification on alcogel thin film, we had an exciting discovery that that is to produce stable silica hydrogel-like thin film from nascent silica alcogel thin film. Stable hydrogel thin film has never been accomplished before. With the availability of different instruments, I was able to learn the techniques, polish my experimental skills, and finally get all my research work done.

2.3 SAMPLE PREPARATION

2.3.1 Materials

Tetraethyl orthosilicate (TEOS 99.9%+), Tetramethyl orthosilicate (TMOS 99+%), 95% ethanol (spectroscopic grade), o-phosphoric acid (85 wt %), fluorescein sodium salt (Fl) and Nile blue chloride (NBC) were purchased from Sigma-Aldrich; chloroform (99.8%+), hydrochloric acid (37.1%) and sodium phosphate were purchased from Fisher Chemicals; sodium phosphate monobasic was purchased from Mallinckrodt AR; 3-Aminopropyltrimethoxysilane (APTS) and methyltriethoxysilane (MTES) were purchased from Gelest Inc.; whereas Rhodamine 6G chloride (R6G) was purchased from Molecular Probes. All chemicals were used as received. R6G and Fl were chosen because of their high fluorescence quantum yields and exceptional photostability. NBC was chosen because it is highly sensitive to pH change and good for pH sensor

development. Chemical structures and the wavelengths of maximum absorption and maximum emission of them are provided in Figure 2.1.

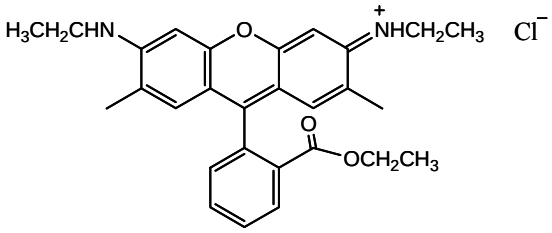

Rhodamine 6G **MW** 479.02 g/mol
λ_{abs}: 528 nm λ_{em}: 551 nm (in methanol)

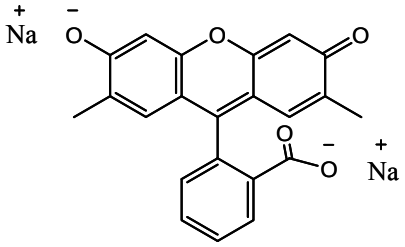

Fluorescein **MW** 376.28 g/mol
λ_{abs}: 494 nm λ_{em}: 521 nm (in water)

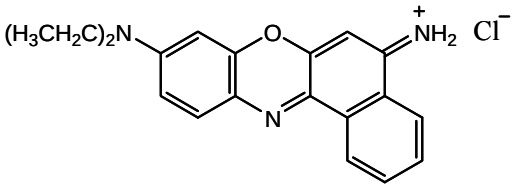

Nile Blue Chloride **MW** 353.85 g/mol
λ_{abs}: 635 nm λ_{em}: 676 nm (in water)

Figure 2.1 Basic information of the three dye molecules used in investigations.

All aqueous reagents, aqueous solutions were prepared using distilled-deionized water, including usage of water during all sample preparations. Microscope cover glasses (Fisher Premium) were purchased from Fisher Scientific. Standard VWR microscope slides and 900nm CVD (chemical vapor deposition) SiO_2/Si wafers were provided by Dr. Matt B. Johnson's lab in the department of physics and astronomy. As the substrates to deposit gel, they have all been thoroughly cleaned by sonications in 10% sodium hydroxide solution (room temperature), distilled water (room temperature), acetone (0 ^{o}C), and distilled-deionized water (room temperature) for 1 hr each before gel deposition. Thin film gel samples were usually deposited on Fisher Premium cover slides unless specified individually.

2.3.2 Preparation of Silica Alcogel Thin Films

The procedure for preparing silica alcogel thin films was the same as previously published protocol from our group.[14] Briefly, a liquid sol was first prepared by an acid-catalyzed hydrolysis reaction of TEOS in an ethanol-water solution mixture in 1:8:7 molar ratios. The materials were added in the following order: 1% by volume diluted phosphoric acid (1.95 μL), distilled-deionized water (100 μL), 95% ethanol (352.1 μL), and TEOS (176.4 μL). The resultant mixture was then sonicated in an ice-water bath for 2 hrs to facilitate hydrolysis and minimize polycondensation, and then became one homogeneous liquid sol.

Blank alcogel thin film samples: after the liquid sol (without any dyes) was aged in dark overnight (18 to 20 hrs), 60 μL of the sol was spun cast onto a cleaned cover slide at 6100 rpm for 1.1 minute

R6G-doped alcogel thin film samples (investigated in Chapter 3): 1.1 μL of 0.11 μM R6G in ethanol was added into the liquid sol immediately after sonication. For thin films to be subjected to post-synthesis grafting, 6.5 μL of 0.11 μM R6G in ethanol was used instead. The larger dye volume employed did not result in a higher R6G concentration in the modified film as plenty of R6G molecules would be washed away during the modification reaction and after repeated rinsing. The R6G-doped liquid sol was then vortexed and allowed to age in darkness overnight. After ~18 to 20 hrs of aging, 60 μL of the R6G-doped liquid sol was spun cast onto a cleaned cover glass at 6100 rpm for 1.1 min. All resultant sol-gel thin films were either subjected to the post-synthesis grafting reactions or used as a regular sample and aged for one more day in the dark before they were ready for single molecule measurements.

Nile blue chloride (NBC)-doped alcogel thin film samples (investigated in Chapter 5): ~80 mg NBC powder was mixed with the liquid sol right after sonication, and the sol was allowed to age overnight (18 to 20 hrs). 60 μL of the NBC-doped sol was spun cast onto a cleaned cover slide at 6100 rpm for 1.1 minute, and NBC-doped alcogel thin film sensor was then obtained. Thin film sensors were kept in dark for two days before pH response, leaching and reversibility investigations.

2.3.4 Surface Modification of Silica Alcogel Thin Films by Post-grafting Synthesis

This procedure is applied to samples studied in Chapter 3. Silica sol-gel pore surface modification was performed immediately after the spincoating process. First, all freshly made alcogel thin films were set to age in the darkness for 1 hr, which was then followed by another 30 minutes in distilled-deionized water. This initial procedure performed on all nascent silica films is called "pre-treatment", and those samples are called "pretreated" samples (reasons for pretreatment will be discussed later in Chapter 3.3.1.1). Afterward, the pretreated films were blown dry by nitrogen gas and be ready for surface grafting. Pore surface modification was carried out by dipping the pretreated sol-gel films into either a 0.4% (v/v) APTS aqueous solution or a 10% (v/v) MTES in chloroform mixture. After a predetermined reaction time for pore surface modification, the films were then taken out of the organosilane solution and rinsed in either water (APTS modification) or chloroform (MTES modification) for 5 minutes. The control samples were prepared by dipping pretreated alcogel films into distilled-deionized water and chloroform respectively, for the same amount of time as the corresponding organosilane modified sample. Finally, the wet films were dried with nitrogen gas and

allowed to age for one more day in the darkness before they are ready for single molecule measurements or contact angle measurements.

2.3.5 Preparation of Silica Hydrogel Monoliths

This procedure is applied to samples studied in Chapter 4. The silica sol solution was prepared by an acid-catalyzed hydrolysis of tetramethylorthosilicate (TMOS) in water.[15] Briefly, 562.5 μL TMOS, 120 μL double-distilled water, and 11.25 μL 0.01 M hydrochloric acid were mixed and sonicated in an ice-water bath for 20 minutes. For dye-doped hydrogel samples, referred as "trapping-first", one volume of sol was mixed with ten volume of 1.0×10^{-5} M R6G or Fl in 0.01 M pH 7.0 phosphate buffer solution. For dye-infused hydrogel samples, referred as "grafting-first", the sol was then mixed with ten times the amount of 0.01M pH 7.0 phosphate buffer solution for hydrogel formation. Before the gel solidified, hydrogel monolith samples for anisotropy measurements were prepared by pipetting 750 μL sol-gel solution into a 1.5 mL-polystyrene cuvet. Usually, gelation takes about 30 minutes. There are two exceptions in sample preparation: samples for chloroform and 10% MTES/chloroform modifications (shown in Figure 4.2) were prepared in glass tubes, and samples in Table 4.1 were 1000 μL-size hydrogel samples in polystyrene cuvets instead of 750 μL-size.

2.3.6 Surface Modification of Silica Hydrogel Monoliths

This procedure is applied to samples studied in Chapter 4. Pore surface modification was performed right after gelation by a top-to-bottom diffusion process. 750 μL of pre-made modification reagents such as 0.4% APTS aqueous solution was added to the top of a monolith sample, and the modification reaction was allowed to happen for two days. For those control samples, distilled-deionized water, chloroform

or 38% ethanol was added to the top instead. After two-day surface modification, "trapping-first" samples would be ready for anisotropy measurement. For "grafting-first" samples, the surface modification solution was decanted, 750 μL of 1 x 10^{-5} M R6G or Fl solution was added, and dye solution was allowed to diffuse one day before the samples were ready for measurements. Some measurements were based on longer-time diffusion, which will be addressed individually. All samples were sealed with Parafilm and stored in dark during surface modification and dye diffusion processes.

2.3.7 Preparation of Silica Hydrogel-like Thin Films and Prototype pH Sensors

All silica hydrogel-like thin films were made from silica alcogel thin film samples. The procedure for preparing silica alcogel thin films was the same as described above in section 2.3.2, referring to blank alcogel thin films. The following procedures are applied to samples investigated in Chapter 5.

Water-modified silica alcogel: nascent alcogel thin films were allowed to age various times from 0 min to 1 hr, and then were dipped into distilled-deionized water for 1 hr to induce the formation of thin film hydrogel-like samples. Resultant thin films were then blown dry with N_2 and kept in dark for one day before subjected to contact angle measurement.

Water-modified silica alcogel doped with fluorescein (Fl): nascent alcogel thin films were allowed to age 0 min (due to the operation gap, the minimum aging time was controlled less than 15 s) or 1 hr, and then were dipped into 1 mM Fl aqueous solution for 1hr to induce the formation of thin film hydrogel-like samples. Resultant thin film samples were rinsed three times with distilled-deionized water and then blown dry to

keep in dark. Before subjected to FRAP experiment, Fl-doped samples were stored overnight in chambers equilibrated with water moisture.

Water-modified silica alcogel doped with Rhodamine 6G (R6G): nascent alcogel thin films were allowed being aged for various times from 0 min to 1 hr before they were dipped into aqueous R6G solutions for 1 hr to induce the formation of thin film hydrogel-like samples. As specified individually later in Chapter 5, humidity control was applied during spincoating and the followed aging process for some preparations, which was realized by adjusting the humidity in the spincoater with a water bubbling system while the sample was inside. Two methods were used for encapsulation of R6G molecules. The first method was labeled as "real-time trapping", and samples were prepared by dipping alcogel thin films into variously concentrated R6G (from 0.1 mM to 1 mM) in 10 mM pH 7 phosphate buffer solutions (PBS), with dye trapped during gel formation. The second method was labeled as "post-trapping", and samples were prepared by dipping alcogel thin films in 10 mM pH 7 PBS to form the gel first and then being soaked in variously concentrated R6G aqueous solutions to trap dye molecules afterwards. Resultant thin film hydrogel-like samples were rinsed three times with distilled-deionized water and then blown dry to keep in dark before they were subjected to absorption spectrum, fluorescence imaging, and thickness measurements 1hr after preparation. SEM and AFM imaging of samples were conducted over a couple of days, but no difference was caught due to sample aging.

Prototype hydrogel-like thin film pH sensor doped with Nile blue chloride (NBC): nascent alcogel thin films were aged for various times from 0 min to 5 min before they were dipped into aqueous NBC solutions for 1 hr to induce the formation of thin film

hydrogel-like samples. Humidity control was applied during spincoating and the followed aging process. NBC aqueous solutions with concentrations of 0.35 mM, 0.035 mM and 0.025 mM either in pure distilled-deionized water or in 5 mM pH 7 phosphate buffer solutions (PBS) were used to induce the formation of hydrogel-like thin films. Resultant prototype hydrogel-like thin film sensors were rinsed three times with distilled-deionized water and then blown dry to keep in dark for two days before pH response, leaching and reversibility investigations.

In Chapter 5, dye-doped hydrogel-like thin film samples were prepared by "real-time trapping" method, unless specified individually. To differentiate the aging time before thin films were dipped into aqueous solution for induction of hydrogel formation from the aging time after sample preparation, the former is labeled as sample "delay time", and the latter is labeled as sample "aging time". Under the same humidity, the delay time which corresponds to the hydrogel-like thin film sample with highest absorbance is labeled as '"peak-delay-time", and the sample is labeled as "peak-delay-sample".

2.4 INSTRUMENTATION

2.4.1 Single Molecule Spectroscopy (SMS)

2.4.1.1 Background information and advantages

In the past two decades, single molecule spectroscopy (SMS) has grown into one of the powerful techniques to study the physical and optical properties of individual molecules in complex local environments. With the experimental advances in solid-state technology, SMS has now been applied into many different systems at either low or room temperature in different fields such as physics,[16-19] chemistry[12,20-22] and biology,[23-27] and its applications continue burgeoning. It is worth pointing out that room-temperature operation has made SMS applications in the biological field to undergo an explosive development.

Intense interest of SMS from so many different research groups is due to its distinct advantages.[18-19,28-29] First of all, compared to all other traditional spectroscopies, SMS completely removes the ensemble averaging, thus provides most detailed information of molecules. For example, the frequency histogram of polarization or survival lifetime of single molecules contains a lot more information than just an average value alone.[30-31] Secondly, SMS is sensitive to spatial heterogeneity, and a single molecule can act as a local reporter of its surrounding nanoenvironment. This is especially important for heterogeneous systems such as polymers, real crystals, glasses and biomolecules.[25,32-33] There's a good review about using dye as probes to explore the pore environment and molecule-matrix interactions in silica sol-gel.[34] Thirdly, SMS makes the study of time-dependent processes much easier than that of ensemble samples. For example, it is always difficult to measure the triplet lifetime by ensemble

measurements, because it requires synchronizing large number of molecules to undergo intersystem crossing, on the contrary, SMS only focuses on one molecule at a time, and removes the difficulty of synchronization process. Additionally, SMS collects the time-dependant data of many single molecules rather than an average value of them. Most importantly, SMS helped discover a lot of new phenomena which have been obscured by ensemble averaging. Famous examples like photon bunching[22] and antibunching,[35] quantum jumps,[36] and observations of conformational states and dynamics of biological molecules.[37] It is believed that SMS will help reveal more and more new effects in unexplored regimes.

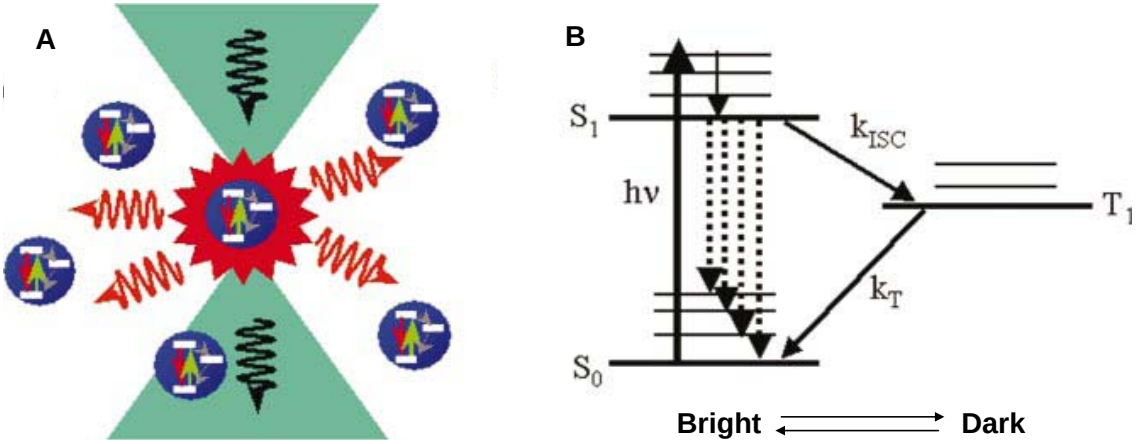

Figure 2.2 (A) An excited single molecule in the optical beam focal region (triangles). (B) The three-state model of a single molecule. Reprinted with permission from Moerner, W. E.; Fromm, D. P. *Rev. Sci. Instrum.* **2003**, *74*, 3597. Copyright 2003, American Institute of Physics.

SMS is achieved by pumping an electronic transition of one molecule resonant with the optical wavelength, and then detecting the fluorescence emission from that molecule, as shown in Figure 2.2. (A). Generally, the process is described by a three-state model.[29,38-39] As illustrated in Figure 2.2. (B), after the molecule absorbs light or more accurately photons (hν), it undergoes transitions from the ground

vibrational level of the ground singlet state (S_0), to different vibrational levels in the first excited singlet state (S_1), and then the molecule rapidly undergoes a nonradiative relaxation process to the lowest level of the first excited singlet state (S_1). If the molecule involves singlet-singlet transition from the lowest level of the first excited singlet state to the ground singlet state, photons will be emitted and fluorescence emission (dotted-line arrows) will be detected. Usually, we call this molecule is in bright state. However, sometimes the molecule undergoes an intersystem crossing (k_{ISC}) from S_1 to T_1, and then decays from the triplet state to the ground state (k_T). When the molecule is trapped in the triplet state, it doesn't emit photons, corresponding to the dark state of the molecule. What we observe is that sometimes the molecules is in bright state, sometimes it is in dark state. This phenomenon is called blinking. Blinking effect is very common in single molecule systems, and is easily detected when the relaxation from triplet state to the ground state is long (millisecond timescale).

2.4.1.2 Instrumental set-up

Currently, there are four well-developed SMS techniques. They are two scanning methods: confocal microscopy and near-field scanning optical microscopy, and two methods for wide-field study: epifluorescence microscopy and total internal reflection microscopy. Compared to wide-field methods, scanning methods involve a smaller illumination volume, thus provide lower background and better single-to-noise ratio, in the meanwhile, scanning methods always come with higher-resolution detectors such as avalanche photodiodes (APDs), they offer higher sensitivity and better temporal resolution. However, wide-field methods are able to observe several single molecules simultaneously, thus offers the real-time observation of molecular motions in

microscopic distances. Details about the experimental set-up, advantages and disadvantages of them were fully reviewed by Moerner and Fromm.[29] In our lab, we use confocal SMS microscopy (as illustrated below in Figure 2.3).

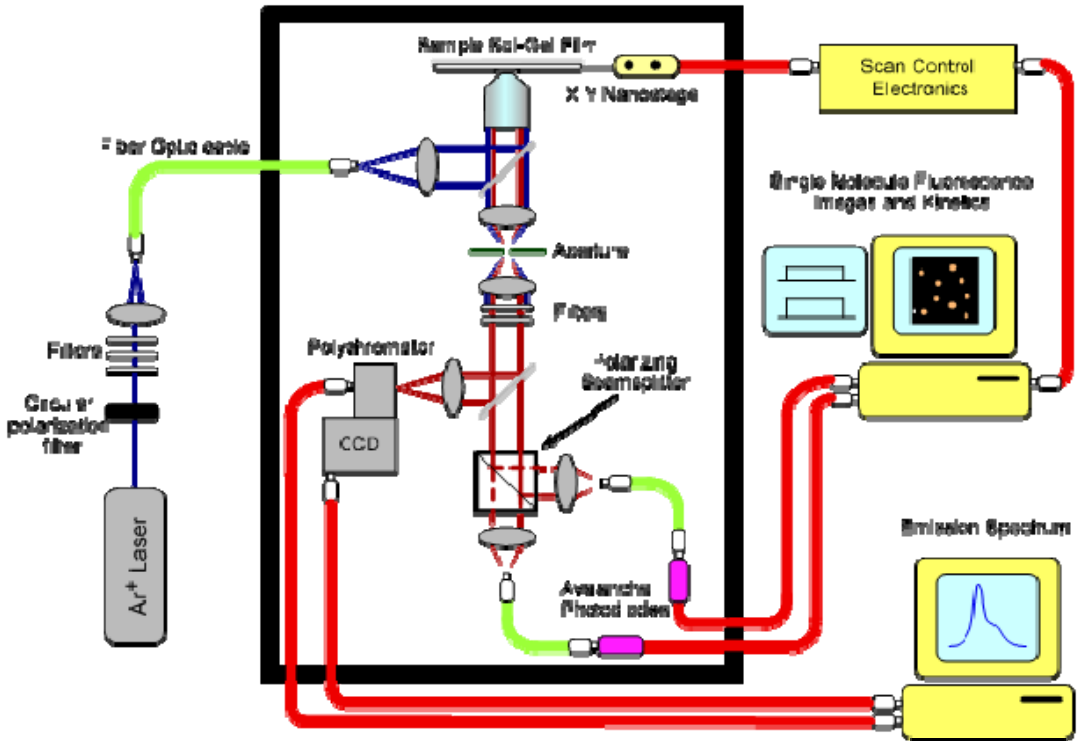

Figure 2.3 Schematic of the confocal microscope for SMS. The major part of the set-up is installed inside a black plexiglass box.

Fluorescence images and kinetic traces of R6G molecules were acquired by this home-built sample scanning confocal microscope equipped with a feedback-controlled nanostage. Briefly, the 514 nm line of an Ar^+ laser was made into circularly polarized, to ensure the even excitation of randomly oriented R6G molecules, and was directed into the epi-illumination port of an inverted microscope (Nikon TE-300). The laser excitation was then reflected up by a dichroic beamsplitter and focused at a silica thin film sample by a 100× 1.25 NA oil immersion objective, which was also used to collect

emission from the sample. After passing the dichroic beamsplitter, emission from the sample was subsequently directed to a polarizing beam splitter cube to be resolved into a parallel ($I_{\parallel}(t)$) and a perpendicular ($I_{\perp}(t)$) polarization component. The polarization resolved emission was then detected by two separate avalanche photodiode (APD) detectors. Fluorescence images were obtained by raster scanning the sample. In a typical experiment, fluorescence images of 10 μm × 10μm were recorded to locate single R6G molecules. Once their locations were identified, the fluorescence kinetics trace of each chosen molecule could be collected by transporting the molecule back to the laser focus and subjected the molecule to continuous laser excitation.

2.4.1.3 Fluorescence imaging

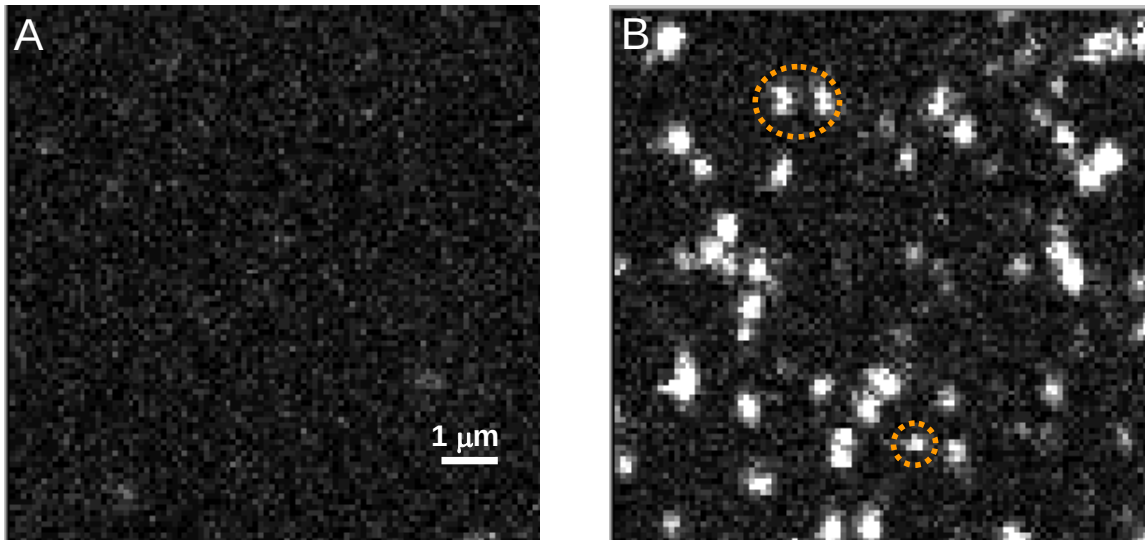

Figure 2.4 Fluorescence images of (A) blank alcogel thin film sample and (B) R6G-doped alcogel thin film sample. Spots in dashed-line circles are molecules experienced photobleaching during scanning.

For single molecule study, the final dye concentration of dye-doped samples was controlled in nM scale, while the exact concentration depends on test conditions, thus

providing lowest background and best single-to-noise ratio. Since fresh samples give streaks on imaging due to active motion of molecules, all samples for fluorescence imaging were aged one day before use. Fluorescence images were obtained by raster scanning the selected 10 μm × 10μm areas in 100 nm step increments (100 x 100 pixels). Typical fluorescence images of one-day-aged alcogel thin film samples are shown in Figure 2.4. With the same excitation intensity, blank alcogel samples usually show background noise within 10 counts, while those bright spots represent individual single molecules with intensity between 50 and 300 counts or even higher. Incompleteness of the spots in dashed-line circles indicates the photobleaching of molecules before the scanning is complete.

2.4.1.4 Kinetic traces of fluorescent molecules by photobleaching

Molecules photobleach during SMS experiments, especially at room temperature under atmospheric conditions. Due to photobleaching, a single molecule only emits a certain number of photons and then doesn't fluoresce any more. The mechanism of photobleaching is still not fully understood, while there are some common features observed during photobleaching studies, such as excitation-intensity dependence, environmental effect (especially atmospheric oxygen), and enhancement by multiple-photon absorption.[40-41]

To study the dynamic behaviors of single molecules, a higher excitation intensity than that for fluorescence imaging was chosen to photobleach the molecules, making sure most molecules survive less than 120 s. Kinetics traces of fluorescent molecules were then obtained. Examples of three different kinetics traces are demonstrated in Figure 2.5. Dark blue trace and red trace represent fluorescence signals of the parallel or

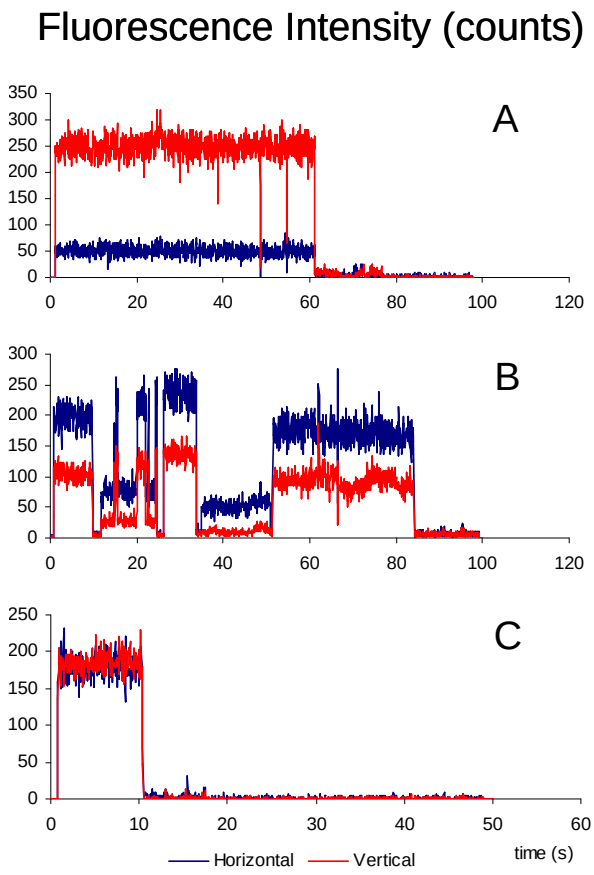

Figure 2.5 Kinetic traces of three different types of R6G molecules (A) a fixed molecule (B) an intermediate molecule and (C) a freely tumbling molecule.

horizontal ($I_{\parallel}(t)$) polarization component and the perpendicular or vertical ($I_{\perp}(t)$) polarization component from two detectors, respectively. In Figure 2.5 (A), both traces of fluorescence signals remain constant along with time, but the intensities of these two traces are different. In Figure 2.5 (B), both traces of fluorescence signals keep fluctuating along with time, sometimes even go down to 0 count, and the intensities of these two traces are different. This molecule demonstrates a good example of blinking phenomena. In Figure 2.5 (C), both traces of fluorescence signals remain constant along with time, and the intensities of these two traces are the same. According to the method of mobility classification which will be discussed later in section 2.5.1, the three molecules in Figure 2.5 are categorized as fixed, intermediate and tumbling molecule, respectively.

2.4.2 Contact Angle Measurements

Contact angle can reflect the hydrophobicity of a surface.[33,42] Usually, hydrophobic surfaces result in large contact angles and hydrophilic surfaces lead to small contact

angles. Contact angle measurement was employed to examine the extent of surface modification by post-synthesis grafting in Chapter 3 and was also used to monitor the surface hydrophobicity change of water-treated thin film samples in Chapter 5.

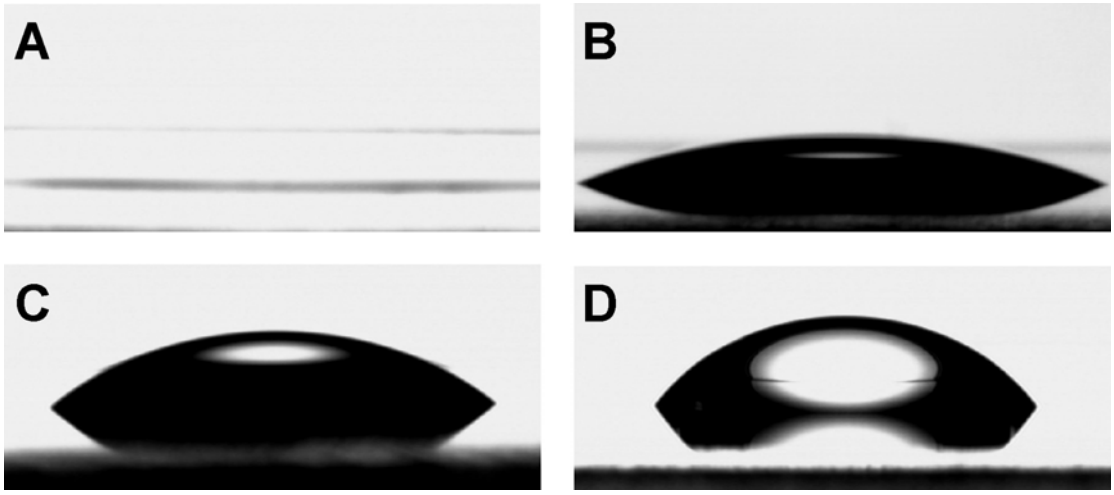

Figure 2.6 Contact angle images of a water droplet on (A) water-treated nascent, (B) pretreated, (C) APTS-grafted, and (D) MTES-grafted silica alcogel films.

All samples subjected to contact angle measurement were aged one day. Static contact angles of differently modified silica sol-gel films were obtained from a model 190-F1 goniometer manufactured by Ramé-Hart. Images of water droplets on different thin film surfaces were captured and then analyzed using the accompanying DROPimage CA software. Water droplet was dripped to the center of each sample, and then five successive images were captured with 20 s intervals for each sample. Typical images of water-treated nascent, pretreated, APTS-, and MTES-modified sol-gel silica films investigated in Chapter 3 are shown in Figure 2.6. The contact angle (θ) is found to increase in the following order $\theta_{nascent} < \theta_{pretreated} < \theta_{APTS} < \theta_{MTES}$. What caused differences between them will be extensively discussed in Chapter 3.3.1.

2.4.3 Thermogravimetric Analysis (TGA)

TGA was used to estimate the amount of organics post-grafted on the silica film surface. Although TGA is a robust technique to determine the amount of surface attached organics on silica surface, it is noted that all previous post-grafted silica research has been focused on silica particles, which have a much larger surface area to mass ratio than our samples.[43-45] In our thin film samples, the surface area to mass ratio is substantially lower, which may not be able to produce a reliable measure on the amount of surface attached APTS or MTES on our silica films. Despite numerous efforts, we saw no discernable weight loss from our sample upon heating to 500 ºC. As a result, we are still not able to provide a quantitative estimate on the amount of surface attached APTS or MTES. This unfortunate outcome is entirely due to the limit of sensitivity of the TGA technique because of the low surface area to mass ratio of our sample.

All the samples were stored in atmospheric condition overnight before subjected to TGA. In a typical TGA experiment, ~ 50 mg of broken microscope coverglass pieces coated with APTS or MTES modified silica film was used. TGA measurement was carried out with DuPont model 951 thermogravimetric analyzer by using a Thermal Analyst 2000 data system., which is capable of detecting weight loss as small as 34 μg. TGA thermograms were collected from 25 ºC to 500 ºC with a heating rate of 20 ºC min^{-1}. The air flow rate was 50 mL/min.

2.4.4 Steady-state Fluorescence Anisotropy Measurements

Quantitative measurements of fluorescence anisotropy were performed on a Shimadzu RF-5310PC fluorometer, which has a single emission channel. Schematic diagrams for the measurements of fluorescence anisotropy are shown in Figure 2.7.[46] For R6G, spectra were collected at λ_{ex} = 514 nm, whereas λ_{ex} = 488 nm for Fl. Typically, four measurements should be performed for each sample to obtain I_{HH}, I_{HV}, I_{VV} and I_{VH}. Fluorescence anisotropy value r will be calculated according to Equations 2.1.[46] I_{HH}, I_{HV}, I_{VV} and I_{VH} represent fluorescence intensities with different polarized excitation and emission. H means horizontally polarized, and V means vertically polarized. G is a correction factor used to correct the birefringence of the fluorometer. Large r values indicate slow rotations or restricted molecules, whereas small r values indicate fast rotations or freely tumbling molecules.

$$r = \frac{I_{VV} - GI_{VH}}{I_{VV} + 2GI_{VH}} \qquad G = \frac{I_{HV}}{I_{HH}} \qquad \textbf{2.1}$$

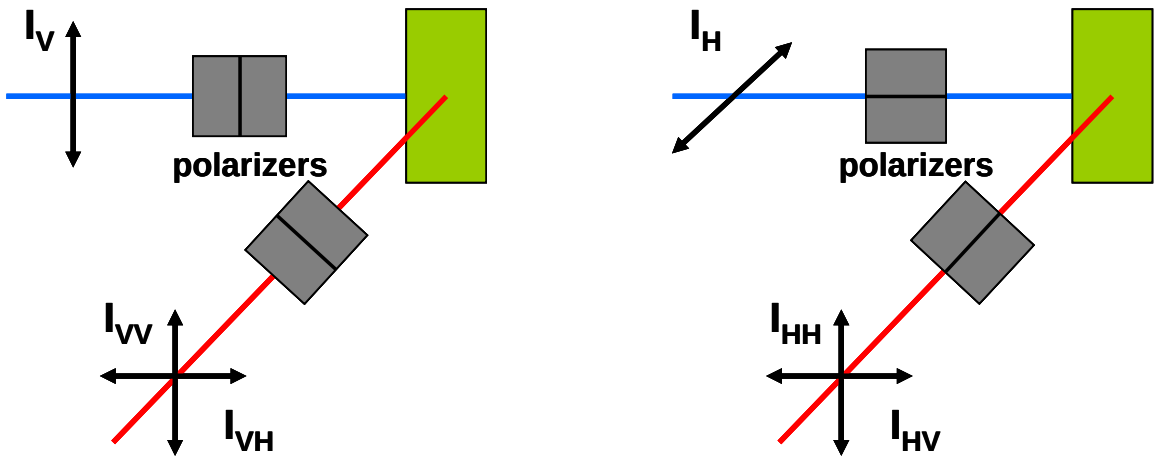

Figure 2.7 Schematic diagrams of fluorescence anisotropy measurements (A) vertically polarized excitation, and (B) horizontally polarized excitation. Figure based on ref. 46.

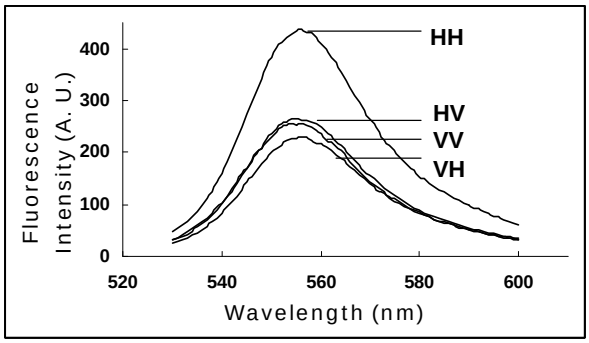

Figure 2.8 Polarized fluorescence intensity of R6G in a water-modified hydrogel sample.

Figure 2.8 shows the four fluorescence emission spectra collected from a water-modified hydrogel sample doped with R6G. The values of I_{HH}, I_{HV}, I_{VV} and I_{VH} were calculated by averaging the twenty emission intensities in ± 10 nm range of λ_{max} (the wavelength corresponding to the peak intensity of each individual spectrum). They were 225.98, 202.67, 386.32 and 234.54 respectively, according to Equations 2.1, G factor was 0.8968, and the anisotropy value would be 0.218, which indicated that most R6G molecules were immobilized in this hydrogel sample.

2.4.5 Absorption Spectra

Absorption spectra of solutions and thin film samples were measured on a Shimadzu UV-2101PC, UV-VIS Scanning Spectrophotometer, operated in the parallel two beam configuration. For consistency, the absorption spectra of R6G doped thin film samples were collected 1 hr after preparation. Two peaks at 532 ± 2 nm and 498 ± 2 nm were observed in the absorption spectra of most R6G doped thin film samples and R6G aqueous solutions (when concentration was higher than 0.01 mM), representing monomer and dimer peaks of R6G respectively. R6G absorption spectra were all fitted with Gaussian equations, and one example will be shown in section 2.5.3. For convenience, only data from R6G monomer peak at 532 nm were plotted and compared in Chapter 5. In Chapter 5, during the pH response, leaching and reversibility

investigations, NBC doped silica hydrogel-like thin film sensors and alcogel thin film sensors were blown dry before taken absorption spectra. Due to the sensitivity of NBC to pH, the major absorption peaks of NBC samples (both solution and doped thin film samples) changed with pH, so no Gaussian fitting was applied to them.

2.4.6 Fluorescence Recovery after Photobleaching (FRAP)[47-49]

FRAP started in 1970s, and was originally used to study molecular mobility in biological samples. It now becomes to a very versatile tool for mobility and interaction measurements in pharmaceutical field, and it is ideal to study mobility or diffusion of molecules and particles on a microscopic level in all kinds of environments, especially in polymers and gels. FRAP experiment is fast and convenient, can be finished in minutes; while provides high resolutions both in spatial (μm) and in temporal (μs); most importantly for biological samples, it allows study in intact samples. Due to the noninvasive nature, it has been widely applied both in *vivo* and in *vitro* experiment.

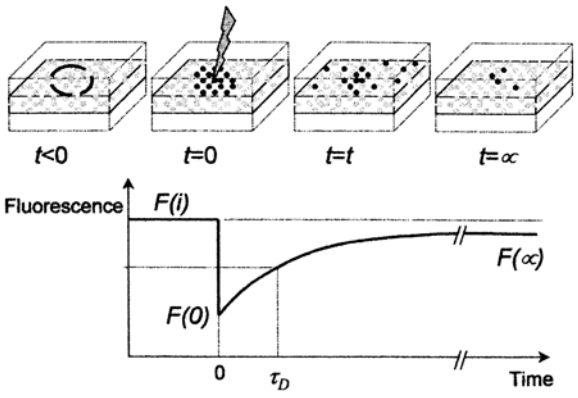

Figure 2.9 Schematic of a FRAP experiment. Reproduced with permission from ref. 47. Copyright 1999 Springer.

FRAPs of fluorescein (Fl) in thin film hydrogel were performed on the home-built sample scanning confocal microscope equipped with a feedback-controlled nanostage described in section 2.4.1.2. A representative schematic of FRAP experiment is shown in Figure 2.9:[47] Basically, an area on the sample was chosen and moved into the laser focus. A low-power probe laser light was used to obtain a stable initial fluorescence

intensity (*F(i)*). Once a stable fluorescence from the selected area has been established, the laser power was then increased by 10^4 ~10^6 fold to photobleach the dye with the selected area for 10 s. Right after the photobleaching, the laser power was decreased back to the probe level to monitor the recovery of fluorescence due to the subsequent diffusion of dye molecules from outside the bleached area.

F(i) is the initial fluorescence before photobleaching, *F(0)* is the fluorescence after beaching, and $F(\infty)$ is the fluorescence after recovery. The FRAP data were fit with Equation 2.2:

$$I(t) = A(1 - \exp(-k_{recover}t)) + C \qquad 2.2$$

Where $I(t)$ is the fluorescence intensity, $k_{recover}$ is the recovery rate constant. A is the recovered fluorescence intensity minus the fluorescence intensity after photobleaching ($F(\infty) - F(0)$), and C is $F(0)$.

2.4.7 Profile Thickness Measurements

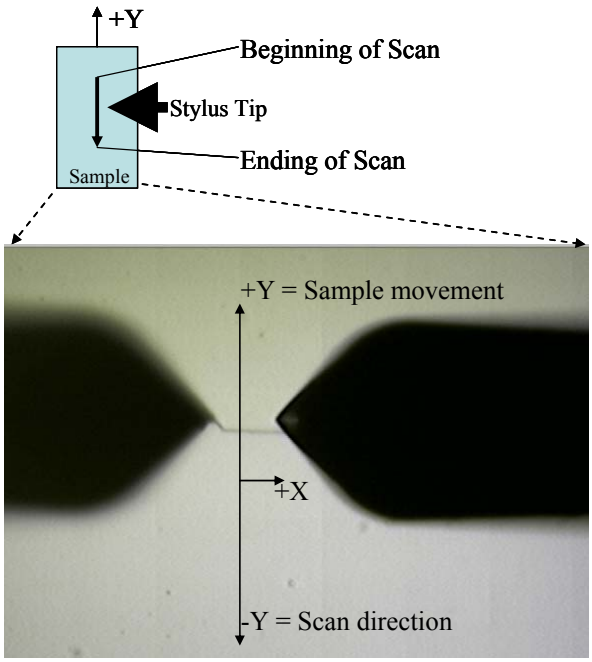

A strip of gel layer from the thin film sample was removed with a razor blade, held in a "snow plow" fashion. The step height was then measured through a XP-2 stylus profilometer by Ambios Technology Inc.. Figure 2.10 shows what actually happens during a scan. Once the stylus tip approaches the sample surface close enough, the camera

Figure 2.10 Schematic of a profile thickness scan.

would be able to capture the motion of stylus and display it in the program window. Typically, two images of the stylus head are found in the captured region. As shown in Figure 2. 10, right one is the real image of the stylus head, and the left one is a mirror image of the stylus due to reflection. First, the interested spot on the sample was located by adjusting the position of the stylus (all directions applicable), once you start the scan, the stylus head moves to –X direction, when the stylus tip hits the sample surface (illustrated by the meet of two images), the stylus will start scanning from +Y to –Y direction. After the scanning completes, a profile of the sample surface will be generated. In my experiment, the scan speed was 0.05 mm/s, measured length was 0.8 mm, the applied force was 0.5 mg, and the range was 10 μm. Usually, sample thickness was measured on the day of preparation, and the thickness was an average of values from at least two spots and four measurements from the sample.

2.4.8 Atomic Force Microscope (AFM)

AFM was invented in 1986 by G. Binnig, C. F. Quate and Ch. Gerber.[50] It is one type of scanning probe microscopy (SPM), which is based on scanning the surface of the sample in an x/y raster pattern with a very sharp tip that moves up and down along the z axis when the surface topography changes. AFM can be used to image virtually both conducting and insulating surfaces at microscopic and nanoscopic levels. It has proven to be a powerful tool for chemical, physical and biological studies.[51-55] There are three imaging modes to operate AFM: contact mode, tapping mode or intermittent mode, and non-contact mode.[51,55] The classification of the operation modes is strictly related to the region of the force field between the tip and the imaging surface. When the microscope works in contact mode, the tip is permanently in contact with the sample

surface, and the repulsive interaction dominates. In tapping mode operation, the tip contacts with the sample surface for only a short time periodically and then is mostly removed from the surface, so the resultant image depends both on the repulsive and attractive forces. For the non-contact mode, the tip-cantilever system is placed at the attractive region all the time, and the force gradients caused by attractive interactions are detected. AFM images are obtained by measuring the force between the tip and the sample, so the performance of an AFM is strongly dependent on the physical characteristics of the tip and the cantilever.

In my experiment, all images were acquired in non-contact mode by TopoMetrix EXPLORER, with a scan rate of 5 μm/s for 5 μm x 5 μm size images and 20μm/s rate for 20μm x 20μm images. Integrated tip sets from MikroMasch were used in all experiments. Three n-type silicon tips were grown on no Al-coated silicon cantilevers (NSC35/ no Al) with spring constant of 4.5, 7.5 or 14.0 N/m respectively. Root mean square (RMS) roughness based on AFM images was calculated by Gwyddion 2.19.

2.4.9 Scanning Electron Microscope (SEM)[56]

The first SEM image was obtained by Max Knoll in 1935, which was an image of silicon steel showing electron channeling contrast. After development of several researchers, SEM was first marketed in 1965 by the Cambridge Instrument Company as the "Stereoscan". Today, SEM becomes into a standard technique to study the surface properties of solid samples. Application fields include chemistry, material science, geology, and biology. SEM images are obtained by scanning the sample surface with a high-energy beam of electrons in a raster scan pattern. It can provide information not only about surface topography but also the composition and other properties such as

electrical conductivity of the sample. SEM can produce very high-resolution images of a sample surface, down to less than 1 to 5 nm in size. Wide range of magnifications from 10 times to more than 500,000 times can all be achieved by SEM.

SEM images of samples with different magnifications from 20x to 100,000x were collected on JEOL JSM-880 high resolution scanning microscope. Silica samples on glass slides were sputter-coated with a ~5nm Au-Pd layer before imaging.

2.5 DATA ANALYSIS

2.5.1 Polarization Calculation, Mobility Classification and the Error Calculation of Mobility Population

Fluorescence polarization reflects the relative angle between the orientation of polarized absorption light and emission light of a fluorophore. The value of polarization is between - 1 and 1. In an isotropic solution, fluorescent molecules are randomly oriented, which results in polarization value of 0. The polarization (*P(t)*) of a single molecule can be calculated from the collected kinetic trace signals $I_{\parallel}(t)$ and $I_{\perp}(t)$, according to Equation 2.3:

$$P(t) = \frac{xI_{\parallel}(t) - I_{\perp}(t)}{xI_{\parallel}(t) + I_{\perp}(t)}. \qquad \textbf{2.3}$$

$P(t)$ is a time-dependent function, and x is a scaling factor to correct for the birefringence accumulated from various optical components plus the different sensitivities of the two APD detectors. The value of x was determined daily by forcing the average of $P(t)$ ($\overline{P}$) of a R6G solution to zero to represent isotropic emission. The standard deviation (σ_{iso}) of $\overline{P}$ from the R6G solution was also determined and used

for classifying the mobility of single R6G molecules in other samples according to the following scheme:[14]

Fixed molecule: $P(t) = \text{constant}$ and $|\overline{P}| > \sigma_{iso}$

Intermediate molecule: $P(t) \neq \text{constant}$

Tumbling molecule: $P(t) = \text{constant}$ and $|\overline{P}| < \sigma_{iso}$

Figure 2.11 nicely demonstrates single molecules in three different mobility states. Green traces in the graphs represent the time dependent $P(t)$, pink straight lines indicate the average of $P(t)$ ($\overline{P}$) for each single molecule. After all $\overline{P}$ s of single molecules were calculated, usually a histogram of $\overline{P}$ was plotted.

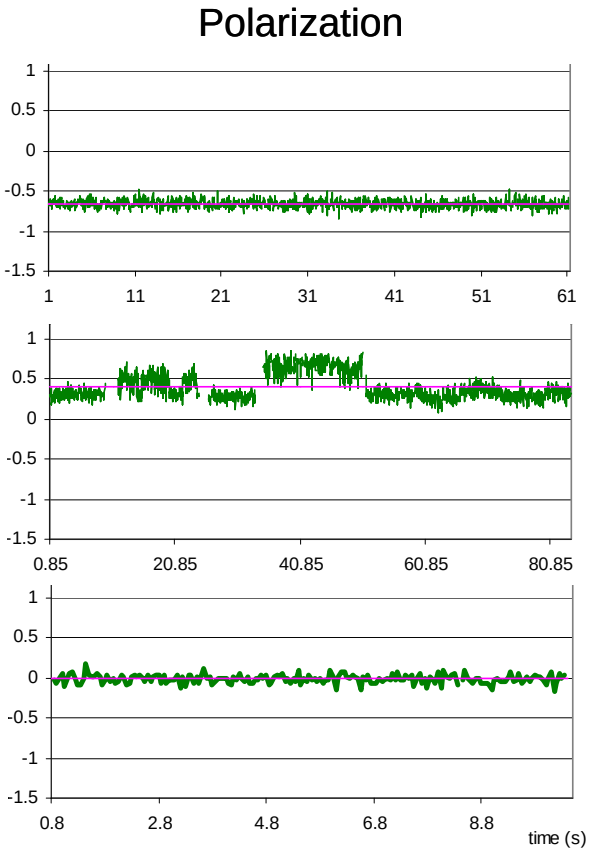

Figure 2.11 Polarization traces of three different types of R6G molecules (A) a fixed molecule (B) an intermediate molecule and (C) a freely tumbling molecule.

Figure 2.12 below shows the polarization distribution of R6G in regular alcogel thin films, based on a collection of 131 R6G single molecules. The frequency distribution followed a Gaussian form, with the mean value of this set of $\overline{P}$ s around 0.4, which suggests that most portion of the molecules are either in fixed or intermediate category.

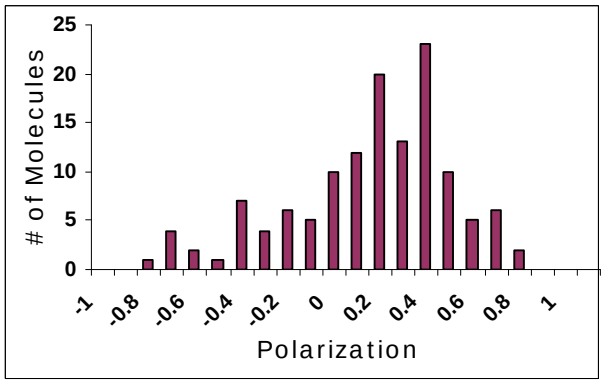

Figure 2.12 A $\overline{P}$ histogram of R6G in regular thin film alcogel samples.

After the category of each single molecule was identified according to its polarization trace, the mobility distribution or percentage of this set of molecules can be calculated. The error for each mobility category percentage was calculated under a binomial sampling distribution assumption according to Equation 2.4.

$$\text{Error} = (p\ q\ n)^{1/2} \qquad \textbf{2.4}$$

The error calculated represents the number of molecules whose category is uncertain. p is the molecule fraction within the category considered, q is the fraction not within the category (1-p), and n is the total number of sampled molecules. As the sampling size increases, the relative uncertainty of categorizing decreases. Usually, we collected 150 to 200 molecules to reduce the sampling error.

2.5.2 Bi-exponential Decay Fitting of Molecular Survival Lifetimes

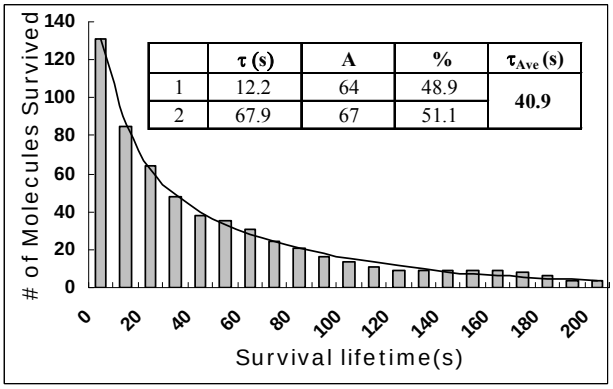

Figure 2.13 Bi-exponential decay fitting of R6G molecular survival lifetimes in regular thin film alcogel samples. Inset table is a summary of fitted data

Using the number of R6G molecules that remains fluorescent upon continuous excitation (*f*) as y axis, the survival lifetime of R6G in all samples are best fitted by a bi-exponential decay function, Equation 2.5, revealing the spatial heterogeneity of the sol-gel silica films. Figure 2.13 shows a typical fitting graph, which based on 131 R6G single molecules in regular thin film alcogel samples. Gray columns are the statistical numbers of molecules remaining survived at each lifetime, and the black curve is the fitting curve according to Equation 2.5.

$$f = A_1 e^{-t/\tau_1} + A_2\, e^{-t/\tau_2} \qquad \textbf{2.5}$$

A_1 is the number of molecules with survival lifetime τ_1, and A_2 is the number of molecules with survival lifetime τ_2. After the fraction (%) of each set of molecule was calculated, the average survival lifetime τ_{ave} of the collected molecules was then able to be obtained. Longer survival lifetime reflects higher photostability of molecule.

2.5.3 Gaussian Fittings of Absorption Spectra

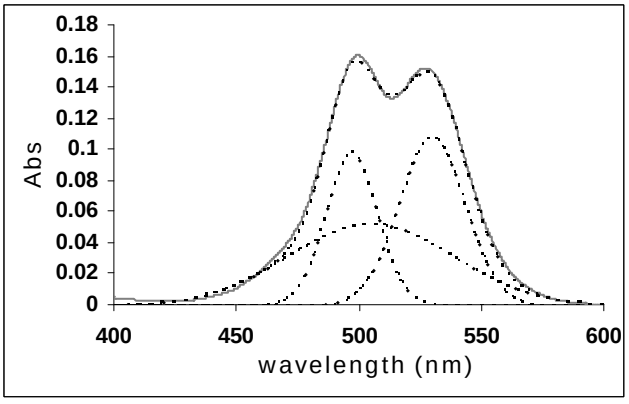

Figure 2.14 Three-peak Gaussian fitting of the R6G absorption spectrum.

As our hydrogel-like thin film samples have a very high dye loading capacity, they are able to accumulate a lot more molecules in a unit volume than in aqueous solution, so dimers are easily formed. As shown in Figure 2.14 (the gray solid line), two peaks at

532 ± 2 nm and 498 ± 2 nm were found in the absorption spectra of most R6G doped thin film hydrogel-like samples, representing monomer and dimer peaks of R6G respectively. There's another peak at 505 ± 2 nm usually was hidden by the other two, representing the vibronic peak of R6G monomer. Figure 2.14 demonstrates a typical three-peak Gaussian fitting of a spectrum. The black dashed-line curve on the top is the fitted curve, and the three bottom black dashed-line curves represent the three components of it. Equation 2.6 was used to do all the Gaussian fittings.

$$A = A_{\max 1} e^{-(\lambda-\lambda_{\max 1})^2/\omega_1^2} + A_{\max 2} e^{-(\lambda-\lambda_{\max 2})^2/\omega_2^2} + A_{\max 3} e^{-(\lambda-\lambda_{\max 3})^2/\omega_3^2} + A_{bkg} \quad \textbf{2.6}$$

A_{max} is the maximum intensity of a single peak, λ_{max} is the wavelength corresponding to A_{max}, and ω is the full width at half maximum (FWHM). Subscripts 1, 2 and 3 represent the three components or the three peaks. A_{bkg} is the background noise.

2.5.4 Error Calculation of Multiple Variables

When the experiment result is determined by several parameters, the uncertainty of the data points is propagated to the parameters, which will affect the determination of the final result. The error or uncertainty of the experiment result, which is determined by two variables, can be calculated according to Equation 2.7.[57]

$$\delta(A/H) = \sqrt{(\delta A)^2 \left(\frac{\partial(A/H)}{\partial A}\right)^2 + (\delta H)^2 \left(\frac{\partial(A/H)}{\partial H}\right)^2} \quad \textbf{2.7}$$

Specifically, we use this equation to calculate the error of the unit absorbance of R6G-doped hydrogel-like thin film samples. Unit absorbance (A/H, μm^{-1}) of a sample helps us to compare the dye loading capacity of each sample by eliminating the thickness influence. A is the average value of absorbance, δA is the variation of

absorption measurements, H is the average value of sample thickness in μm, and δH is the variation of thickness measurements.

2.6 CONCLUSION

This chapter presented the general protocols of sample preparation, basic background information of the instruments, different types of experimental data obtained from those instrumental measurements, and methods of data analysis. All those fundamental information makes the discussions in the following chapters possible.

2.7 CHAPTER 2 REFERENCES

(1) Stöber, W.; Fink, A.; Bohn, E. *J Colloid Interf Sci* **1968**, *26*, 62.

(2) Wu, X.; Choi, M. M. F.; Xiao, D. *Analyst* **2000**, *125*, 157.

(3) Nogami, M.; Moriya, Y. *J Non-Cryst Solids* **1980**, *37*, 191.

(4) Brinker, C. J.; Keefer, K. D.; Schaefer, D. W.; Ashley, C. S. *J Non-Cryst Solids* **1982**, *48*, 47.

(5) Ellerby, L. M.; Nishida, C. R.; Nishida, F.; Yamanaka, S. A.; Dunn, B.; Valentine, J. S.; Zink, J. I. *Science* **1992**, *255*, 1113.

(6) Yu, D.; Volponi, J.; Chhabra, S.; Brinker, C. J.; Mulchandani, A.; Singh, A. K. *Biosensors and Bioelectronics* **2005**, *20*, 1433.

(7) Krupa, I.; Nedelčev, T.; Račko, D.; Lacík, I. *Journal of Sol-Gel Science and Technology* **2010**, *53*, 107.

(8) Sakka, S.; Kamiya, K.; Makita, K.; Yamamoto, Y. *J Non-Cryst Solids* **1984**, *63*, 223.

(9) Huang, M. H.; Soyez, H. M.; Dunn, B. S.; Zink, J. I.; Sellinger, A.; Brinker, C. J. *Journal of Sol-Gel Science and Technology* **2008**, *47*, 300.

(10) Huang, M. H.; Dunn, B. S.; Zink, J. I. *Journal of the American Chemical Society* **2000**, *122*, 3739.

(11) Wang, H.; Bardo, A. M.; Collinson, M. M.; Higgins, D. A. *The Journal of Physical Chemistry B* **1998**, *102*, 7231.

(12) Mei, E.; Bardo, A. M.; Collinson, M. M.; Higgins, D. A. *The Journal of Physical Chemistry B* **2000**, *104*, 9973.

(13) Brinker, C. J.; Scherer, G. W. *Sol-Gel Science: the physics and chemistry of sol-gel processing*; Academic press: San Diego, 1990.

(14) Viteri, C. R.; Gilliland, J. W.; Yip, W. T. *Journal of the American Chemical Society* **2003**, *125*, 1980.

(15) Zhou, Y. Y.; Yip, W. T. *J Phys Chem B* **2009**, *113*, 5720.

(16) Ambrose, W. P.; Basche, T.; Moerner, W. E. *J Lumin* **1992**, *53*, 62.

(17) Kohler, J.; Disselhorst, J. A. J. M.; Donckers, M. C. J. M.; Groenen, E. J. J.; Schmidt, J.; Moerner, W. E. *Nature* **1993**, *363*, 242.

(18) Moerner, W. E. *J Phys Chem B* **2002**, *106*, 910.

(19) Orrit, M. *The Journal of Chemical Physics* **2002**, *117*, 10938.

(20) Conley, N. R.; Biteen, J. S.; Moerner, W. E. *J Phys Chem B* **2008**, *112*, 11878.

(21) Lu, Z. K.; Liu, N.; Lord, S. J.; Bunge, S. D.; Moerner, W. E.; Twieg, R. J. *Chemistry of Materials* **2009**, *21*, 797.

(22) Orrit, M.; Bernard, J. *Phys Rev Lett* **1990**, *65*, 2716.

(23) Moerner, W. E. *P Natl Acad Sci USA* **2007**, *104*, 15584.

(24) Biteen, J. S.; Moerner, W. E. *Csh Perspect Biol* **2010**, *2*.

(25) Lord, S. J.; Lee, H. L. D.; Moerner, W. E. *Analytical Chemistry* **2010**, *82*, 2192.

(26) Ferris, M. M.; Habbersett, R. C.; Wolinsky, M.; Jett, J. H.; Yoshida, T. M.; Keller, R. A. *Cytom Part A* **2004**, *60A*, 41.

(27) Werner, J. H.; McCarney, E. R.; Keller, R. A.; Plaxco, K. W.; Goodwin, P. M. *Analytical Chemistry* **2007**, *79*, 3509.

(28) Jung, Y.; Barkai, E.; Silbey, R. J. *J Chem Phys* **2002**, *117*, 10980.

(29) Moerner, W. E.; Fromm, D. P. *Rev Sci Instrum* **2003**, *74*, 3597.

(30) Viteri, C. R.; Gilliland, J. W.; Yip, W. T. *Journal of the American Chemical Society* **2003**, *125*, 1980.

(31) Lei, Q.; Yip, W. T. *The Journal of Physical Chemistry C* **2009**, *113*, 21130.

(32) Klichko, Y.; Khashab, N. M.; Yang, Y. W.; Angelos, S.; Stoddart, J. F.; Zink, J. I. *Micropor Mesopor Mat* **2010**, *132*, 435.

(33) Venkateswara Rao, A.; Latthe, S. S.; Nadargi, D. Y.; Hirashima, H.; Ganesan, V. *J Colloid Interf Sci* **2009**, *332*, 484.

(34) Dunn, B.; Zink, J. I. *Chemistry of Materials* **1997**, *9*, 2280.

(35) Basche, T.; Moerner, W. E.; Orrit, M.; Talon, H. *Phys Rev Lett* **1992**, *69*, 1516.

(36) Basche, T.; Kummer, S.; Brauchle, C. *Nature* **1995**, *373*, 132.

(37) Weiss, S. *Science* **1999**, *283*, 1676.

(38) Molski, A.; Hofkens, J.; Gensch, T.; Boens, N.; De Schryver, F. *Chemical Physics Letters* **2000**, *318*, 325.

(39) Barkai, E.; Jung, Y. J.; Silbey, R. *Annual Review of Physical Chemistry* **2004**, *55*, 457.

(40) Deschenes, L. A.; Vanden Bout, D. A. *Chemical Physics Letters* **2002**, *365*, 387.

(41) Zondervan, R.; Kulzer, F.; Kol'chenko, M. A.; Orrit, M. *J Phys Chem A* **2004**, *108*, 1657.

(42) Onda, T.; Shibuichi, S.; Satoh, N.; Tsujii, K. *Langmuir* **1996**, *12*, 2125.

(43) Lin, J.; Siddiqui, J. A.; Ottenbrite, R. M. *Poly. Adv. Technol.* **2001**, *12*, 285.

(44) Zengin, H.; Hu, B.; Siddiqui, J. A.; Ottenbrite, R. M. *Poly. Adv. Technol.* **2006**, *17*, 372.

(45) Zengin, H.; Siddiqui, J. A.; Ottenbrite, R. M. *Poly. Adv. Technol.* **2008**, *19*, 105.

(46) Lakowicz, J. R. *Principles of Fluorescence Spectroscopy*; 3rd ed.; Springer 2006.

(47) Meyvis, T.; De Smedt, S.; Van Oostveldt, P.; Demeester, J. *Pharmaceutical Research* **1999**, *16*, 1153.

(48) Reits, E. A. J.; Neefjes, J. J. *Nat Cell Biol* **2001**, *3*, E145.

(49) Braeckmans, K.; Peeters, L.; Sanders, N. N.; De Smedt, S. C.; Demeester, J. *Biophys J* **2003**, *85*, 2240.

(50) Binnig, G.; Quate, C. F.; Gerber, C. *Phys Rev Lett* **1986**, *56*, 930.

(51) Louder, D. R.; Parkinson, B. A. *Analytical Chemistry* **1995**, *67*, 297A.

(52) Silva, L. P. d. *Protein and Peptide Letters* **2002**, *9*, 117.

(53) Giessibl, F. J. *Rev Mod Phys* **2003**, *75*, 949.

(54) Borionetti, G.; Bazzali, A.; Orizio, R. *The European Physical Journal Applied Physics* **2004**, *27*, 101.

(55) Alessandrini, A.; Facci, P. *Measurement Science and Technology* **2005**, *16*, R65.

(56) Skoog, D. A.; Holler, F. J.; Nieman, T. A. *Principles of Instrumental Analysis*; 5th ed.; Thomson Learning, 1997.

(57) Bevington, P. R. *Data Reduction and Error Analysis for the Physical Sciences*; McGraw-Hill Book Company: New York, 1969.

CHAPTER 3 PROBING THE EFFECT OF POST-SYTHESIS GRAFTING ON GUEST-HOST INTERACTIONS IN SOL-GEL SILICA WITH SINGLE-MOLECULE MOBILITY AND PHOTOSTABILITY

3.1 ABSTRACT

The mobility and photostability of single rhodamine 6G (R6G) molecules encapsulated in organosilane modified silica alcogel films were used to examine how post-synthesis grafting alters guest-host interactions. While physical confinement remains the major factor that controls mobility in modified alcogels, both R6G mobility and photostability register discernable changes after surface charges are respectively reversed and neutralized by aminopropyltriethoxysilane (APTS) and methyltriethoxysilane (MTES) grafting to weaken R6G/silica attraction on pore surfaces. Among the two methods, the change in R6G photostability was found to be more sensitive to surface grafting, which is more capable of inducing localized dynamic motions than full scale molecular rotation under the stringent physical confinement inside alcogel films. In addition, silica film modification by 0.4% APTS is as efficient as that by pure MTES in lowering R6G photostability, which suggests that surface charge reversal is more effective than charge neutralization in disrupting R6G/silica attraction. Collectively, our results demonstrate that single-molecule mobility and photostability can be used to monitor the extent of grafting reaction underneath a film

surface and complement other surface characterization techniques that are only sensitive to modifications made on a film surface.

3.2 INTRODUCTION

Mesoporous silica synthesized by the sol-gel process has long been a subject of intense interest. The ease of guest molecule encapsulation, its ability to protect the encapsulated molecules from degradation and denaturation, the inertness of silica, and the benign chemical reactions involved in the sol-gel process have made sol-gel silica a popular substrate for widespread applications ranging from nonlinear optics[1] to anticorrosion coatings[2-3] to chemical and biosensor developments.[4-9] A major advantage of the sol-gel process is that it is highly adaptable to modifications, which makes it quite easy to alter the external appearance, internal structure, as well as the surface property of the resultant silica. Thus, silica sol-gel can be dip-coated or spin-coated into thin films upon rapid drying or it can be made into thick monoliths if allowed to solidify slowly. In addition, it can be prepared as an alcogel[10] that possesses a dense internal structure or as a hydrogel[11-14] consisting of a highly porous framework that filled with water. Finally, the surface chemistry of silica sol-gel, both internally and externally, can be fine tuned by additional reaction with organosilanes either through a one-pot synthesis carried out simultaneously with the sol-gel formation process[15-22] or in a stepwise fashion as a post-gelation modification approach.[23-27] It is worth pointing out that even when the same organosilane modifying reagent is employed, the two approaches do not usually produce silica sol-gel with similar internal microstructures.

The ease of the one-pot approach to introduce alternative functionality to regular sol-gel silica together with more homogeneously distributed functional groups have

been the major driving force for the study of organically modified siloxanes (ormosils). Numerous investigations have been devoted to examining the properties of ormosils and their potential applications.[28-30] Unlike the one-pot approach, post-synthesis surface grafting has received much less attention, partly because of the more lengthy stepwise reaction involved. Poor diffusion, especially in the denser alcogel, has also called into question of whether the internal pore surface of a silica sol-gel is accessible to silane modifications. Nevertheless, post-synthesis grafting does offer distinct advantages in a better defined silica structure and more accessible functional groups that are unmatched by the one-pot approach.[31] With the handful of studies on post-synthesis grafting, it has already been demonstrated that a gas sensor can be built from the dielectric response of a modified film;[32] thiol functionalized films have been made into an electrochemical sensor of metal ions;[33] and even gold nanowires can be grown inside amino derivatized films.[34]

Various X-ray techniques such as photoelectron spectroscopy (XPS), small angle scattering (SAXS), and reflectometry (XRR) are regularly used to characterize the internal structure of silica films.[31] Film surface morphology can be examined by various scanning probe microscopic techniques like TEM, SEM, and AFM, whereas the extent of modification can be monitored by contact angle measurements, FTIR, solid-state NMR, and thermogravimetric analysis (TGA).[35-36] Besides these basic structural analyses, there has been a gathering interest in characterizing the functional group imparted into the silica films. An earlier report based on nitrogen adsorption/desorption and bromination kinetics suggested that functional groups anchored on the external surface or near channel openings are more available for reactions.[37] Most recently,

amino-functionalized mesoporous silica films were found to be reactive toward amidation, with ~37% post-gelation grafted amino groups available for the reaction as opposed to ~16% from films obtained through a one-pot reaction.[31] Together, these two studies reveal that relative to the one-pot approach, functional groups introduced by post-synthesis grafting have a bigger influence on silica pores and channels that are readily accessible to external reagents. This has a strong implication in the design of silica based sensor, reactor, and catalyst as their performance are almost certainly originated from chemical species encapsulated inside those more accessible pores and channels.

In addition to accessibility, understanding how guest-host interactions can be affected by silane modifications is also critical to sensor development. In this study, we employ the mobility and photostability of rhodamine 6G (R6G) to examine how guest-host interactions are altered by post-synthesis grafting. R6G is a positively charged molecule, which is normally attracted to the negatively charged silica surface at neutral pH. Capping the silica surface with amino and methyl functional group respectively using aminopropyltriethoxysilane (APTS) and methyltriethoxysilane (MTES) has the potential of weakening R6G-silica interactions. In previous single-molecule investigations on regular silica sol-gels, we have successfully demonstrated that both mobility and photostability can be measured simultaneously from single molecules, that enhanced photostability of an encapsulated probe is mostly due to increasing constraint imposed by the mesoporous silica, and that mobility of the encapsulated probe can be enhanced by neutralizing the surface charge of silica with a low pH buffer.[38-41] Since mobility and photostability are very sensitive to the local

environment surrounding a silica encapsulated molecule, they are ideal for monitoring changes in guest-host interaction as a result of post-synthesis grafting. Moreover, single-molecule measurements were used exclusively in this investigation in order to identify subtle changes in guest-host interactions that may otherwise escape ensemble detection due to the averaging effect. The ability to resolve spatial heterogeneity in the nanometer length scale has made single-molecular spectroscopy one of the powerful techniques to examine amorphous materials like mesoporous silica. The applications of single-molecule spectroscopy in studying silica sol-gel materials have been reviewed recently.[42]

3.3 RESULTS AND DISCUSSION

3.3.1 Sol-Gel Pore Surface Modification

3.3.1.1 Initial water treatment

The extent of surface modification was monitored by contact angle measurement. For a hydrophobic surface, a large contact angle will be resulted, whereas a hydrophilic surface should lead to a smaller contact angle.[35] Figure 3.1 (A) shows the effect of water on the contact angle of silica so-gel film spun-cast on glass coverslips. In this experiment, freshly prepared silica sol-gel films were dipped in water for various durations that range from 0 to 26 hr. The contact angles of all films were then measured 24 hr after the water treatment. As illustrated, a 24-hr old silica sol-gel film that had not been treated with water (treatment time = 0) exhibits a fairly hydrophobic surface, producing a contact angle of 45º±2º. The process of dipping a nascent silica sol-gel film in water dramatically reduces the contact angle to well below 10º. Afterward, water

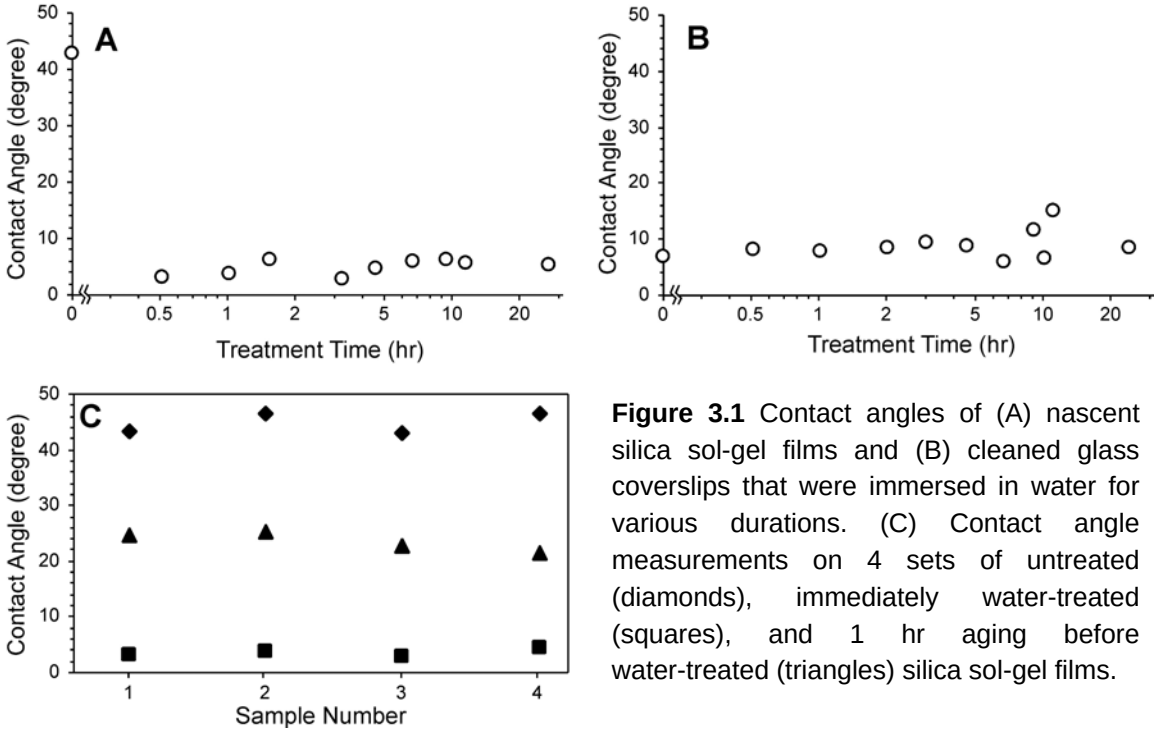

Figure 3.1 Contact angles of (A) nascent silica sol-gel films and (B) cleaned glass coverslips that were immersed in water for various durations. (C) Contact angle measurements on 4 sets of untreated (diamonds), immediately water-treated (squares), and 1 hr aging before water-treated (triangles) silica sol-gel films.

does not seem to have much effect as the contact angle from samples subjecting to longer water treatment only fluctuate mildly around 5º±1º. This suggests that whatever causes the substantial reduction in contact angle initially is most likely completed in 30 minutes, the shortest treatment time employed in this study.

Figure 3.1 (B) indicates that when cleaned glass coverslips (with no silica film) underwent an identical water treatment, the contact angle was found to cluster around 9º±3º. The difference in contact angle between the silica film and coverslip suggests that the dramatic reduction of contact angle in silica film upon water treatment was not caused by peeling off of the silica film and exposing the underlying coverslip surface. Indeed, upon closer inspection, the once clear nascent silica film always turned into an opaque white film after the water treatment. This opaque silica film is most likely due to the rapid coarsening of the film surface when in contact with water, indicating that the silica film surface is still chemically active immediately after spin-coating. It is known

that silica colloids with mean hydrodynamic radius ranging from 1.5 nm to 4.5 nm are produced when sodium silicate is added to an aqueous solution to form silica hydrogel.[13-14,43-44] A similar reaction could be happening to the nascent silica film surface, which contains many reactive nucleation sites for colloidal silica particle to grow, except that the silica particles so produced would stay on the film surface instead of dispersing into the solution, leaving behind an opaque white film. The fact that an apparently rougher surface could lead to a surprisingly smaller contact angle implies that the opaque silica film were made of extremely water rich hydrogel colloids, hence a very small resultant contact angle. It is worth noting that this chemically active stage does not last long, as Figure 3.1 (C) indicates that letting the nascent silica film age under ambient conditions for 1 hr first before dipping in water for 30 minutes would result in a clear silica film with an intermediate contact angle of 24º±2º, suggesting that the film no longer support silica particle growth after 1 hr of aging. Since optical measurements can be easily obscured by strong scattering from the opaque silica film and that chemically active silica film may influence surface modification in an unpredictable fashion, freshly spin-coated silica films for all subsequent studies were immediately set to age in air for 1 hr and then dipped in water for another 30 minutes before they were subjected to different post-synthesis grafting reactions. Hereafter, this initial procedure performed on all nascent silica films will be called pre-treatment, and those samples are called “pretreated” samples. This pre-treatment protocol would consistently prepare silica films with contact angle of 24º±2º before any surface modification.

3.3.1.2 Aminopropyltriethoxysilane (APTS) modified silica film

Figure 3.2 (A) illustrates the effect of APTS surface modification on a chemically active nascent film. The contact angle of the nascent film decreases gradually upon exposing to 0.4% aqueous APTS. The contact angle eventually settled at ~10º after 10 hr of treatment. This resultant contact angle is substantially lower than the 41º±3º observed from a 0.4% APTS modified glass coverslip as illustrated in Figure 3.2 (B). It is apparent that the surface chemistry of the former sample is influenced by the combination effects of water on nascent film and APTS modification as the resultant contact angle appears to sandwich between 5º and 41º, respectively. The production of water-rich silica colloid on a film surface might have significantly lowered the number of surface modification site and thus caused the contact angle of the APTS modified film to drop from 41º to ~10º.

When nascent silica films were subjected to the pre-treatment protocol first, the

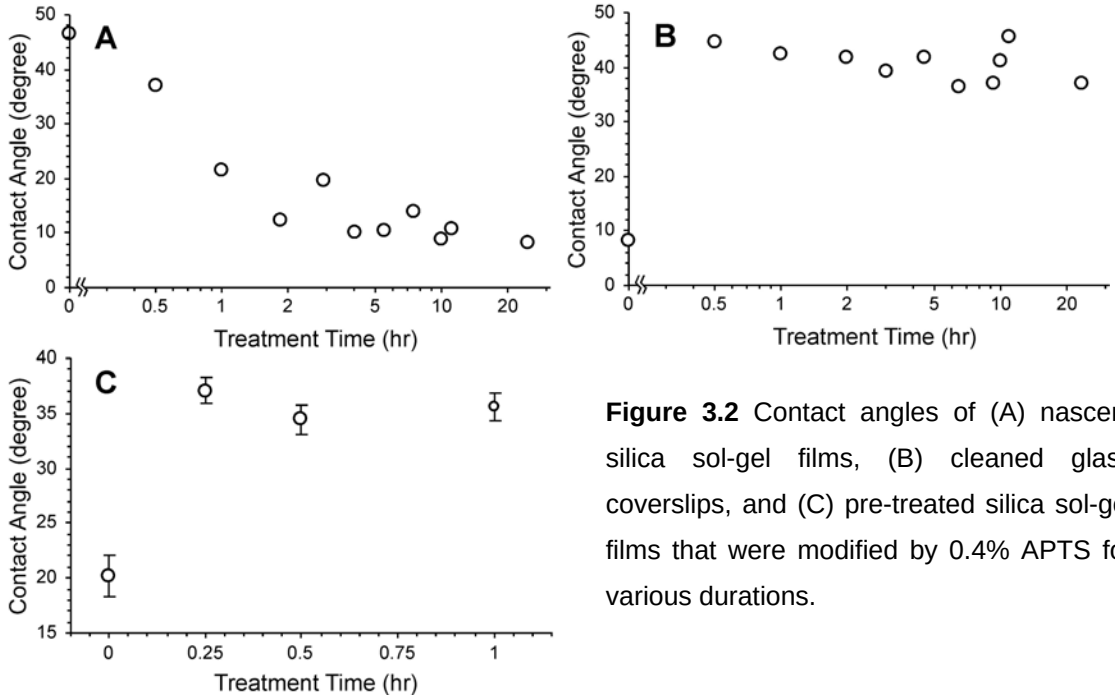

Figure 3.2 Contact angles of (A) nascent silica sol-gel films, (B) cleaned glass coverslips, and (C) pre-treated silica sol-gel films that were modified by 0.4% APTS for various durations.

effect of water on nascent films appeared to be eliminated. The end result is that the effect of APTS became more reproducible as well as more consistent with those observed from glass coverslips. Figure 3.2 (C) shows the contact angles of modified silica films as the reaction time of APTS modification varies. It is obvious from the plot that surface modification is practically completed in as little as 15 minutes. The contact angle increases from 20º±2º to 37º±1º after 1 hr of APTS modification, approaching that of an APTS modified glass coverslip. It is worth noting that despite the hydrophilic amino group, the relatively high contact angle shown in APTS grafted silica sol-gel surface indicates that the hydrophobic propyl group in APTS has a more dominant effect in altering surface chemistry. It is quite possible that the amino-tail of APTS is attracted to the silica film surface either through Coulombic attraction as positively charged ammonium ion or through H-bonding as the neutral amine,[45-47] forcing APTS molecules to lie flat on the film surface and exposing the propyl group to result in a more hydrophobic surface, hence the high contact angle observed. Since there is practically no increase in contact angle between a 0.5-hr and a 1-hr modified sample, all APTS modified samples employed in this work were prepared by dipping the silica film in 0.4% APTS for 0.5 hr after the pre-treatment protocol. 0.4% APTS was chosen since the use of a moderately higher 1.0% APTS would lead to irreproducible, thick, and uneven coating on the silica film (data not shown). The fast reaction kinetics observed here is typical of silane modifying reaction using APTS. It has been suggested by previous reports that this unique characteristic of APTS is likely due to the catalytic effect of the amino group possibly serving to enhance the nucleophilicity of surface

silanols to facilitate the condensation of APTS directly onto the silica film by bypassing the hydrolysis of its ethoxy groups altogether.[48]

The contact angle of our sample is consistently lower than the approximately 60º reported by others, where glass and silicon substrates were modified with higher concentration of anhydrous APTS followed by drying at elevated temperatures.[49-50] The use of anhydrous APTS would eliminate the hydrolysis of APTS and limit all reactions at the solid-liquid interface, which prevents APTS condensation from occurring at high concentration and avoids the formation of uneven surface coating. A higher APTS concentration may ensure a more complete surface modification and thus a higher resultant contact angle. In addition, any residual water inside or on a modified surface would be vaporized after the drying process, leaving the modified surface less hydrophilic, hence a higher contact angle. Regardless of the treatments, most studies register an approximately 20º increase in contact angle upon APTS modification, which is fairly consistent with what have been observed in our samples.[49-51]

3.3.1.3 Methyltriethoxysilane (MTES) modified silica film

MTES of 3% and 10% in chloroform were used to determine the optimal concentration for MTES modification. As illustrated in Figure 3.3, the contact angles of

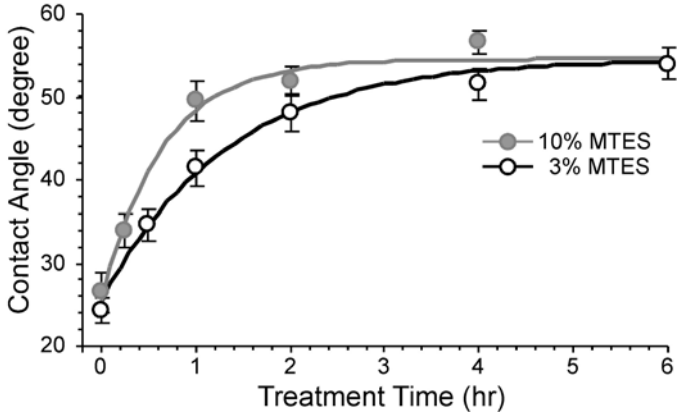

Figure 3.3 Rising of contact angle as a function of MTES modification time. Solid lines are fitting to the data according to Equation 3.1

all silica films seem to settle above 50º regardless of MTES concentration used, which probably signifies the completion of surface modification reaction. However, the rate of surface modification (k) does depend on MTES concentration, with the lower the MTES concentration, the longer it takes for a modification reaction to complete. Assuming a first order rate law, the contact angles (θ) in Figure 3.3 were fit to the following Equation 3.1:

$$\theta = \theta_i + \left(\theta_f - \theta_i\right)\left(1 - e^{-kt}\right) \qquad \textbf{3.1}$$

Where θ_i and θ_f are initial and final contact angles, respectively. According to the fitting, the rate constant for the 3% MTES reaction stands at 0.75º hr^{-1} whereas the 10% MTES reaction displays a faster rate constant at 1.55º hr^{-1}. Thus, the reaction employing 10% MTES exhibits a noticeably faster reaction rate as it takes approximately 1 hr to raise the contact angle toward 50º. In about 2 hours of reaction time, the surface modification reaction appears to almost complete in 10% MTES as the contact angle increases from 26º±2º to 52º±2º. Although the contact angle continues to rise marginally, the data from the 2- and 4-hr samples suggest that there is little gain in stretching the MTES surface modifying reaction beyond 2 hours. Unlike APTS where its amino-tail catalyzes the surface modifying reaction, MTES contains no catalytic functional group and the surface modifying reaction could only proceed normally with a considerably slower reaction rate.

It is also noted that MTES produces a surface with a higher contact angle than that from APTS, consistent with the more hydrophobic nature of MTES relative to APTS, as the amino end group inevitably reduces the overall hydrophobicity of APTS. In addition to hydrophobicity, surface roughness also plays a significant role in determining the

contact angle of a surface, with smoother surface usually leads to smaller contact angles.[52] It is also known that the amino-tail of a surface attached APTS can catalyze its own dissociation from the film surface, especially in the presence of water.[53] This may kinetically favor a process similar to Ostwald ripening where smaller scale surface roughness due to uneven APTS coverage can be removed by APTS dissociation during the course of the surface modification reaction. This would result in a smoother film and hence a smaller contact angle than that from MTES modification where both surface association and dissociation of MTES are not catalyzed. Since the concentration of MTES employed appeared to only influence the reaction time to complete surface modification, all MTES modified samples employed in this work were prepared by dipping the silica film in 10% MTES for 1 hr after the pre-treatment protocol, which corresponds to more than 90% completion of the surface modification reaction. Similar to the case of APTS, the contact angle of our MTES modified film is lower than the approximately 80º reported in the literature for short *n*-alkyl organosilanes modification.[54-55] In this case, it seems that removing water by drying contributes mostly to the discrepancy as the 10% MTES concentration employed in this study is comparable to those in other studies. In fact, when drying at an elevated temperature is not included, our results seems to agree quite well with the literature where an advancing and receding contact angle of 58º and 54º have been reported, respectively.[56]

3.3.1.4 Thermogravimetric analysis (TGA) of APTS and MTES modified silica thin films

Thermogravimetric curves in Figure 3.4 were obtained from pretreated alcogel thin film, MTES-grafted alcogel thin film, APTS-grafted alcogel thin film, and pure APTS

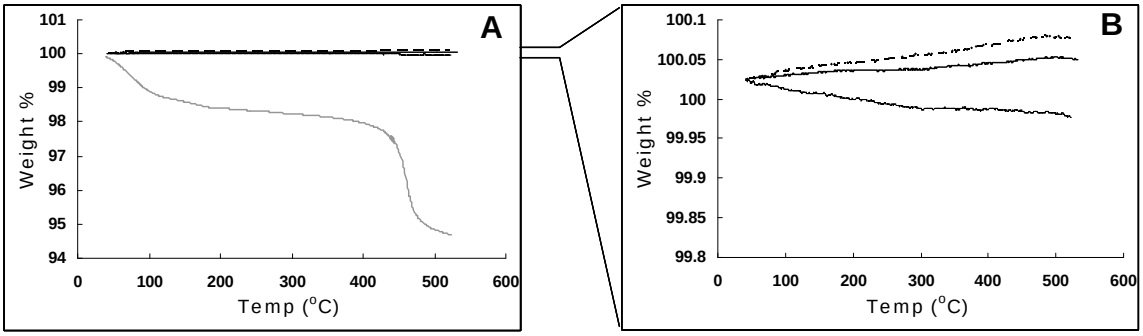

Figure 3.4 (A) From top to the bottom, thermogravimetric curves of MTES-grafted alcogel thin film (black long-dashed line), pretreated alcogel thin film (black solid line), APTS-grafted alcogel thin film (black short-dashed line), and pure APTS coated alcogel thin film (gray solid line). (B) is an expanded view of (A) near 100 weight %.

coated alcogel thin film, respectively. Pure APTS coated alcogel thin film was prepared by adding large amount of pure APTS on the surface of an alcogel thin film sample for 30 min and then let dry overnight. The sample surface turned rough and irregular with a thick layer of APTS. The purpose of this pure APTS coated alcogel thin film was to make sure weight loss of $–CH_2CH_2CH_2NH_2$ groups could be detected within 500 ^oC range by the instrument. As shown in Figure 3.4 (A), pure APTS coated alcogel thin film showed ~ 1% weight loss of adsorbed solvent (which should be the liquid APTS residue) when T < 120 ^oC, and ~ 3% weight loss at 400 ~500 ^oC, which corresponded to the decomposition of $–CH_2CH_2CH_2NH_2$ groups.[57] As a control sample, pretreated alcogel thin film was not expected any weight loss, which was nicely demonstrated in Figure 3.4 (B). Neither MTES-grafted alcogel thin film nor APTS-grafted alcogel thin film showed discernable weight loss, even in the expanded Figure 3.4 (B). The slight upwards or downwards trend of those three samples in Figure 2.7 (B) was indeed due to the fluctuations of the measurement. This suggests that either the concentration of

APTS or MTES on the silica film surface is very low or weight loss by the decomposition of surface attached APTS or MTES was below the detection limit of the instrument. We believe it is the latter case that led to the apparent absence of weight loss implied by the thermogram. To support our argument, we provide an estimate of the weight loss that would have been observed in our TGA measurements.

Based on pervious reports of grafting APTS on surface etched non-porous glass beads with surface area to mass ratio between 4 and 500 $m^2 g^{-1}$, the amount of weight loss from TGA measurements was found to be around 5 ~ 6 %.[58-60] Our silica films were spun-coated on 1" × 1" microscope coverslips that weight ~0.244 g per slide. As a result, the surface area to mass ratio is approximately 1 square inch per 0.244 g, which is equivalent to 2.644×10^{-3} $m^2 g^{-1}$. Assuming the smallest surface area to mass ratio of 4 $m^2 g^{-1}$ from the previous reports, this would still translate to a factor of ~1500 less surface area in our sample for the same amount of material used in a TGA measurement. Using the 6 percent weigh loss from the previous reports, the percentage weight loss in our sample would be around 0.004 %, which is equivalent to 2 μg. This is clearly below the detection limit of our TGA instrument (34 μg) and therefore explains why we were not able to observe any prominent weight loss from TGA experiment.

3.3.2 The Effect of Surface Modification on Rotational Mobility

Contact angle measurement is a surface probing technique that is sensitive to changes occurring at macroscopic length scales. While contact angle can respond to changes in hydrophobicity roughness of a silica film surface, its usefulness in reporting chemical modification below the film surface is questionable. In this part, the rotational mobility of R6G is employed to examine whether silane modification can alter the

internal chemical composition of an alcogel film, which is characterized by mesopores that are known to significantly impair diffusion or even completely block the infusion of molecules that are much bigger than the silica pores. This will cause the internal structure of an alcogel film less accessible to external reactants and potentially render the approach of post-synthesis grafting ineffective.

3.3.2.1 APTS modified film

In Table 3.1, the mobility distributions of R6G in silica film with and without APTS modification are compared. Similar to our previous reports, R6G molecules are separated into three categories of rotational mobility in accordance with their respective emission polarizations.[39] For R6G trapped inside regular sol-gel silica films, approximately 40% were found to be fixed, with a good majority of the remaining molecules (~56%) exhibiting limited mobility. Since physical confinement is the major factor that control mobility inside alcogels where silica pores are usually no more than a few nanometers big, R6G encapsulated inside is expected to display rather restricted mobility.

Sample	Tumbling	Fixed	Intermediate	Number of molecules studied
Dry silica sol-gel	**4.6** ± 1.8 %	**39.7** ± 4.3 %	**55.7** ± 4.3 %	**131**
After immersion in water	**1.2** ± 0.8 %	**62.3** ± 3.7 %	**34.5** ± 3.7 %	**170**
After modified by 0.4% APTS	**6.2** ± 1.7 %	**57.9** ± 3.4 %	**35.9** ± 3.3 %	**209**

Table 3.1 Mobility distribution of R6G before and after APTS modification.

The ~5% tumbling R6G molecules recorded are either trapped inside bigger pores or residing near the film surface and possibly fairly unrestrained. These molecules are relatively free to rotate and therefore emit un-polarized fluorescence. However, these same molecules are possibly most vulnerable to rinsing and thus can be easily washed away upon immersion in water, which can cause a significant shift in R6G mobility. Since R6G-doped silica films are dipped into 0.4% APTS solution during APTS grafting, the effect of rinsing should not be neglected. To account for the rinsing effect and to really determine whether APTS grafting can reach below the film surface, R6G mobility in an APTS modified film should be compared to an identically prepared film that was immersed in water for the same amount of reaction time as the APTS modified film.

As indicated in Table 3.1, the percentage of fixed R6G molecule after rinsing increases dramatically from ~40% to ~62%. This is accompanied by a concomitant decrease in the more mobile tumbling and intermediate molecules as they are more likely to be washed off. In an APTS modified film, however, there is a noticeable increase in the percentage of tumbling molecule at the expense of the fixed molecules while the percentage of intermediate molecule remains unchanged. The approximately 5-fold (1.2% $\rightarrow$ 6.2%) increase in the percentage of tumbling molecule in the APTS treated silica film may be an indication of successful APTS pore surface modification. Since the capping of a pore surface with APTS will effectively reverse the surface charge from negative $Si–O^-$ to positive $Si–O–R–NH_3^+$ at neutral pH. As a result of this charge reversal, positively charged R6G will be more likely to repel from the pore surface instead of being attracted to it, hence a higher rotational mobility. It is also

evident from Table 3.1 that despite the 5-fold increase in tumbling molecules, the mobility of R6G in the silica film is still dominated by fixed molecules (~58%), implying that either there are a lot of pores that are inaccessible to APTS modification or R6G are physically confined in pores that are too small to permit rotation even though APTS has turned the pore surface repulsive to R6G. The facts that APTS is a fairly small molecule and that guest-host interactions are usually dominated by physical confinement in alcogel samples has led us to believe that the latter explanation is most likely responsible for the lack of R6G mobility in an APTS modified silica film. This argument is also supported by the study of R6G photostability in subsequent sections.

3.3.2.2 MTES modified film

Although MTES does not introduce any positive charge to a silica pore surface, it is still capable of capping the negative surface $Si–O^-$ group with a non-polar methyl group and thereby weakening the attraction of R6G toward the surface and enhancing R6G mobility. Thus, it has been reported that the mobility of Nile Red was found to increase with the amount of isobutyltrimethoxysilane used in an ormosil film.[61-62] Similar to the case of APTS modification, Table 3.2 indicates that a significant amount of mobile R6G molecules were washed off upon immersing the silica film in chloroform, the solvent used for MTES modification reaction. Relative to the dry film, the percentage of fixed R6G molecule increased from ~40% to ~65% after treating the film with chloroform. Unlike water, however, a chloroform wash only decreases the percentage of tumbling molecule marginally from 4.6% to 3.6%. Presumably tumbling molecules are fully solvated by water or water/ethanol mixture in a dry silica film and that access to this group of molecule is effectively blocked by the surrounding solvent

shell as chloroform and water are fairly immiscible. On the other hand, intermediate molecules may lack the protection of a complete solvent shell and are more likely to be washed away by chloroform. This may explain why only a dramatic decrease in the percentage of intermediate molecule was observed after the chloroform treatment.

Sample	Tumbling	Fixed	Intermediate	Number of molecules studied
After immersion in $CHCl_3$	**3.6** ± 1.5 %	**64.8** ± 3.7 %	**31.5** ± 3.6 %	**165**
After modified by 10% MTES	**5.6** ± 1.7 %	**55.0** ± 3.7 %	**39.4** ± 3.6 %	**180**
After modified by pure MTES	**8.8** ± 2.0 %	**53.4** ± 3.5 %	**37.8** ± 3.4 %	**204**

Table 3.2 Mobility distribution of R6G before and after MTES modification

Table 3.2 also illustrates that the methyl group in MTES has a moderate effect on R6G mobility. The percentage of tumbling molecule only increases slightly upon MTES modification, although there is a noticeable transfer of fixed molecules to intermediate molecules. Despite a different surface capping group than APTS, MTES produces very similar R6G mobility distributions in a silica film. This suggests that both charge reversal (APTS) and charge neutralization (MTES) are able to alter R6G and silica pore surface interactions to a similar extent. Moreover, when pure instead of 10% MTES was used for surface modification, we found that the mobility of encapsulated R6G molecules can be further enhanced, yielding 8.8% tumbling R6G molecules as opposed to 5.6%. This is very different from APTS modification as concentration as low as 1.0% APTS would lead to irreproducible, thick, and uneven silica film due to APTS condensation. When considering that like-charge repulsion is more effective in inducing motion than non-charge interaction, the higher percentage of tumbling molecule

achievable in MTES suggests that post-synthesis grafting can be driven to higher surface coverage in MTES than in APTS simply because of a much wider workable concentration range.

Although rotational mobility is able to reveal the effect of silane modification on R6G/pore surface interactions, the observed increase in R6G mobility as a result of charge reversal (APTS) and neutralization (MTES) is rather marginal. These subtle shifts in rotational mobility is arguably due to the fact that physical confinement dominates R6G mobility in silica alcogel such that full scale molecular rotation rarely occurs even though R6G is attracted to the silica surface to a lesser extent after silane modifications. This is possibly an inevitable outcome of the post-gelation modification approach as Coulombic attraction between R6G and silica oligomers has been the major guiding force to a tight silica pore structure surrounding all R6G molecules during the gelation process.[63] After gelation, successful silane modification can only alter pore surface chemistry but it is expected to have a negligible effect on the already formed mesoporous silica structure. As physical confinement continues to restrict molecular rotation, hence the very small change in R6G rotational mobility observed after silane modification.

3.3.3 The Effect of Surface Modification on Photostability

Intuitively, photostability should provide a more sensitive probe to R6G/silica interaction than molecular rotation when R6G is under stringent physical confinement. Since photostability strongly depends on the dynamic interaction between a guest molecule and its local surrounding, any subtle change in R6G/silica interaction because of silane modification will be reflected by the change in R6G photostability. In this

work, both APTS and MTES serve to reduce the attraction between R6G and silica pore surface, which will allow more dynamic motions in a less surface-bound R6G molecule. As more dynamic motions usually lead to additional photodegradation pathways, R6G photostability is expected to decrease upon APTS and MTES modification. As long as R6G becomes less surface-bound, this decrease in photostability should apply even to those R6G molecules that are elusive to rotational mobility detection because of their trapping in very tight cavities that preclude full scale molecular rotation.

Table 3.3 lists the survival lifetimes of R6G in silica films before and after silane modification. As illustrated, the survival lifetime of R6G in all samples, as the fraction of R6G that remains fluorescent (*f*) upon continuous excitation, are best fitted by a bi-exponential decay function, Equation 3.2, revealing the spatial heterogeneity of the sol-gel silica films. Evidently, silane modification does not seem to alleviate the spatial heterogeneity inside the modified films.

$$f = A_1 e^{-t/\tau_1} + \left(1 - A_1\right) e^{-t/\tau_2} \qquad \textbf{3.2}$$

Sample	A_1	τ_1 (s)	τ_2 (s)	τ_{avg}(s)	χ^2
Dry	**0.54** ± 0.07	**14.1** ± 1.9	**72.0** ± 8.3	**40.7** ± 6.3	0.150
Water	**0.63** ± 0.03	**19.6** ± 1.4	**112** ± 9	**53.2** ± 5.1	0.061
0.4% APTS	**0.57** ± 0.02	**5.19** ± 0.32	**43.0** ± 2.3	**21.5** ± 1.4	0.148
$CHCl_3$	**0.74** ± 0.04	**18.5** ± 1.2	**108** ± 14	**41.7** ± 5.6	0.143
10% MTES	**0.47** ± 0.02	**7.20** ± 0.66	**73.1** ± 3.6	**41.9** ± 2.5	0.341
Pure MTES	**0.69** ± 0.02	**7.04** ± 0.35	**70.8** ± 5.1	**27.1** ± 2.1	0.168

Table 3.3 Survival lifetime of R6G in various silica alcogel thin films.

The survival lifetime of R6G in a dry, unmodified silica film is fairly close to evenly split between 14 s and 72 s, which lead to a τ_{avg} of 40.7 s. After immersing in

water, there is a noticeable increase in both τ_1 and τ_2 for the remaining molecules. The longer τ values, which signify a higher photostability, is the direct result of a loss in R6G mobility after the more mobile molecules had been washed away. The bigger resultant τ_{avg} value of 53.2 s relative to the 40.7 s of a dry film is consistent with the idea that less mobile molecules exhibit less dynamic motions that cause photodegradation, hence a higher photostability and therefore a longer τ_{avg} in the water treated silica film.

Compared to water, the effect of $CHCl_3$ is less pronounced as τ_{avg} only increases marginally to 41.7 s after a dry film is immersed in chloroform. As pointed out before, $CHCl_3$ is much less effective in removing mobile R6G molecules from the dry film because water and $CHCl_3$ are immiscible. As a result, both rotational mobility and τ_{avg} register only minor changes to lower mobility after the $CHCl_3$ treatment. Despite a small change in τ_{avg}, there are unmistaken signs in the longer τ_1 and τ_2 that the remaining R6G molecules are less prone to photodegradation after the $CHCl_3$ wash, indicating that the remaining R6G molecules are less mobile and more photostable.

Table 3.3 also indicates that R6G becomes much less photostable in an APTS modified silica film as the attraction between R6G and silica surface is effectively eliminated. Relative to the water treated film, the value of τ_{avg} drops dramatically from 53.2 s to 21.5 s, implying that R6G is capable of much more dynamics motions in an APTS modified film, which lead to a lower photostability. This lower photostability is also reflected in τ_1 and τ_2 as both values decrease by ~4-fold and ~3-fold, respectively. Such a big decrease in survival lifetime suggests that charge-charge repulsion is very effective in disrupting R6G/silica attraction. Although the tight silica cavity in alcogel

still disfavors full scale R6G rotation in an APTS modified film, as seen in the rotational mobility measurements, the release of R6G from silica surface attraction to permit more localized dynamic motions upon APTS capping is sufficient to impart a significant drop in R6G photostability.

Similar to the case of rotational mobility, the effect of surface charge neutralization by MTES on R6G photostability is much more subdued than seen in APTS modification. When a silica film is modified by 10% MTES, it causes almost no change to the τ_{avg} value of R6G relative to that from the $CHCl_3$ treated film. This agrees quite well with the rotational mobility study, where R6G mobility only increases marginally upon 10% MTES modification. Although there are more than 2-fold decrease in τ_1 and ~32% decrease in τ_2 to signify a less photostable R6G after MTES modification, the averaged R6G photostability instead remains statistically identical to those from the $CHCl_3$ treated sample as the apparent loss of R6G photostability is more than compensated by the considerable amount of population transfer from less to more photostable R6G. When pure instead of 10% MTES was used, however, there is a more discernable effect of MTES on the photostability of R6G. While τ_1 and τ_2 remain practically the same in both MTES modified films, there is a significant reversal of population transfer from more to less photostable R6G when pure MTES was used, causing a substantial drop in τ_{avg} from 41.9 s to 27.1 s. The constancy in τ_1 and τ_2 suggests that the local environment surrounding R6G inside the modified film did not change very much when higher MTES concentration was used. Rather, the shift in R6G population implies that pure MTES only led to more comprehensive pore surface modification inside the silica film, causing a more noticeable drop in R6G photostability. This is further supported by the

considerable higher contact angle of 65.7º observed in silica films modified by pure MTES relative to the ~55º obtained from the 10% MTES modification protocol. It is worth noting that both τ_1 and τ_2 in the MTES modified film are longer than those in APTS modified film, indicating that R6G is more likely to be more mobile in an APTS than a MTES modified film. This reinforces the notion that charge repulsion is more effective in inducing localized dynamic motions of R6G than charge neutralization. Generally speaking, since charge-charge interaction is expected to be stronger than non-charge interaction, we believe that this observation should not be limited to R6G alone but apply to all kinds of guest molecules encapsulated inside silica films. In retrospect, the bigger effect of pure MTES modification on silica sol-gel encapsulated R6G is not completely surprising as we have demonstrated that the concentration of MTES used in a modification reaction appears to only affect the time it takes to reach a desirable level of surface modification. In addition to being an uncatalyzed reaction, the fact that water and $CHCl_3$ are immiscible seems to also play a part in the much longer time required in MTES modification. Thus pure MTES is going to provide the most comprehensive pore surface modification in the shortest period of time. We also believe that if not for the less polar silica surface to facilitate $CHCl_3$ and MTES diffusion, the reaction time for MTES modification would have been much longer. Nevertheless, MTES modification is not expected to reach very deep into a silica film because of the immiscibility issue. Finally, the ability to cause a significant decrease in τ_{avg} in APTS and MTES modified films whereas the same modification only result in a small change in R6G mobility distribution has confirmed that photostability is a more sensitive probe

for guest-host interactions than molecular rotation when a guest molecule is tightly constrained inside a cavity that disfavors full scale molecular rotation.

3.4 CONCLUSIONS

Post-synthesis grafting protocols to modify sol-gel pore surfaces using APTS and MTES have been developed, which is potentially applicable to tailor local environments to manipulate guest-host interactions. It is discovered that nascent silica film prepared by the spin coating method contains many active sites and is unsuitable for post-synthesis grafting. Thus, an hour-long aging followed by a 30-minute water treatment is necessary to prepare the silica film for pore surface modification. Contact angle measurement alone is capable of monitoring chemical modifications on a film surface, but it does not provide any clue on the extent of modification underneath. Due to the limited sensitivity of TGA technique, it can't detect the weight loss of APTS and MTES modified silica thin films because of the low surface area to mass ratio of our samples. Using R6G as a fluorescence probe, we measured the change in rotational mobility and photostability from single molecules to monitor post-synthesis grafting beneath the film surface. The inclusion of repeated rinsing after the grafting reaction helps remove all surface-bound R6G and ensure that emission is mostly originated from R6G trapped inside the silica films. It was found that R6G experiences a 5-fold increase in the percentage of tumbling molecule in APTS modified samples as a result of charge reversal, but only a slight increase in the percentage of tumbling molecule when modified by MTES. R6G photostability decreased upon both APTS and MTES modifications, which suggested that pore surface grafting induces more R6G dynamic

motions that lead to faster photodegradation. In both cases, only a very small change in R6G rotational mobility was observed after silane modification, and fixed molecule was still the dominate category, which emphasized that physical confinement is still the major factor that control guest-host interaction in modified alcogel films. Nevertheless, we have demonstrated that photostability measurement is a more sensitive technique to probe guest-host interactions when full scale molecular rotation is disfavored. The substantial changes in R6G photostability caused by surface grafting also convinced us that the grafting reaction can be controlled to reach deep underneath the film surface. In the case of MTES grafting, the further decrease in R6G photostability upon using pure MTES is entirely the result of population shift toward less photostable R6G, which can be attributed to the result of more extensive surface grafting. The practically constant R6G survival lifetime for the dual population of R6G regardless of MTES concentration is also consistent with the notion that organosilane reagents only alter the chemical composition of silica pore surface. They have very little influence on the already formed pore structure, which should have a more direct impact on the survival lifetime of an encapsulated guest molecule.

Most of the results in this chapter have been published in 2009 on Journal of Physical Chemistry C. (Lei, Q.; Yip, W. T., *J. Phys. Chem. C* **2009**, *113 (50)*, 21130-21138.)

3.5 CHAPTER 3 REFERENCES

(1) Innocenzi, P.; Lebeau, B. *J. Mater. Chem.* **2005**, *15*, 3821.

(2) Lopez, D. A.; Rosero-Navarro, N. C.; Ballarre, J.; Duran, A.; Aparicio, M.; Cere, S. *Surf. Coat. Technol.* **2008**, *202*, 2194.

(3) Chou, T. P.; Chandrasekaran, C.; Limmer, S. J.; Seraji, S.; Wu, Y.; Forbess, M. J.; Nguyen, C.; Cao, G. Z. *J. Non-Cryst. Solids* **2001**, *290*, 153.

(4) Holthoff, E. L.; Bright, F. V. *Accounts Chem. Res.* **2007**, *40*, 756.

(5) Chaudhury, N. K.; Gupta, R.; Gulia, S. *Def. Sci. J.* **2007**, *57*, 241.

(6) Carrington, N. A.; Xue, Z. L. *Accounts Chem. Res.* **2007**, *40*, 343.

(7) Jeronimo, P. C. A.; Araujo, A. N.; Montenegro, M. *Talanta* **2007**, *72*, 13.

(8) Melde, B. J.; Johnson, B. J.; Charles, P. T. *Sensors* **2008**, *8*, 5202.

(9) Lukowiak, A.; Strek, W. *J. Sol-Gel Sci. Technol.* **2009**, *50*, 201.

(10) Forest, L.; Gibiat, V.; Woignier, T. *J. Sol-Gel Sci. Technol.* **1998**, *13*, 329.

(11) Balkose, D. *J. Chem. Technol. Biotechnol.* **1990**, *49*, 165.

(12) Brinker, C. J.; Scherer, G. *Sol-Gel Science, The Physics and Chemistry of Sol-Gel Processing*; Academic Press: San Diego, 1989.

(13) Geddes, C. D.; Birch, D. J. S. *J. Non-Cryst. Solids* **2000**, *270*, 191.

(14) Birch, D. J. S.; Geddes, C. D. *Chem. Phys. Lett.* **2000**, *320*, 229.

(15) Schmidt, H. *J. Sol-Gel Sci. Technol.* **1994**, *1*, 217.

(16) Sanchez, C.; Ribot, F. *New J. Chem.* **1994**, *18*, 1007.

(17) Schubert, U.; Husing, N.; Lorenz, A. *Chem. Mat.* **1995**, *7*, 2010.

(18) Wen, J. Y.; Wilkes, G. L. *Chem. Mat.* **1996**, *8*, 1667.

(19) Collinson, M. M. *Trac-Trends Anal. Chem.* **2002**, *21*, 30.

(20) Sanchez, C.; Julian, B.; Belleville, P.; Popall, M. *J. Mater. Chem.* **2005**, *15*, 3559.

(21) Palmisano, G.; Le Bourhis, E.; Ciriminna, R.; Tranchida, D.; Pagliaro, M. *Langmuir* **2006**, *22*, 11158.

(22) Pagliaro, M.; Ciriminna, R.; Man, M. W. C.; Campestrini, S. *J. Phys. Chem. B* **2006**, *110*, 1976.

(23) Maschmeyer, T.; Rey, F.; Sankar, G.; Thomas, J. M. *Nature* **1995**, *378*, 159.

(24) Brunel, D.; Cauvel, A.; Di Renzo, F.; Fajula, F.; Fubini, B.; Onida, B.; Garrone, E. *New J. Chem.* **2000**, *24*, 807.

(25) Brunel, D.; Lentz, P.; Sutra, P.; Deroide, B.; Fajula, F.; Nagy, J. B. In *Porous Materials in Environmentally Friendly Processes*; Kiricsi, I., PalBorbely, G., Nagy, J. B., Karge, H. G., Eds.; Elsevier Science Publ B V: Amsterdam, 1999; Vol. 125, p 237.

(26) Brunel, D. *Microporous Mesoporous Mat.* **1999**, *27*, 329.

(27) Brunel, D.; Cauvel, A.; Fajula, F.; DiRenzo, F. In *Zeolites: a Refined Tool for Designing Catalytic Sites*; Bonneviot, L., Kaliaguine, S., Eds.; Elsevier Science Publ B V: Amsterdam, 1995; Vol. 97, p 173.

(28) Dash, S.; Mishra, S.; Patel, S.; Mishra, B. K. *Adv. Colloid Interface Sci.* **2008**, *140*, 77.

(29) Tripathi, V. S.; Kandimalla, V. B.; Ju, H. X. *Sens. Actuator B-Chem.* **2006**, *114*, 1071.

(30) Nicole, L.; Boissiere, C.; Grosso, D.; Quach, A.; Sanchez, C. *J. Mater. Chem.* **2005**, *15*, 3598.

(31) Calvo, A.; Joselevich, M.; Soler-Illia, G.; Williams, F. J. *Microporous Mesoporous Mat.* **2009**, *121*, 67.

(32) Domansky, K.; Liu, J.; Wang, L. Q.; Engelhard, M. H.; Baskaran, S. *J. Mater. Res.* **2001**, *16*, 2810.

(33) Yantasee, W.; Lin, Y. H.; Li, X. H.; Fryxell, G. E.; Zemanian, T. S.; Viswanathan, V. V. *Analyst* **2003**, *128*, 899.

(34) Gu, J. L.; Shi, J. L.; Hua, Z.; Xiong, L. M.; Zhang, L. X.; Li, L. *Chem. Lett.* **2005**, *34*, 114.

(35) Rao, A. V.; Latthe, S. S.; Nadargi, D. Y.; Hirashima, H.; Ganesan, V. *J. Colloid Interface Sci.* **2009**, *332*, 484.

(36) Liu, N. G.; Assink, R. A.; Smarsly, B.; Brinker, C. J. *Chem. Commun.* **2003**, 1146.

(37) Lim, M. H.; Stein, A. *Chem. Mat.* **1999**, *11*, 3285.

(38) Viteri, C. R.; Gilliland, J. W.; Yip, W. T. *Journal of the American Chemical Society* **2003**, *125*, 1980.

(39) Gilliland, J. W.; Yokoyama, K.; Yip, W. T. *Chem. Mat.* **2004**, *16*, 3949

(40) Gilliland, J. W.; Yokoyama, K.; Yip, W. T. *Chem. Mat.* **2005**, *17*, 6702.

(41) Gilliland, J. W.; Yokoyama, K.; Yip, W. T. *J. Phys. Chem. B* **2005**, *109*, 4816.

(42) Ye, F. M.; Collinson, M. M.; Higgins, D. A. *Phys. Chem. Chem. Phys.* **2009**, *11*, 66.

(43) Birch, D. J. S.; Geddes, C. D. *Phys. Rev. E* **2000**, *62*, 2977.

(44) Geddes, C. D.; Karolin, J.; Birch, D. J. S. *J. Phys. Chem. B* **2002**, *106*, 3835.

(45) Golub, A. A.; Zubenko, A. I.; Zhmud, B. V. *J. Colloid Interface Sci.* **1996**, *179*, 482.

(46) Rochester, C. H.; Yong, G. H. *Journal of the Chemical Society-Faraday Transactions I* **1980**, *76*, 1158.

(47) Fripiat, J. J.; Vanderme, C.; Touillau.R; Jelli, A. *J. Phys. Chem.* **1970**, *74*, 382.

(48) Blitz, J. P.; Murthy, R. S. S.; Leyden, D. E. *J. Colloid Interface Sci.* **1988**, *126*, 387.

(49) Qin, M.; Hou, S.; Wang, L. K.; Feng, X. Z.; Wang, R.; Yang, Y. B.; Wang, C.; Yu, L.; Shao, B.; Qiao, M. Q. *Colloid Surf. B-Biointerfaces* **2007**, *60*, 243.

(50) AJ, N.; JY, C.; ML, W.; CM, S. *Applied Materials & Interfaces* **2009**, *1*, 373.

(51) Cui, N. Y.; Liu, C. Z.; Brown, N. M. D.; Meenan, B. J. *Appl. Surf. Sci.* **2007**, *253*, 6932.

(52) Marmur, A. *Soft Matter* **2006**, *2*, 12.

(53) Etienne, M.; Walcarius, A. *Talanta* **2003**, *59*, 1173.

(54) Park, J. M.; Kim, J. H. *J. Colloid Interface Sci.* **1994**, *168*, 103.

(55) Lavin, P.; McDonagh, C. M.; Maccraith, B. D. *J. Sol-Gel Sci. Technol.* **1998**, *13*, 641.

(56) Wang, Z. H.; Jin, G. *Colloid Surf. B-Biointerfaces* **2004**, *34*, 173.

(57) Liu, N.; Assink, R. A.; Smarsly, B.; Brinker, C. J. *Chemical Communications* **2003**, *10*, 1146.

(58) Lin, J.; Siddiqui, J. A.; Ottenbrite, R. M. *Poly. Adv. Technol.* **2001**, *12*, 285.

(59) Zengin, H.; Hu, B.; Siddiqui, J. A.; Ottenbrite, R. M. *Poly. Adv. Technol.* **2006**, *17*, 372.

(60) Zengin, H.; Siddiqui, J. A.; Ottenbrite, R. M. *Poly. Adv. Technol.* **2008**, *19*, 105.

(61) Bardo, A. M.; Collinson, M. M.; Higgins, D. A. *Chem. Mat.* **2001**, *13*, 2713.

(62) Martin-Brown, S. A.; Fu, Y.; Saroja, G.; Collinson, M. M.; Higgins, D. A. *Anal. Chem.* **2005**, *77*, 486.

(63) Zhou, Y. Y.; Yip, W. T. *J. Phys. Chem. B* **2009**, *113*, 5720.

CHAPTER 4 USING DYE AS PROBES TO MONITOR THE SURFACE MODIFICATION INSIDE SILICA HYDROGEL

4.1 ABSTRACT

Rhodamine 6G (R6G) and fluorescein (Fl) molecules were used as probes to monitor the surface modification inside silica hydrogel. The modification process can be easily tracked by locating R6G dye band, or be precisely monitored by measuring anisotropy values of doped dyes. Due to the larger pore sizes, pore surface modification inside hydrogel was more effective than in alcogel. Surface modifications by post-grafting of 3-Aminopropyltrimethoxysilane (APTS) and methyltriethoxysilane (MTES) showed significant effect on guest molecule mobility, whereas surface modifications by physical method, that is by using 1.0 M sodium chloride to increase ionic strength or by adding pH 2.0 hydrochloric acid to neutralize pore surfaces, barely showed any effect. Charge-reversal by APTS is a more effective way to modify pore surfaces than hydrophobic capping from MTES, simply because Columbic interactions dominate inside hydrogel. Multiple-step section measurements revealed more than bulk measurements did, and demonstrated that pore surface modification showed a combined effect from the pore fluid and post-grafted functional groups. The ease of tracking surface modification inside hydrogel by locating R6G dye band, and the negligible pore fluid effect on R6G in modified hydrogel makes R6G a better probe than Fl to monitor the pore surface modification process in silica hydrogel monoliths.

4.2 INTRODUCTION

Even since the pioneer work of H. Schmidt in 1985 on the preparation and investigation of inorganic-organic hydrid silica gel (ormosils),[1] and the first report about an organic dye doped silica gel (composites) by Avnir et al.,[2] sol-gel research has experienced an explosion of development. They also marked the second important period of sol-gel process.[3-4] When Braun et al. successfully trapped enzymes into TEOS-derived sol-gel matrix with remained bioactivities in 1990,[5] intense interest has been focused the development of biocomposites associated with organically modified silica matrix.[6-7] There are two different approaches to synthesize organically modified silica gel: one-pot co-condensation and stepwise post-grafting.[8-10] Tailoring the surface of silica matrix with organic groups improves its biocompatibility,[6-7,11] and replaces the brittleness with rubber elasticity; however, the mechanical strength is compromised if one-pot approach was used,[12] whereas post-grafting can introduce almost any functionality without changing the framework and distorting porosity.[13] In addition, post-grafting provides better defined silica structure, better hydrothermal stability, and more accessible functional groups than one-pot method does even with the same organosilane modifying reagent.[8,10] Among all silica gels, hydrogel attracted attentions because it contains more than 50% of water, which generates large pore sizes and makes itself highly biocompatible. Up to date, most biocomposites studies were based on one-pot synthesized silica gel, such as polymer hybrid hydrogel, a lot of stabilizing additive mixed gel, and ormosils, [6-7] instead of post-synthesis grafted silica hydrogel.

No one has ever reported post-synthesis grafting on highly hydrated silica hydrogel monolith. To well tailor the mesoporous structure of silica hydrogel to be adapted to

trapped molecules, investigations on surface modification effect to encapsulated molecules become important. Our previous research on post-synthesis grafted alcogel thin film samples has demonstrated that:[14] (1) Sol-gel pore surfaces can be successfully modified after sol-gel network is formed. (2) By introducing positively-charged groups, such as amino groups, to sol-gel pore surface, positively charged R6G molecules become more freely tumbling because charge-reversal on the pore surfaces. (3) By introducing hydrophobic groups, such as methyl groups, to sol-gel pore surface, the interactions between negatively charged sol-gel network and positively charged R6G molecules are weakened and partially replaced by van der Waals' forces, which leads to more free R6G molecules. But due to the dense structure of alcogel thin films, even though pore surfaces have been modified, R6G molecules were still strictly confined inside those pores, and only a subtle change in R6G mobility was observed after silane modifications. Compared to alcogel thin film samples, hydrogel samples exhibit larger pore sizes and should provide the possibility of higher efficiency for pore surface modification after gelation; the dominating electrostatic interactions inside hydrogel system should lead to a much more sensitive response to pore surface modification. In this study, 3-aminopropyltrimethoxysilane (APTS) and methyl triethoxysilane (MTES) have been used to introduce new functional groups to the pore surfaces by chemical bonding, pH 2.0 HCl has been used to minimize the electrostatic interaction between dyes molecules and pore surfaces, and 1.0 M NaCl solution has been used to increase ionic strength and weaken electrostatic interactions. A protocol was developed to modify hydrogel pore surfaces by post-grafting, and R6G and Fl were used as probes to

track the modification process by locating dye band and by fluorescence anisotropy measurements.

4.3 RESULTS AND DISCUSSION

4.3.1 Development of the Experimental Protocol

A lot of efforts have been made to develop the protocol, such as to determine whether trapping dyes into hydrogel before surface modification or modifying the pore surfaces before dye infusion, to determine the suitable sample size for the measurements, the duration of pore surface modification, and the duration of dye infusion. In this research, R6G and Fl solutions were used as reference samples, and had been measured whenever taking the anisotropy measurements of hydrogel samples.

4.3.1.1 APTS modification

Since 0.4% APTS was aqueous solution, silica hydrogel samples modified by pure distilled-deionized water were prepared as the corresponding control samples. Table 4.1 compares the anisotropy values of R6G and Fl in aqueous solutions and in silica hydrogel prepared by two different procedures described in Chapter 2.3.5 and 2.3.6. In aqueous solution, R6G and Fl are freely mobile molecules, as expected, they both showed very small *r* values close to 0.01. But after they have been encapsulated into silica hydrogel, they behave dramatically different. These phenomena have been reported and explained by many groups. [15-17]

R6G showed a significant loss of mobility in hydrogel, registering a big r between 0.24 and 0.27 when prepared by both “grafting-first” and “trapping-first” methods. Even though in both cases, R6G molecules were quite immobilized, there’s a major

difference between them. When encapsulated by "trapping first" method, R6G molecules were trapped during gel formation and were embedded deep inside, resulting in physical confinement dominating; if encapsulated by "grafting-first" method, R6G molecules infused into gel matrix after gel network had formed, and they had relatively more freedom to choose where to stay, with larger-size pores more preferable. In this case, Columbic interactions dominated. Due to the strong Columbic attractions between positively-charged R6G and negatively-charged pore surfaces, most R6G molecules were still immobilized. While larger pores restricted R6G molecules less than those in smaller pores by "trapping first" method, leading to the slight drop of anisotropy value of R6G from 0.264 in "trapping-first" method to 0.243 in "grafting-first". On the contrary, there's no detectable difference between anisotropy values of Fl when encapsulated by either method, with r less than 0.02 in both cases, due to the remarkably strong Columbic repulsions between negatively-charged Fl and pore surfaces.

	Solution	**Hydrogel**			
		Trapping-first		**Grafting-first**	
		H_2O	**APTS**	**H_2O**	**APTS**
R6G	**0.013** ±0.007	**0.264** ±0.003	**0.267** ±0.004	**0.243** ±0.003	**0.122** ±0.009
Fl	**0.011** ±0.005	**0.019** ±0.006	**0.018** ±0.006	**0.015** ±0.003	**0.076** ±0.015

Table 4.1 Comparison of anisotropy values of R6G and Fl (based on 1000 μL-size. samples)

To study the effect of APTS modification to trapped molecules, hydrogel samples encapsulated with R6G or Fl molecules by both methods were examined. In "trapping-first" method, dye molecules were doped inside hydrogel before surface modification by 0.4% APTS. For R6G and Fl, neither APTS modified sample showed any change of anisotropy value compared to unmodified samples: R6G samples stayed

~ 0.26, and Fl kept ~0.02. This indicates that either the surface modification reaction didn't happen or the modified surface with amino groups couldn't affect the motion of pre-trapped molecules. The first assumption can't be true, since APTS modified silica materials by post-grafting have been intensively studied by many groups, including the mechanism of the reaction and the surface properties after grafting.[14,18-23] With the presence of water, it's a fast self-catalyzed reaction. However, the objects they studied were porous silica powder, glass slides, silicon wafers or silica alcogel thin films, and the organosilane modification reaction can easily happen on the surfaces or very thin films. No one has ever reported an APTS post-grafting on pores inside thick silica hydrogel monoliths. The modification inside hydrogel monolith could be hindered by the slow top-to-bottom diffusion of APTS, and the grafting didn't go deep enough to affect the overall anisotropy value of the sample. Even in the top part of hydrogel that APTS molecules had reached, there were two situations which would result in no observation of surface modification effect: (1) APTS was able to access the pores and amino groups were introduced to pore surfaces, however, R6G molecules were strictly confined inside the pores beforehand, they can't move around even though there's strong Columbic repulsions between positively-charged R6G and positively-charged amino groups; (2) APTS couldn't access some of the pores which had R6G molecules trapped inside. Overall, if samples were prepared by "trapping-first", slow diffusion, physical confinement, and pore accessibility all possibly concealed the effect of pore surface modification on guest molecules, which made "trapping-first" method unsuitable for dye encapsulation.

Whereas, in "grating-first" method, dye molecules infused into gel after surface modification completed. Dramatic change of anisotropy values of both R6G and Fl samples were observed. There's a 50% drop of *r* value from 0.243 to 0.122 for positively-charged R6G, and there's a 5-fold increase of *r* from 0.015 to 0.076 for negatively-charged Fl. Since pore surfaces were modified before dye molecules were trapped, those dye molecules can access and then stay inside those modified pores, unlike the first method APTS cannot access some of those pores trapped with dyes. Introduction of positively-charged amino groups to originally negatively-charged pore surfaces turned R6G molecules more mobile, and slowed Fl molecules down. When investigating samples prepared by this method, only charge-charge interactions dominated and the effect of pore surface modification was clearly demonstrated. Because "grafting-first" method provided us the evidence of successful surface modification and helped tracking the modification process, hereafter, all samples were prepared by "grafting-first" method.

Figure 4.1 APTS modified hydrogel infused with R6G by "grafting-first" method. Short solid line indicates the top boundary of the gel sample, and the dashed line marks the bottom of R6G dye band, which represents the boundary of unmodified region. Rectangle points out the observation area.

As shown in Figure 4.1, R6G encapsulated in APTS modified hydrogel can be used as an indicator to track the modification process. The yellow band, where most R6G molecules accumulate, provided us the information about how far R6G molecules could diffuse to, or precisely, how deep the APTS modification can go. The bottom of dye band, showed as dash line in Figure 4.1, marked the interface of modified and unmodified regions. Without the charge-reversal from APTS modification, R6G molecules would be strongly attracted by negatively-charged pore surfaces and get stuck at the very top of gel sample; as the modification went deeper with time, the dye band moved deeper. R6G dye band provided us an easy way to track the modification process inside silica hydrogel. Dye band was also used to help optimizing experiment protocol. As the study object, the modified region should fit in the observation window, and the dye band should pass beyond the window. APTS modification before dye infusion were tested with different times from 24hr to 72hr, and it was found that 24hr-modification was not long enough to exclude dye band out of observation window, while 48hr and 72hr modifications marginally did. For another 24hr, the dye band of 72hr-modified sample was wider and only a little bit deeper. The gain was not impressive, so 48hr-modification was chosen as the standard process for sample preparation. Regarding the sample size, it takes longer for modification reagents and dye molecules to diffuse down if larger volume gel sample size was used, finally, 750 μL was determined to be a proper sample size, as it only took one-day dye diffusion to fit the observation window.

4.3.1.2 MTES modification

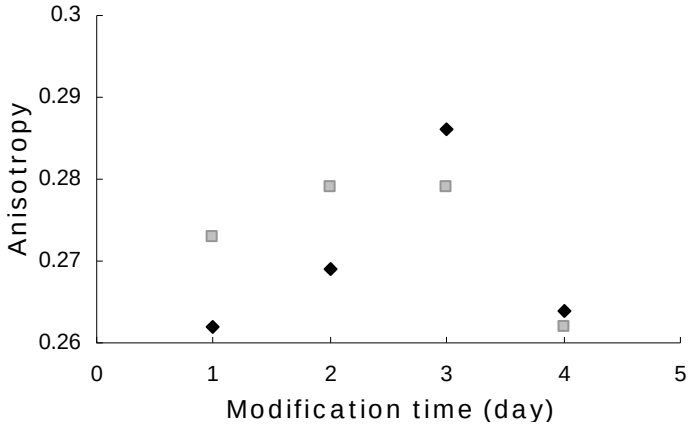

Figure 4.2 Anisotropy value change of R6G in $CHCl_3$ modified hydrogel (diamonds) and 10% MTES/$CHCl_3$ modified hydrogel (squares) with modification time.

At the beginning, 10% of MTES in chloroform was used to modify hydrogel pore surfaces. Various MTES modification times from 1-day to 4-day have been tested, and R6G solution was allowed to diffuse one day before the measurements were taken. Since MTES was dissolved in chloroform, chloroform modified hydrogel was used as a control sample for MTES modification. As shown in Figure 4.2, the anisotropy values of R6G were practically unchanged before and after MTES modification. Even after being modified for as long as four days, samples didn't show a certain upward or downward trend in anisotropy values. The average *r* of all chloroform control samples was 0.270±0.011, and the average *r* of all MTES/$CHCl_3$ samples was 0.273±0.008. The small difference between those values falls in the error range of the technique. We believe that MTES in $CHCl_3$ mixture didn't modify pore surfaces in hydrogel.

What caught our attention was the immiscibility of chloroform with water, as observed, a thin layer of dye stuck to the glass tube surface instead of penetrating into hydrogel samples. Hydrogel contains more than 90% of water, which makes it hard for MTES/chloroform mixture to diffuse into the gel. The modification reaction possibly could only happen on the surface of the gel. Whereas the modification of alcogel thin

films by 10% MTES/$CHCl_3$ were successful,[14] one reason is that alcogel thin films are dry samples, MTES in chloroform can easily get into pores by natural diffusion, and another reason could be those samples are very thin (~200 nm). For those ~ 2 cm-thick hydrogel monolith samples filled with water, the solvent for MTES must be miscible with water to help MTES diffusing into the gel and then modifying the pore surfaces. Ethanol with a concentration (vol %) from 38% to 95% were tested, MTES cannot dissolve well in ethanol when its concentration was less than 38%. To make sure the concentration of ethanol wouldn't become an issue to cause the change of anisotropy values, a series of control hydrogel samples modified by different concentrated ethanol from 38% to 95% were prepared and compared. As shown in Figure 4.3, the concentration of ethanol did affect the motion of R6G molecules, the higher the concentration of ethanol, the faster R6G molecules move. In this graph, data of 0% ethanol, which is pure distilled-deionized water, were also included. The anisotropy value reached to a plateau as the ethanol concentration dropped. The anisotropy values dropped about 25% from the plateau ~0.21 to the minimum ~0.16. As reported by P. J. Davis, G. W. Scherer *et al*.,[24-26] pore structure can be affected by the pore fluid during aging, and larger pore volumes were observed for gels aged in ethanol compared to those dried in water. R6G in larger pores of ethanol modified samples would be less restricted than those in water modified samples. At the same time, R6G has a better solubility in ethanol than in water, which also helps to improve the mobility of R6G molecules thus decreasing anisotropy values. Both factors are contributing to the anisotropy value drop of R6G with increased ethanol concentration. When comparing the anisotropy values of R6G in 38% ethanol modified hydrogel samples and

distilled-deionized water modified samples, they were 0.202±0.008 and 0.212±0.012, respectively, and they both fell into the plateau region. The difference of those two samples was small enough to be neglected, so it won't become an issue if we try to compare samples modified by organosilane reagents dissolved in these two solvents. Thereafter, 38% ethanol was used as the solvent for MTES modification.

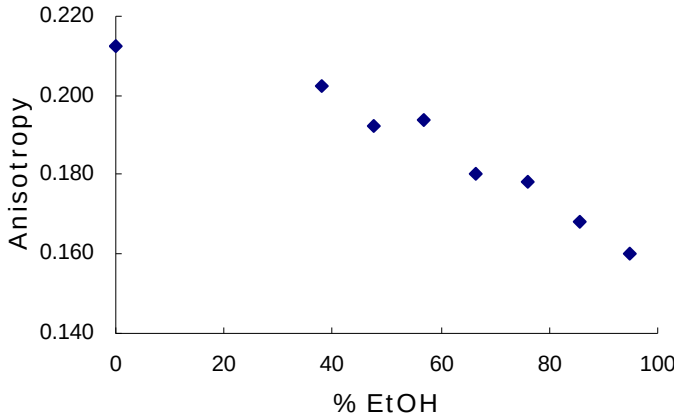

Figure 4.3 Anisotropy values of R6G encapsulated into hydrogel modified by variously concentrated ethanol.

4.3.2 R6G Study

4.3.2.1 Bulk measurements

Basically, the four I_{HH}, I_{HV}, I_{VV} and I_{VH} spectra were collected by sampling what fits in the observation window of that hydrogel sample, and the anisotropy value calculated was an average. It is known that at neutral pH, silica sol-gel network is negatively charged, R6G molecule is positively charged, and the strong Columbic attractions dominate in this hydrogel system. To study the effects of surface modification on the electrostatic interactions between R6G molecules and the gel, four different reagents were used to attempt to weaken the Columbic attractions. APTS was used to introduce positively-charged amino groups to the pore surfaces, MTES was used to introduced nonpolar methyl groups to capping the negative surfaces, pH 2.0 hydrochloric acid was used to neutralize the negatively-charged pore surfaces, and 1.0

M sodium chloride was used to increase ionic strength to weaken Columbic interactions and hydrogen bonding between R6G molecules and the pores. In Table 4.2, the anisotropy values of R6G in hydrogel modified by different reagents are compared. Since 1.0 M sodium chloride solution, pH 2.0 hydrochloric acid and 0.4% APTS are aqueous solution, and MTES is dissolved in 38% ethanol, hydrogel samples modified by pure distilled-deionized water and 38% ethanol were prepared as control samples.

	H_2O	1.0 M NaCl	pH 2.0 HCl	0.4% APTS	38% EtOH	10% MTES
r	**0.210** ±0.012	**0.226** ±0.006	**0.218** ±0.003	**0.070** ±0.007	**0.202** ±0.008	**0.163** ±0.002

Table 4.2 Comparison of anisotropy values of R6G after different modifications.

As shown in Table 4.2, the anisotropy value of R6G in hydrogel with or without the existence of 1.0 M NaCl barely changed. It has been reported by several groups[27-29] that ionic strength affected not only the adsorption rate of R6G on negatively charged silica surface, but also the amount of adsorbate. The presence of electrolytes e.g. NaCl caused the decrease of R6G adsorption on silica substrate due to the change of the structure of electric double layer near the surface. Because of the much smaller size, Na^+ is sterically more competitive than positively charged R6G to occupy the site of compact layer, and then reduce the amount of R6G absorbed, leaving more R6G freely moving in pore solution. The anisotropy value would be expected to decrease. However, those studies were all based on a simple one layer water/silica interface model, and focused on a few molecules on the silica surface. For the highly porous hydrogel monolith we studied, there are numerous pores inside, and when bulk measurements were performed, the anisotropy value should reflect the average motion of R6G

molecules, not just those absorbed on the pore surfaces but all of them in the pore solution. As a result, addition of 1.0 M NaCl didn't change the anisotropy value of R6G in hydrogel based on bulk measurement.

pH 2.0 HCl solution was used to equilibrated with pH 7 hydrogel for two days, and the purpose was to neutralized negative $Si\text{-}O^-$ on pore surfaces by protons and disrupt the attraction between R6G and hydrogel, but no effect was observed. We know that it's very difficult to change the pH value of this type of hydrogel because of the slow diffusion process and the buffer capacity of the gel itself. After being equilibrated by pH 2.0 HCl for two days, the pH value of hydrogel could still be around 7, and we know that the isoelectric point of HCl catalyzed silica is 2.0±0.2,[29-30] therefore, the hydrogel pore surfaces were still negatively-charged even after two-day equilibrium with pH 2.0 HCl. In addition, Zheng et al. reported that the number of adsorbed R6G molecules on silica surface is independent of bulk acidity, [31] which suggests that even there's a slight pH drop of pH 2.0 HCl sample, it would not affect the amount of R6G adsorbed on pore surfaces, so no change on the population of adsorbed and freely moving molecules in the gel matrix. Hence, no change of R6G anisotropy values would be expected, which matched up with our observation from pH 2.0 HCl modified hydrogel sample. The anisotropy values of R6G in H_2O modified and pH 2.0 HCl modified hydrogel samples were 0.210 and 0.218 respectively, and the small difference was probably due to fluctuation of anisotropy measurements.

For R6G encapsulated inside 0.4% APTS modified hydrogel, the anisotropy dropped ~67% to a value of 0.07 relative to 0.21 obtained from the water modified control sample. This is a dramatic improvement of mobility from mostly immobilized to

mostly mobile, unlike those R6G molecules in APTS modified alcogel thin film samples, in which the majority ~58% of trapped R6G remained fixed as compared to ~62% fixed in water immersed alcogel samples, and only 5% more tumbling molecules were observed after modification.[14] This big difference of molecular behaviors after APTS modification confirmed our hypothesis that larger pore size of hydrogel provides a higher efficiency for pore surface modification than inside alcogel. As the pore sizes are larger, the steric hindrance becomes less when APTS diffuses into the pores, and more negative $Si\text{-}O^-$ would be accessible to be turned into positive $Si\text{-}O\text{-}R\text{-}NH_3^+$ at neutral pH. As a result of this charge reversal on the pore surface, R6G will be repelled from the surface instead of being strongly attracted to it, hence *r* dropped to 0.07 from 0.21.

Table 4.2 also illustrated that the introduced methyl groups had a moderate effect on R6G mobility. The anisotropy value of R6G dropped ~20% from ~0.20 to ~0.16 after pore surface modification. MTES modified hydrogel pore surfaces turned more hydrophobic, which weakened the charge-charge attractions between R6G and gel network, thus made the R6G guest molecules relatively more mobile. Similarly, the effect of MTES modification on R6G molecules in hydrogel is greater than that in alcogel,[14] due to the same reason (larger pores) as explained earlier for APTS modification. When compared to the ~67% drop of anisotropy value caused by APTS modification, ~20% drop by MTES modification was not comparably effective. In summary, in silica hydrogel the non-charge interactions such as van der Waals forces are not as competitive as charge-charge interactions, as a result, charge neutralization by

MTES was not efficient as charge-reversal by APTS to modify pore surfaces in silica hydrogel.

In addition to the change of R6G anisotropy values, it was noticed that MTES modified hydrogel strongly accumulated R6G at the interface of dye solution and the gel, and retarded dyes to diffuse deeper. After 24 hr dye diffusion, the color of the top dye solution in MTES sample was a lot lighter than the solution in EtOH sample, and the R6G dye band was much darker than the one in EtOH soaked gel. After two weeks diffusion, the differences became even more obvious, as demonstrated by the emission and absorbance spectra of EtOH sample and MTES sample in Figure 4.4 (A) and 4.4 (B). With the same amount of R6G molecules being added to the top of EtOH and MTES modified hydrogel samples respectively, the amount of dyes left (after two-week diffusion) in top solution of EtOH sample was ~17 times that of MTES sample (indicated Figure 4.4 (A)), which suggests that MTES modification helped attracting and then encapsulating a lot more R6G molecules into the gel. As further substantiated by the absorption spectra of EtOH sample and MTES sample in Figure 4.4 (B), the amount of R6G trapped in MTES sample was ~2.1 times that in EtOH sample. After the absorption spectra were resolved by Gaussian fitting, the monomer/dimer ratio was found to be ~16 in EtOH sample and ~13.8 in MTES sample, and a 6 nm red-shift of λ_{max} (peak wavelength) from 526 nm in EtOH sample to 531 nm in MTES sample was observed (a 7 nm red-shift was also observed from emission spectra). Apparently, nonpolar methyl groups helped the formation of R6G dimers and aggregates, and were also responsible for the slight red shift. Studies from other groups have proved that less polar and more hydrophobic groups such as methyl groups can help dye molecules form

cluster on the inhomogeneous silica surface, both the polarity change of the local environments of dyes and the aggregation of dyes could cause the red shift of absorption and emission peaks.[28-29,32-34] And because of the large size of dimers and aggregates, R6G molecular diffusion inside hydrogel was hindered and they accumulated in the very thin top layer of hydrogel sample.

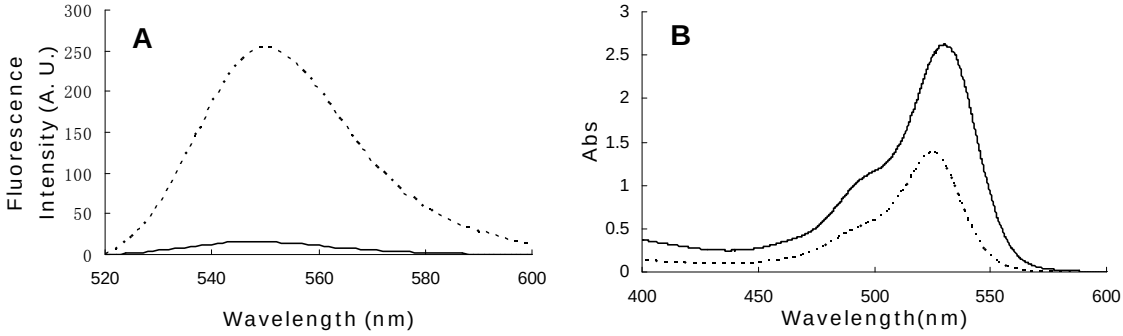

Figure 4.4 (A) Fluorescence emission spectra and (B) absorption spectra of R6G in 38% EtOH modified gel (dashed line) and 10% MTES modified gel (solid line) after two-week dye diffusion.

4.3.2.2 Section measurements

Although bulk measurements can provide us an overall picture of the surface modification effect, some details could be overlooked. Modification reagents couldn't penetrate as deep as 2 cm of the whole monolith sample in two days, the deeper inside the gel, the less extent of modification would be achieved. From top to the bottom of those samples, there should be a transition from completely modified, partially modified to unmodified regions. To track the heterogeneity of the modification process and study its effect on the motion of guest molecules, section measurements were then taken by collecting the fluorescence emission spectra of the gel samples from top to the bottom every 1.6 mm (accessible depth was ~13mm).

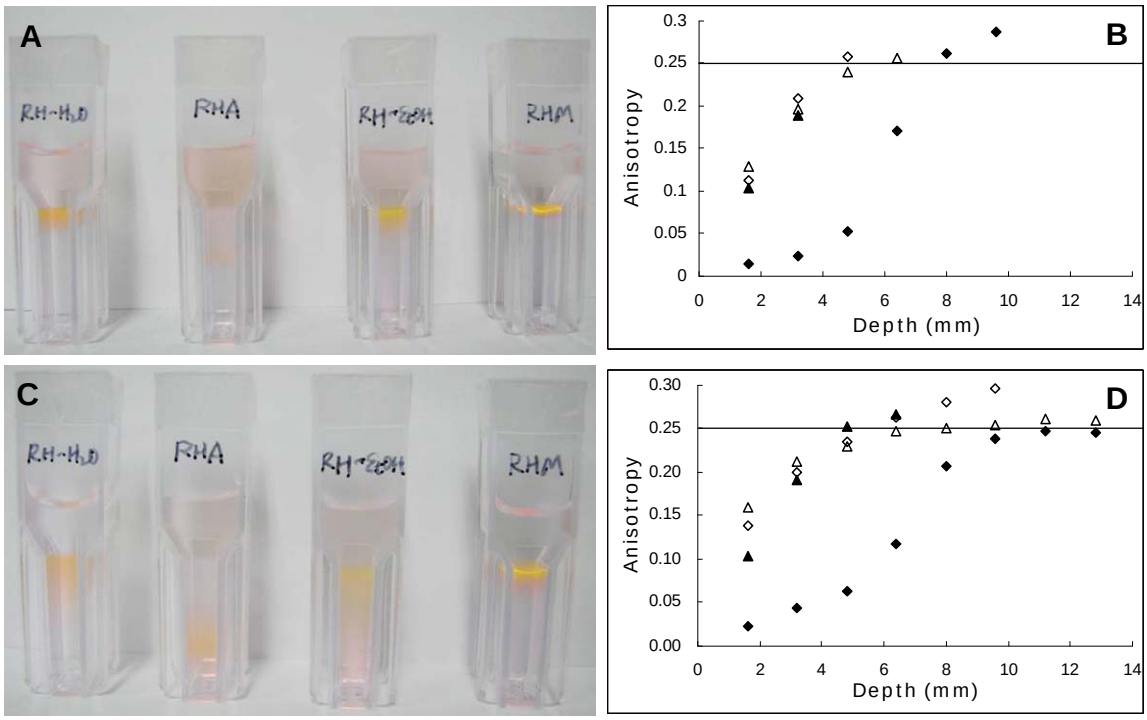

Figure 4.5 (A) from left to right, samples modified by H_2O, 0.4% APTS, 38% EtOH and 10% MTES for two days, followed by one-day dye diffusion, (B) section measurement of anisotropy values of R6G in samples from (A), (C) same samples as in (A), with thirteen more days dye diffusion, (D) section measurement of anisotropy values of R6G in samples from (C). In (B) and (D), hollow diamonds, solid diamonds, hollow triangles and solid triangles represent H_2O, 0.4% APTS, 38% EtOH and 10% MTES modified samples, respectively. The solid line at 0.25 in (B) and (D) indicates the boundary of unmodified region.

As illustrated clearly in Figure 4.5 (A) and (C), the locations, the shapes and colors of R6G dye bands provided us a rough idea about how different modification reagents greatly affected the travelling of R6G molecules inside the gel. For H_2O and EtOH samples, after one day diffusion (as shown in Figure 4.5 (A)), most R6G molecules were concentrated at the top of gel and hardly diffused into the unmodified region, because they were strongly attracted by negatively charged pore surfaces and got stuck

once they diffused into the gel. In MTES sample, R6G molecules were restricted in an even smaller area (the dye band was thinner than that of H_2O and EtOH samples), as explained earlier, methyl groups turned the pore surface more hydrophobic, which helped the aggregation of R6G molecules, because the size of the aggregates are larger than monomer, the downward dye diffusion became harder, and the molecules then piled up in a narrower space. In APTS sample, R6G molecules went as deep as the modification had reached, indicated by the dye band located at the half way of the sample, because positively charged amino groups on the modified surface drove positively charged R6G molecules mobile. After another thirteen-day dye diffusion (as shown in Figure 4.5 (B)), the dye band of H_2O, EtOH and MTES samples didn't migrate deeper, but only became wider due to natural diffusion, and more R6G molecules diffused into the unmodified region. It's worth to point out that, in EtOH sample, a lot of R6G molecule traveled all the way down to the bottom of the gel, probably because the remaining small amount of ethanol around the molecules lowered the surface tension[26] and made the diffusion easier than in H_2O sample. APTS sample behaved differently; not only more dye diffused into the unmodified region, but the dye band migrated deeper from half way to the bottom, this is because APTS not only turned the pore surfaces positively charged to drive R6G molecules mobile, but also made the surface more hydrophobic, which helps decrease surface tensions[35] and makes the molecular diffusion of R6G easier.

Anisotropy data of samples were demonstrated in Figure 4.5 (B) and (D). The transition from modified to unmodified region was clearly shown, and the anisotropy values of all samples settled between 0.25 and 0.30 regardless of the modification

reagents used. We defined the region with anisotropy values between 0.25 and 0.30 as the unmodified region for two reasons: (1) Immobilized R6G molecules in hydrogel register an anisotropy value ≥ 0.25 (referring to section 4.3.1.1), (2) the anisotropy value of R6G at 0.25 always corresponded to the 1.6 mm section of the sample, in which the bottom of the dye band was included. We thus believe *r* at 0.25 marked the boundary of unmodified region. However, the samples didn't show the same rate or pattern of anisotropy value increment. MTES sample was the fastest one, and APTS sample was the slowest.

In Figure 4.5 (D), for the first 1.6 mm-thick section of the samples, all of them registered an anisotropy value ⩽ 0.16. R6G in H_2O sample and EtOH sample should be affected by pore fluid effect, as reported by C. J. Brinker et al., before drying, gel structure and chemistry can be dramatically changed by the varied aging conditions such as time, temperature, pH and pore fluid.[26,36-38] The condensation and cross-linking reactions didn't stop at the gel point, but continue during aging, which could last a few weeks to months.[39] When H_2O, 0.4% APTS, 38% EtOH and 10% MTES/38% EtOH were added to the top of monolith samples right after gelation, they would involve in the ongoing cross-linking, condensation processes and increased the molar ratio of water : sol in some extent. Higher ratio of water : sol made the pore size larger, which leads to a smaller anisotropy value of trapped dyes. This explains the much smaller anisotropy value ~0.15 of H_2O and EtOH samples in the first 1.6mm region compared to those values of ~ 0.25 in unmodified region. R6G molecules in APTS and MTES samples would be affected not only by introduced organic groups but also the solvent of organosilane reagents, and the anisotropy values of R6G should reflect a combined

effect of chemically post-grafting and pore fluid, between which surface grafting dominated. The anisotropy value of the 1st 1.6 mm region of APTS sample was as low as 0.023, which is comparable as the value 0.013 ± 0.007 of R6G in aqueous solution. This suggests a highly amino groups covered pore surface. The anisotropy value of R6G in APTS sample gradually increased as it went deeper, until dye got restricted and started accumulating at 8 mm depth with an anisotropy value of 0.207, and then the dye band stopped at 12.8 mm. On the contrary, MTES didn't help R6G molecules migrate deeper, but only turned R6G molecules more mobile, as a relatively low value of 0.103 was observed from the 1st 1.6 mm region of MTES sample. Most R6G molecules in MTES sample were restricted at 3.2 mm depth with an anisotropy value of 0.192, and the dye band stopped at 4.8mm depth, similarly as those R6G in H_2O sample and EtOH sample. Overall, both post-grafting samples showed very obvious effect on the mobility of encapsulated R6G molecules, especially at the very top layer of the gel which was in direct contact with modification reagents. This suggests that as long as the hydrogel monolith is thin enough, post-synthesis grafting can modify pore surfaces completely or at least to a very high extent. That's what we couldn't realize in silica alcogel thin films.

4.3.3 Fl Study

Similarly as R6G study, both bulk and section measurements were taken to study the surface modification effect on Fl molecules. Results from bulk measurements were summarized in Table 4.3. Because of the strong Columbic repulsion between negatively charged Fl and negatively charged gel network, all Fl samples were quite mobile regardless of what modifications had been done, and no dye band was observed in any sample. Thus, in Fl doped hydrogel samples, the modification process can only be

tracked by monitoring the change of anisotropy values, unlike R6G samples can be monitored both by locating dye band and measuring anisotropy values. Control samples modified by H_2O and 38% EtOH registered anisotropy values of 0.017±0.005 and 0.012 ±0.002 respectively, which are very close to the anisotropy value of Fl in aqueous solution 0.011±0.005.

	H_2O	**pH 2.0 HCl**	**0.4% APTS**	**0.4% APTS-1M NaCl**	**38% EtOH**	**10% MTES**
r	**0.017** ±0.005	**0.064** ±0.005	**0.097** ±0.008	**0.087** ±0.006	**0.012** ±0.002	**0.029** ±0.005

Table 4.3 Comparison of anisotropy values of Fl after different modifications

Fl in pH 2.0 HCl equilibrated sample showed slightly restricted rotation, as the anisotropy value increased to 0.064±0.005. This was possibly due to the neutralization of negative $Si\text{-}O^-$ on surfaces by protons, which weakened the repulsion between Fl and hydrogel. But it has to be pointed out that pH 2.0 HCl not only introduced protons into hydrogel surfaces and but also lead to protonation of Fl molecules, because a ~75% drop of the fluorescence intensity was observed. As reported,[40-42] the fluorescence of Fl is very pH sensitive, especially at pH values lower than 7.0. The relative fluorescence intensity dropped dramatically from 82.7 to 10.0 when pH changed from 6.99 to 5.11.[41] The protonation of some Fl molecules from Fl^{2-} to less charged Fl^- and neutral Fl species could weaken the repulsions between Fl and silica pore surfaces, which caused the increase of anisotropy value.

Fl in 0.4% APTS modified sample showed a 6-fold increase of anisotropy value (0.017 to 0.097), indicating that Fl molecules moved slower due to the charge-reversal

on pore surfaces by positively-charged amino groups. When 1.0 M NaCl was mixed with Fl solution to be introduced to APTS modified hydrogel, the increased ionic strength was expected to weaken the charge-reversal by APTS modification, thus increase the mobility of Fl molecules,[43] but it would be arguable if we attribute the slight anisotropy value drop of 0.01 (from 0.097 to 0.087) to the increased ionic strength, because this small difference fell in the error range of our technique (±0.01). 10% MTES modified sample showed a 2.5-fold increase of anisotropy value (0.012 to 0.029), accredited to the introduced hydrophobic methyl groups, which helped capping the highly negatively charged surface and weakened the repulsion between Fl and pore surfaces. Although both post-synthesis grafting reagents showed effects on Fl mobility, charge-reversal by APTS was more effective than hydrophobic capping.

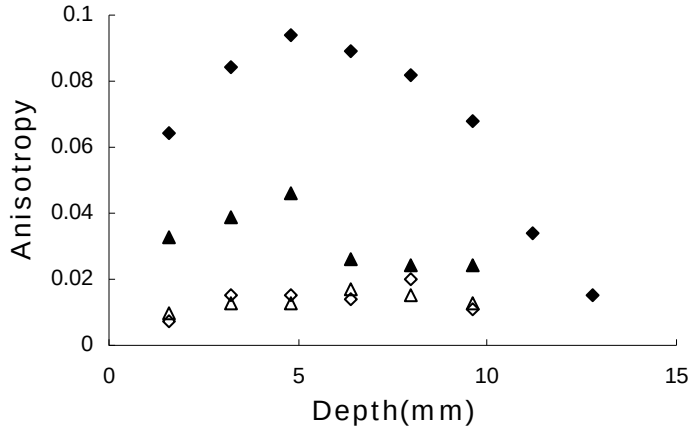

Figure 4.6 Section measurements of anisotropy values of Fl in H_2O (hollow diamonds), 0.4% APTS (solid diamonds), 38% EtOH (hollow triangles), 10% MTES (solid triangles) modified silica hydrogel samples.

From section measurements as illustrated in Figure 4.6, Fl molecules can penetrate as deep as 10 mm in all samples after two-week diffusion. H_2O and EtOH samples showed a flat line pattern with an anisotropy value of 0.014±0.003, suggesting that those two samples were homogeneous from top to the bottom. Solvent effect was negligible for H_2O and EtOH samples. However, after Fl molecules were restricted by introduced amino and methyl groups, solvent effect cannot be neglected. From previous

R6G study we know that solvents caused anisotropy values drop, the effect was very clear at the top layer of gel, and then attenuated with the depth of the gel (illustrated in Figure 4.5 (D)). Without any solvent mixed, if Fl doped hydrogel samples were modified by pure MTES or APTS, the anisotropy values should increase, but because of the top-to-bottom diffusion modification process, the deeper the smaller the increase of anisotropy value. When the solvent effect was comparable to the post-synthesis grafting effect on Fl molecules, these two effects were combined to create a gradual increase to a peak and then slow decreased pattern of APTS and MTES samples shown in Figure 4.6.

4.4 CONCLUSIONS

Post-grafting protocol to modify silica hydrogel pore surfaces has been developed. Using dye as probes, the process of pore surface modification inside hydrogel can be monitored by locating R6G dye band, or be precisely tracked by monitoring the change of anisotropy values. R6G dye band has also been used to optimize the protocol. As a continued work of our previous publication,[14] this study verified the applicability of our post-synthesis grafting protocol, and confirmed the hypothesis that pore surface modification is more effective in silica hydrogel than that in silica alcogel. To eliminate the effect of physical confinement on guest molecules and the limited accessibility of modification reagents to pores, dye molecules must be infused into hydrogel after pore surfaces have been modified. It was found that chloroform was an unsuitable solvent for MTES modification in hydrogel because of the immiscibility of chloroform with water, which hindered MTES from penetrating highly hydrated hydrogel; ethanol was a good solvent for MTES modification, although it showed pore fluid effect and caused a slight decrease of anisotropy value. From bulk measurements, we found that increasing ionic strength by 1.0 M sodium chloride didn't help weakening the strong Columbic interactions between guest R6G or Fl molecules and pore surfaces. Introducing protons to cap the negatively charged pore surfaces by pH 2.0 hydrochloric acid didn't affect the mobility of R6G molecules, but did slow Fl molecules down, which possibly because that R6G was not sensitive to pH, but Fl was, and some Fl^{2-} turned into Fl^{-} and Fl by protonation. Charge-reversal of pore surfaces by APTS modification showed a greater effect on guest molecules mobility than the hydrophobic capping by MTES modification: APTS modification caused the anisotropy value of R6G to drop ~67%,

and MTES modification only caused a ~20% drop; For Fl molecules, APTS modification showed a 6-fold increase of anisotropy value, whereas MTES only brought a 2.5-fold increase. Thus, charge-reversal is believed to be a more effective way to modify pore surfaces than hydrophobic capping in silica hydrogel. The multiple-step section measurement of anisotropy values provided more information than bulk measurement did, and it helped to understand the top-to-bottom diffusion modification process better by tracking the gradual change of anisotropy values. From section measurements, we found that the mobility of encapsulated molecules were affected not only by post-grafting of surfaces but also the solvent for modification reagents, though, for R6G molecules the solvent effect was negligible compared to post-grafting modification, for Fl molecules solvent effect can't be neglected. Moreover, the ease of locating dye band to track modification process was another reason to make R6G a better probe than Fl to monitor the pore surface modification in silica hydrogel.

4.5 CHAPTER 4 REFERENCES

(1) Schmidt, H. *J Non-Cryst Solids* **1985**, *73*, 681.

(2) Avnir, D.; Levy, D.; Reisfeld, R. *The Journal of Physical Chemistry* **1984**, *88*, 5956.

(3) Mackenzie, J. D. *Journal of Sol-Gel Science and Technology* **2003**, *26*, 23.

(4) Dimitriev, Y.; Ivanova, Y.; Iordanova, R. *Journal of University of Chemical technology and Metallurgy* **2008**, *43*, 181.

(5) Braun, S.; Rappoport, S.; Zusman, R.; Avnir, D.; Ottolenghi, M. *Materials Letters* **1990**, *10*, 1.

(6) Pierre, A. C. *Biocatal Biotransfor* **2004**, *22*, 145.

(7) Avnir, D.; Coradin, T.; Lev, O.; Livage, J. *J Mater Chem* **2006**, *16*, 1013.

(8) Lim, M. H.; Stein, A. *Chemistry of Materials* **1999**, *11*, 3285.

(9) Nicole, L.; Boissiere, C.; Grosso, D.; Quach, A.; Sanchez, C. *J Mater Chem* **2005**, *15*, 3598.

(10) Calvo, A.; Joselevich, M.; Soler-Illia, G. J. A. A.; Williams, F. J. *Micropor Mesopor Mat* **2009**, *121*, 67.

(11) Reetz, M. T. *Advanced Materials* **1997**, *9*, 943.

(12) Mackenzie, J. D.; Huang, Q.; Iwamoto, T. *Journal of Sol-Gel Science and Technology* **1996**, *7*, 151.

(13) Angelomé, P. C.; Soler-Illia, G. J. d. A. A. *Chemistry of Materials* **2005**, *17*, 322.

(14) Lei, Q.; Yip, W. T. *The Journal of Physical Chemistry C* **2009**, *113*, 21130.

(15) Tleugabulova, D.; Sui, J.; Ayers, P. W.; Brennan, J. D. *The Journal of Physical Chemistry B* **2005**, *109*, 7850.

(16) Zhou, Y. Y.; Yip, W. T. *J Phys Chem B* **2009**, *113*, 5720.

(17) Tleugabulova, D.; Duft, A. M.; Zhang, Z.; Chen, Y.; Brook, M. A.; Brennan, J. D. *Langmuir* **2004**, *20*, 5924.

(18) Vandenberg, E. T.; Bertilsson, L.; Liedberg, B.; Uvdal, K.; Erlandsson, R.; Elwing, H.; Lundström, I. *J Colloid Interf Sci* **1991**, *147*, 103.

(19) Murthy, R. S. S.; Leyden, D. E. *Analytical Chemistry* **1986**, *58*, 1228.

(20) Vrancken, K. C.; Vandervoort, P.; Gillisdhamers, I.; Vansant, E. F.; Grobet, P. *J Chem Soc Faraday T* **1992**, *88*, 3197.

(21) Cui, N.-Y.; Liu, C.; Brown, N. M. D.; Meenan, B. J. *Applied Surface Science* **2007**, *253*, 6932.

(22) Chiang, C. H.; Ishida, H.; Koenig, J. L. *J Colloid Interf Sci* **1980**, *74*, 396.

(23) Blitz, J. P.; Shreedhara Murthy, R. S.; Leyden, D. E. *J Colloid Interf Sci* **1988**, *126*, 387.

(24) Scherer, G. W. *J Non-Cryst Solids* **1988**, *100*, 77.

(25) Scherer, G. W. *J Non-Cryst Solids* **1989**, *109*, 183.

(26) Davis, P. J.; Jeffrey Brinker, C.; Smith, D. M.; Assink, R. A. *J Non-Cryst Solids* **1992**, *142*, 197.

(27) Hansen, R. L.; Harris, J. M. *Analytical Chemistry* **1998**, *70*, 2565.

(28) Zheng, X.-Y.; Harata, A.; Ogawa, T. *Spectrochimica Acta Part A: Molecular and Biomolecular Spectroscopy* **2001**, *57*, 315.

(29) Chen, Z.; Tang, Y.-J.; Xie, T.-T.; Chen, Y.; Li, Y.-Q. *Journal of Fluorescence* **2008**, *18*, 93.

(30) Parks, G. A. *Chemical Reviews* **1965**, *65*, 177.

(31) Zheng, X.-Y.; Wachi, M.; Harata, A.; Hatano, Y. *Spectrochimica Acta Part A: Molecular and Biomolecular Spectroscopy* **2004**, *60*, 1085.

(32) Dutta, A. K.; Salesse, C. *Langmuir* **1997**, *13*, 5401.

(33) Zheng, X.-Y.; Harata, A.; Ogawa, T. *Chemical Physics Letters* **2000**, *316*, 6.

(34) Imhof, A.; Megens, M.; Engelberts, J. J.; de Lang, D. T. N.; Sprik, R.; Vos, W. L. *The Journal of Physical Chemistry B* **1999**, *103*, 1408.

(35) Zarzycki, J.; Prassas, M.; Phalippou, J. *Journal of Materials Science* **1982**, *17*, 3371.

(36) Davis, P. J.; Jeffrey Brinker, C.; Smith, D. M. *J Non-Cryst Solids* **1992**, *142*, 189.

(37) Deshpande, R.; Hua, D.-W.; Smith, D. M.; Brinker, C. J. *J Non-Cryst Solids* **1992**, *144*, 32.

(38) Davis, P. J.; Deshpande, R.; Smith, D. M.; Brinker, C. J.; Assink, R. A. *J Non-Cryst Solids* **1994**, *167*, 295.

(39) Brinker, C. J.; Scherer, G. W. *Sol-Gel Science: the physics and chemistry of sol-gel processing*; Academic press: San Diego, 1990.

(40) Diehl, H.; Horchak-Morris, N. *Talanta* **1987**, *34*, 739.

(41) Diehl, H.; Markuszewski, R. *Talanta* **1989**, *36*, 416.

(42) Peterson, C. *Water, Air, Soil Pollut.* **2010**, *209*, 473.

(43) Bahga, S. S.; Bercovici, M.; Santiago, J. G. *ELECTROPHORESIS* **2010**, *31*, 910.

CHAPTER 5 DEVELOPMENT OF SILCA HYDROGEL-LIKE THIN FILM FOR FAST SENSOR MATRIX

5.1 ABSCTRACT

The protocol to produce stable hydrogel-like thin film was developed and optimized. Contact angle measurement, fluorescence imaging, fluorescence recovery after photobleaching (FRAP), absorption spectrum, profilometry, atomic force microscopy (AFM), and scanning electron microscopy (SEM) were used to characterize this new thin film material. Homogeneous hydrogel-like thin film samples with thickness between 100 nm and 300 nm were produced. This new film was highly hydrophilic, enabled high-guest-loading capacity, and supported molecular diffusion. The reproducibility of sample preparation was greatly improved by controlling environmental humidity, guest loading capacity of samples was improved more than ten times by using buffer solutions, and the concentration of R6G trapped inside hydrogel-like thin film could reach as high as 900 times of its saturated aqueous solution. Encapsulation of guest dye molecules can be accomplished simply by dipping a chemically reactive precursor alcogel film into a dye-doped buffer solution. Because alcohol exposure can be kept to a minimum during dye encapsulation, this new silica thin film makes a promising candidate for biomolecule encapsulation and thus biosensor development. A prototype hydrogel-like thin film pH sensor doped with Nile blue chloride (NBC) was constructed and it showed faster response time than the corresponding alcogel thin film sensor.

5.2 INTRODUCTION

In 1984 Avnir et al. first reported the entrapment of an organic dye in silica gel (composites),[1] and soon it was discovered that the trapped molecules in sol-gel matrix were sensitive to solvent environment.[2-3] Those findings led people to think about the possibilities for construction of silica gel-based chemical sensors. Since then, silica sol-gel has been extensively studied for sensor development.[4-11] Based on their functions, the requirement of response time, sensitivity, detection limit and loading capacity of functional molecules, several practical sensor configurations have been developed. Packed powder, doped monoliths, coated optical fibers, sandwich configuration, coated electrodes, and thin films are the common types.[12-14] Thin film has been recognized as the most promising configuration, due to low materials cost, fast response, adaptability to device miniaturization and less cracking upon liquid exposure.[9,11,15] Most work to date has focused on silica alcogel thin films. Highly porous silica hydrogel thin films have never been successfully prepared, because high water content renders hydrogel mechanically fragile.[16] The essential elements of a fast sensory matrix, such as thin, high porosity films and high loading capacity of functional guest molecules, can all be realized simultaneously if a stable hydrogel thin film could be produced. Many attempts have been made to improve the mechanical strength of silica hydrogel, such as to make an intertwined or crosslinked hybrid network of hydrogel by doping the silica with hydrophilic polymers,[17-19] or to create double-network hydrogels to provide a stronger support.[20-21] Despite those improvements, the hydrogel composites are still produced into either monoliths or thick films.

Here we report an optimized protocol to produce stable silica hydrogel-like thin films. With thickness around 200 nm, our silica hydrogel-like film is expected to be a better substrate for devices that demand faster response than thick monoliths. Stable thin film hydrogel with such a small thickness has never been accomplished before. The hydrogel-like film is derived from a silica-alcogel thin film, which also determines the final film thickness. It was produced by immersing nascent silica alcogel thin film to aqueous solution, and showed a very hydrophilic surface, high dye loading capacity and the support of molecular diffusion. We suspected that the hydrophilic film was made of extremely water rich surface-bound hydrogel colloids, produced by the rapid coarsening of the chemically reactive nascent silica film upon contacting water. It was also discovered that the chemical reactive stage to produce hydrogel-like thin film from alcogel could last 10 min under ambient conditions. Through extensive characterizations of this new gel material by different techniques, such as contact angle measurement, absorption spectrum, fluorescence imaging, atomic force microscope (AFM), scanning electronic microscope (SEM) and profile thickness measurement, we understood more about its characteristics, improved the reproducibility of film preparation and the guest loading capacity, and were able to extend the reactive stage of the precursor alcogel thin film matrix. The microstructure of hydrogel-like thin films was also examined. The underlying chemistry and mechanism of gel formation were proposed. At the end, a prototype hydrogel-like thin film pH sensor doped with Nile blue chloride (NBC) was developed and tested.

5.3 RESULTS AND DISCUSSION

5.3.1 Characteristics of silica hydrogel-like thin films

5.3.1.1 Hydrophilic surface

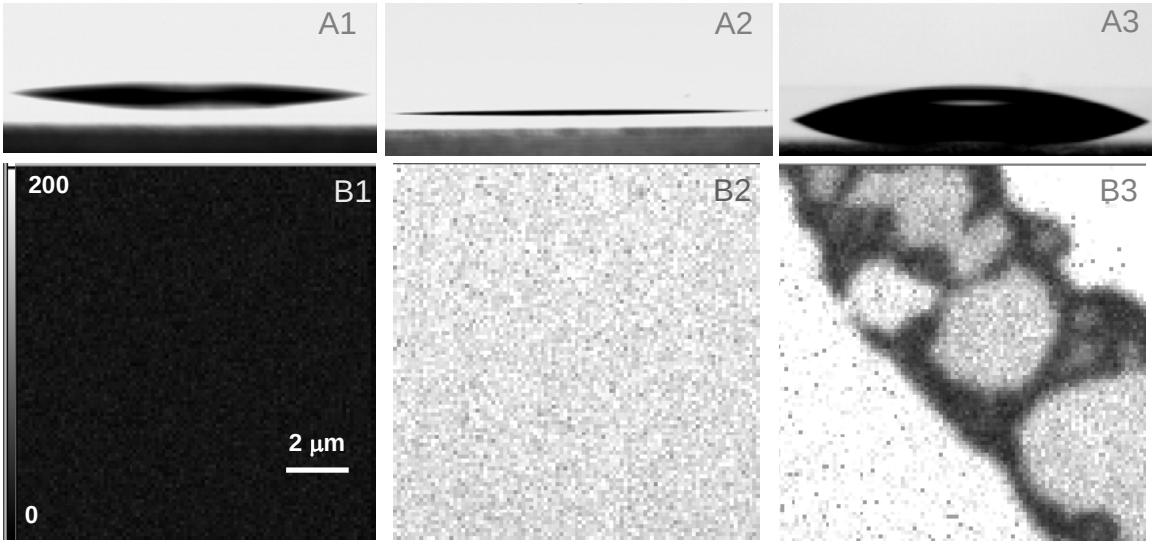

Figure 5.1 Contact angles of (A1) bare coverslip; (A2) water-modified nascent alcogel; (A3) water-modified 1 hr-delayed alcogel. Fluorescence images of rhodamine 6G (R6G) doped (B1) bare coverslip; (B2) water-modified nascent alcogel. (B3) water-modified 1 hr-aged alcogel.

Contact angle can reflect the hydrophobicity of a surface.[22-23] Usually, hydrophobic surfaces result in large contact angles and hydrophilic surfaces lead to small contact angles. Figure 5.1 illustrates the significant difference in contact angle between a clean bare coverslip (A1), an alcogel film that reacted with water right after spincoating (A2), and an alcogel film that reacted with water one hour after spincoating (A3). As stated in Chapter 2.3.7, the aging time before reacting with water is labeled as "sample delay time" in this chapter. If allowed to age for one hour before reacting with water, the alcogel surface appears fairly hydrophobic, with contact angle of 24 ± 2^{o} (A3). This is in sharp contrast to the contact angle 5 ± 1^{o} obtained from an alcogel that

reacts with water immediately after spin-coating (A2). Such a small contact angle in (A2) can be due to: (1) the alcogel turning into a very hydrophilic film after reacting with water or (2) the washing off of the alcogel film to expose the fairly hydrophilic coverslip underneath. The noticeable difference in contact angle between the bare coverslip in (A1) (9º±3º) and the film in (A2) (5º±1º) is consistent with the first interpretation (1). This is further substantiated by the corresponding fluorescence images collected from the rhodamine (R6G) doped samples. As shown in Figure 5.1 (B1) and (B2), the R6G fluorescence intensity from water-modified nascent alcogel is substantially higher than that from the R6G-doped bare coverslip, which is indicative of the presence of a thin layer of porous silica matrix remaining on the coverslip for efficient R6G encapsulation. Meanwhile, the fluorescence image in Figure 5.1 (B3) reveals that R6G distribution inside this film is not homogeneous as dark areas might mark regions that were less accessible to R6G molecules. The considerable differences in contact angle and R6G distribution between these two alcogel films suggest that reacting a nascent alcogel with water at different aging times will produce thin films with different characteristics. It is well known that a silica hydrogel monolith can be prepared by adding a large amount of aqueous buffer to silica sol or sodium silicate.[24] We suspect that the surface of a nascent alcogel film will still be in a chemically reactive stage that resemble a thin film of liquid sol, and that a similar reaction leading to hydrogel formation will occur when a nascent alcogel film reacts with water. This may lead to a rapid coarsening of the film surface and produce a highly porous hydrogel-like film that is made of extremely water-rich surface-bound silica colloids, which trap whatever guest molecules are present in water while the colloids are forming.

5.3.1.2 High guest loading capacity

Absorbance of R6G doped hydrogel-like thin films can reflect the guest loading capacity of them. As discussed above, sample delay time is an important factor that affects characteristics of produced thin films, we thus prepared a series of R6G doped hydrogel-like thin film samples with delay time ranging from 0 min to 60 min to explore the guest loading capacity of them (referring to Chapter 2.3.7 for sample preparation). Figure 5.2 (A) compares the maximum absorption of R6G monomer at 532 nm from different samples. R6G absorbance underwent a rapid increase at short delay time, reached the peak at 3±0.5 min before its rapid decline back to the background level at 10 min delay time. The decline in R6G absorbance after 3±0.5 min can be understood as the nascent alcogel becomes less reactive toward water at longer delay time, rendering the resultant film more alcogel-like and less capable of trapping R6G. So the chemical reactive stage to produce hydrogel-like thin film from alcogel

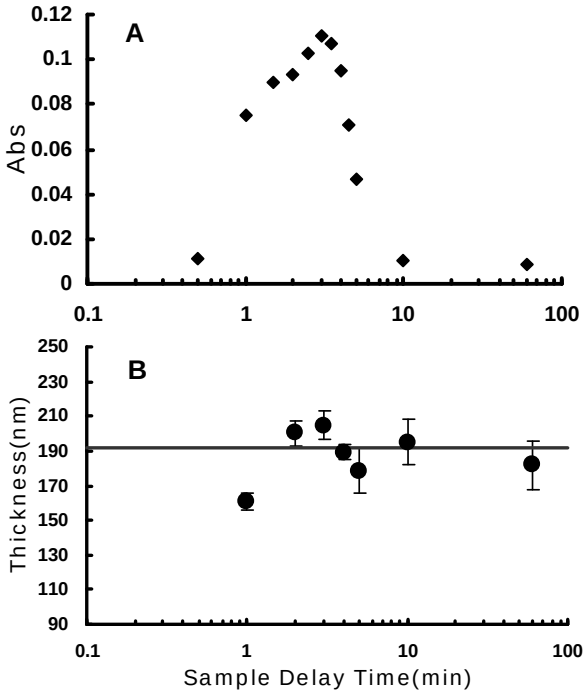

Figure 5.2 Variation of (A) R6G absorbance of monomer peak and (B) film thickness with sample delay time. Gray line in (B) is the average thickness (192 nm) of all films with 2-min or longer delay times. Samples in (A) and (B) are comparable samples.

could last 10 min under ambient conditions. It is worth noting that the dye loading capacity is approximately 18 times higher in the 3-min delayed hydrogel-like film when compared to the 60 min-delayed alcogel-like film, presumably due to higher porosity of the hydrogel-like film. The low R6G absorbance recorded from the very short delay time was most likely caused by the partial wash off of the nascent alcogel film by water before it had sufficient time to develop a stable 3-dimensional gel network. This led to a thinner film and thus lower R6G loading.

The thicknesses of R6G doped hydrogel-like thin film samples with different delay times are shown in Figure 5.2 (B). The 0-min delayed film was too thin to produce a reliable estimate whereas the 1-min delayed sample was about 161±5 nm thick. This is ~30 nm thinner than the average thickness of all other films with 2-min or longer delay times, which stabilized at 192±10 nm. These thickness measurements helped confirm our previous interpretation that the very low R6G absorbance at short delay time was indeed due to partial gel loss, and that the subsequent decrease in R6G absorbance after the peak at 3-min delay time was only caused by declining nascent alcogel reactivity with aging and was unrelated to film thickness, which remains practically unchanged. Also worth mentioning is even for the more hydrogel-like sample that displays the largest R6G absorbance, its thickness is not far from a similarly prepared alcogel film. This should provide reliable thickness control for the hydrogel-like film by adjusting the thickness of the precursor alcogel film.

5.3.1.3 Support of molecular diffusion

Because our new films are derived from alcogel films, molecular transport inside is expected to lie between that of an alcogel and a hydrogel. Diffusion of small molecules

inside the new film was examined by fluorescence recovery after photobleaching (FRAP) using fluorescein (Fl) as the probe (Procedures for FRAP experiment are described in Chapter 2.4.6). It is known that physical confinement and electrostatic interactions are the dominating factors that control guest mobility in alcogel and hydrogel, respectively.[25] As such, Fl in alcogel is expected to be physically immobilized and display no FRAP, which is nicely demonstrated in trace B in Figure 5.3. Being more alcogel-like, the alcogel that aged for an hour before reacting with water (trace C) doesn't show FRAP either. This is because the aging time had resulted in the loss of chemical reactivity and thus inefficient Fl trapping, producing poor signal and no fluorescence recovery.

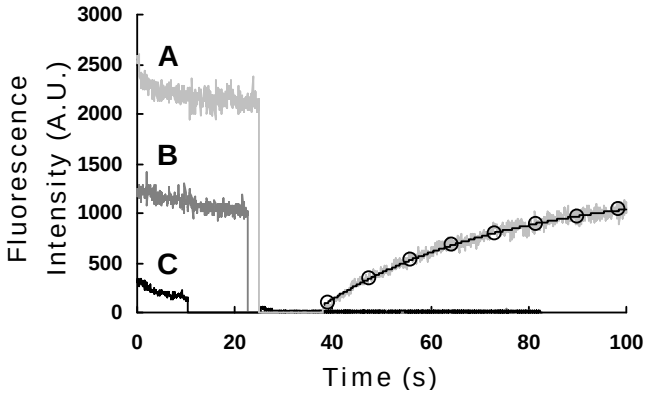

Figure 5.3 FRAP traces from Fl (A) in a treated nascent alcogel film, (B) an alcogel thin film, and (C) a treated 1h-delayed alcogel film. The abrupt drop to zero fluorescence in all traces is due to the blocking of detector while the samples were being photobleached for approximately 10 seconds. The solid black line with open circles in the recovery portion represents the fit according to Equation 5.1

The presence of a substantial FRAP signal from the treated nascent film in Figure 5.3 (trace A) reveals that Fl has a high degree of mobility in this film. Unlike the other two samples (trace B and C), mobility inside the new film appears to be dominated by electrostatic repulsion, which might render Fl mobile by keeping the anionic Fl away from silica surfaces. The much higher Fl mobility thus leads us to believe that the structural characteristics of the new film are more hydrogel-like than alcogel-like. To quantify the diffusion rate of Fl inside this new film, we fit the recovery portion of the

FRAP traces collected from different locations of the new film according to a normalized first-order rate equation (Equation 5.1).

$$I(t) = A(1 - \exp(-k_{recovery}t)) + I(0) \qquad \textbf{5.1}$$

where $I(t)$ is the fluorescence intensity; $k_{recovery}$ is the recovery rate constant; A is the recovered fluorescence intensity minus the fluorescence intensity immediately after photobleaching ($I(\infty) - I(0)$). The solid black line with open circles in Figure 5.3 illustrates one example of six such fittings. The average $k_{recovery}$ is 0.019±0.005 s^{-1}. Using 6.4 x 10^{-6} cm^2 s^{-1} for the diffusion coefficient of Fl in water as a reference,[26] the averaged recovery rate of 0.019±0.005 s^{-1} found in the hydrogel-like silica film would translate to a Fl diffusion coefficient of ca. 1.7 x 10^{-7} cm^2 s^{-1}. This is about a factor of 10 slower than the diffusion of Fl in a regular hydrogel monolith. The smaller Fl diffusion coefficient could be due to the close proximity of Fl to silica surfaces or lower water content because of fast evaporation from such a thin film. Higher humidity resulting in faster recovery rate was indeed observed, which is discussed in section 5.3.3.3.

In summary, this new hydrogel-like thin film exhibits highly hydrophilic surface, and a much higher dye loading capacity relative to that of a typical alcogel film. The chemical reactive stage to produce hydrogel-like thin film from alcogel could last 10 min under ambient conditions, and the thickness can be controlled via the precursor silica alcogel film. FRAP measurements revealed that this new film can support molecular diffusion.

5.3.2. The Change of Gel Characteristics with Sample Delay Time

The characteristics of our hydrogel-like thin films showed high dependence on the sample delay time, as nicely demonstrated from the contact angle measurements and fluorescence imaging (Figure 5.1), FRAP (Figure 5.3), and the investigation of guest loading capacity with sample delay time (Figure 5.2). To understand more about the change of gel characteristics with samples delay time, we extended the contact angle measurement and fluorescence imaging to a series of thin film samples with different delay times, just like the guest loading capacity and sample thickness investigations discussed in section 5.3.1.2.

5.3.2.1 Contact angle measurements

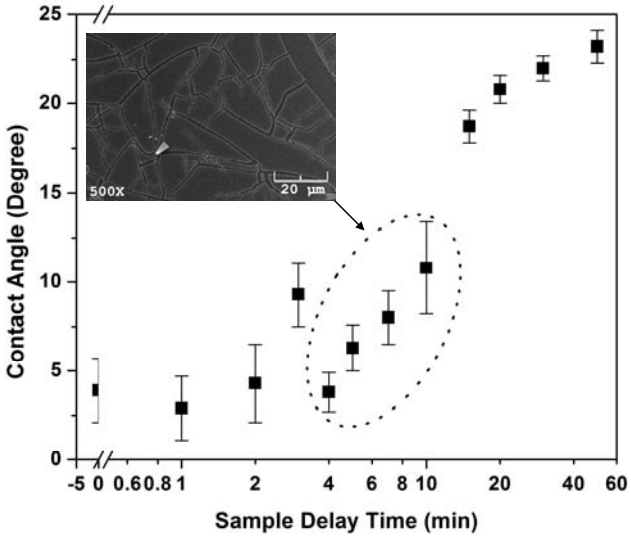

Figure 5.4 Variation of contact angle with sample delay time. Inset: one typical SEM image of circled samples.

To investigate how sample delay time affects the surface hydrophobicity of sample after water treatment, a series of thin film samples with different delay time ranging from 0 min to 50 min were prepared in pure distilled-deionized water (referring to Chapter 2.3.7 for sample preparation). 24 hr after sample preparation, the contact angles of all resultant thin film samples were then measured. Figure 5.4 shows a representative pattern of how contact angle changed with sample delay time under ambient conditions.

The contact angles slightly increased from 4 ± 2^{o} to 9 ± 2^{o} in 0 min to 3 min range, followed by a sudden drop to 4 ± 1^{o} at 4 min-delay, and then a rapid increase until contact angle settled down at 23 ± 1^{o} after about 1 hr delay. Both the slight increase and the later rapid increase can be understood as that aging of sample turned the surface more hydrophobic. There are two major reasons for increased hydrophobicity with aging time: (1) During aging, the ongoing condensation reactions consumed Si-OR groups and hydrophilic Si-OH groups to produce more and more hydrophobic Si-O-Si bonds as silica samples were aged longer. (2) As aging progresses, more and more Si-OR groups were consumed, upon water treatment, less and less amount of hydrophilic Si-OH groups will be produced from Si-OR hydrolysis.

The sudden drop of contact angle at 4 min delay corresponded to an opaque white film sample, unlike those clear samples with 0 to 3 min delay or beyond 15 min delay. Upon closer inspection of sample by SEM (Figure 5.4 inset), the opaqueness of sample was found due to the cracking of gel surface. Samples with delay time from 4 min to 10 min showed whole to partial opaqueness on the film, which corresponded to high to low extent of cracking of the sample surface. It is known that cracking is caused by the differential contraction in the gel network and it occurs when the stress in the network exceeds its strength; usually, silica alcogel thin films thinner than ~ 0.5 μm do not crack, regardless of the drying rate.[24] Our hydrogel-like thin film samples are all thinner than 0.35 μm. What caused the cracking of samples with delay time from 4 min to 10 min is possibly related the hydrogel-like structure of those samples. Silica hydrogel has larger-size pores and less dense structure than alcogel, which makes hydrogel mechanic fragile. As demonstrated in section 5.3.1.2, the chemical reactive stage of nascent

alcogel samples lasted 10 min under ambient conditions, so samples with delay time no longer than 10 min should have all resembled hydrogel after being treated by water. Water modified thin film samples with delay time longer than 10 min resembled more alcogel-like, that's why they didn't crack. But why cracking didn't happen to the hydrogel-like samples with short 0 min to 3 min delay but only those with 4 min to 10 min delay is still not clear.

Based on the profile thickness measurements (Figure 5.2 (B)), we've noticed that hydrogel-like thin film samples produced from nascent alcogel thin films with very short delay time were thinner than the rest due to the gel loss in sample preparation, and the sample thickness stabilized after 2 ~ 3 min delay time. It's highly possible that it is the thickness that influenced the hydrogel-like thin films to crack or not. When a film is thin enough, the energy invested to form the crack is greater than the elastic energy released by cracking a thin film, cracking won't happen.[24,27] This argument was also supported by Thouless' work,[28] who reported that the stress intensity at the tip of a crack is proportional to the square root of the thickness of film, when the thickness is small enough, the stress intensity falls below the critical stress intensity of this material. This theory can also be applied to our hydrogel-like thin film samples. Because silica hydrogel is more fragile than silica alcogel, hydrogel thin film must be thinner than alcogel thin film to keep stable configuration. Since the thickness corresponding to cracking samples was 190±10 nm, we assume the maximum thickness of stable hydrogel-like thin film produced in water ($h_{max, water}$) should be less than 190 nm.

Fortunately, later the cracking problem was solved by preparing thin film samples in dye solutions or dye-doped pH 7 PBS. Considering the fluid-like nature of nascent

alcogel thin film, it resembled a thin film of liquid sol, when dipped into water or aqueous solution, the condensation-gelation would happen to strengthen the structure of gel network. The trapped R6G molecules made the surface more hydrophobic, which helped to reduce surface tension and contributed to less cracking of gel network.[29]

It has to be pointed out that even though the contact angle-sample delay time experiment followed the same pattern on different days, the delay time corresponding to the first cracking sample varied from day to day. As we'll discuss later in section 5.3.3.1, humidity affected the thickness of hydrogel thin films. When humidity changed from day to day, the delay time it took for $h_{max,\ water}$ to be reached would vary from day to day, and so caused the shift of the first cracking sample. The interesting shift was also observed in absorption-sample delay time experiment: the peak-delay-time (see definition in Chapter 2.3.7) varied from day to day. Usually higher humidity resulted in a longer peak-delay-time and lower humidity corresponded to a shorter peak-delay-time. Details about how humidity affects the absorbance and thickness of hydrogel-like samples are discussed in section 5.3.3.

5.3.2.2 Fluorescence imaging

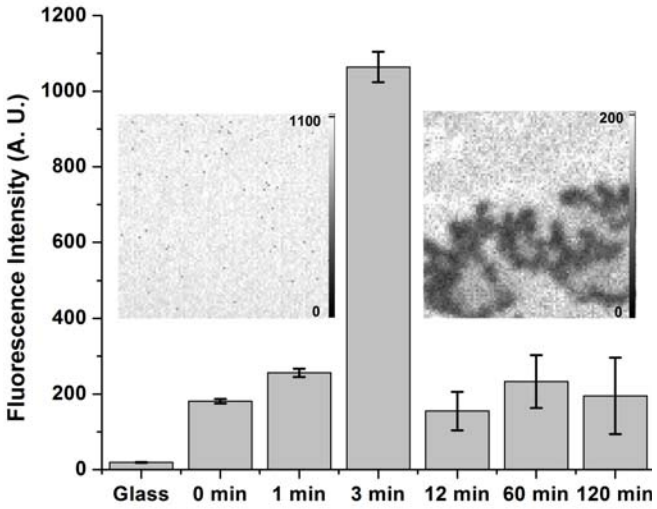

Figure 5.5 Variation of R6G fluorescence intensity with sample delay time. Insets: (left) fluorescence image of 3 min-delay sample, (right) fluorescence image of 12 min-delay sample.

Fluorescence images were collected from water modified thin film samples prepared in 1 mM R6G solution under ambient conditions, and the fluorescence intensity of each sample was quite consistent from day to day. As shown in Figure 5.5, the 0 min-delay alcogel thin film treated by R6G solution showed fluorescence intensity 10 times as that of bare glass substrate, which indicates that the resultant hydrogel-like thin film encapsulated a lot more R6G molecules than what physically adsorbed on bare glass. Along with sample delay time, the fluorescence intensity first increased and reached a peak-intensity over 1000 at 3 min-delay, then started to decrease, which matched the trend of absorbance-sample delay time experiment discussed in section 5.3.1.2 (Figure 5.2 (A)). The pattern of fluorescence intensity change with sample delay time should be due to the same reasons as that of the absorbance change. The initial loss of fluorescence intensity was partially caused by gel loss of those samples, and the intensity drop after 3 min-delay resulted from loss of chemical activity upon aging. With the samples resembling alcogel more, the pore sizes continued to shrink, leading to poor or no dye encapsulation in some areas, hence, the fluorescence dropped with sample delay time. Samples with delay time from 0 to 3 min showed homogeneous fluorescence images, as shown in Figure 5.5 inset (left), once the alcogel thin film was aged as long or longer than 12 min before dipped into R6G solution, the resultant thin film samples all showed a heterogeneous distribution of encapsulated R6G in fluorescence images. As interpreted in section 5.3.1.1, dark areas in Figure 5.5 inset (right) might represent regions with such small-size pores that no dye molecules could diffuse into, and they also contributed to the big standard deviation of fluorescence intensities from samples with 60 min and 120 min delay times.

Absorption measurements, contact angle measurements and fluorescence imaging based on a full set of delay time samples all revealed that nascent alcogel thin films were chemically reactive, the reactive stage persisted ~ 10 min under ambient conditions, and most importantly the sample delay time resulted in dramatically different characteristics of produced thin film samples, with shorter-delay-time samples resembling hydrogel more and longer-delay-time samples resembling alcogel more. Both contact angles and absorption spectra were affected by environmental humidity, whereas fluorescence imaging was not so sensitive to it.

5.3.3 The Change of Gel Characteristics with Humidity

5.3.3.1 Profile thickness measurements

It has been mentioned earlier in the contact angle-sample delay time and absorbance-sample delay time studies, humidity could affect the thickness of produced thin film samples. As described in Chapter 2.3.7, the humidity control during sample preparation was realized by adjusting the humidity in spincoater through a water bubbling system while the sample was inside. Figure 5.6 demonstrates how humidity

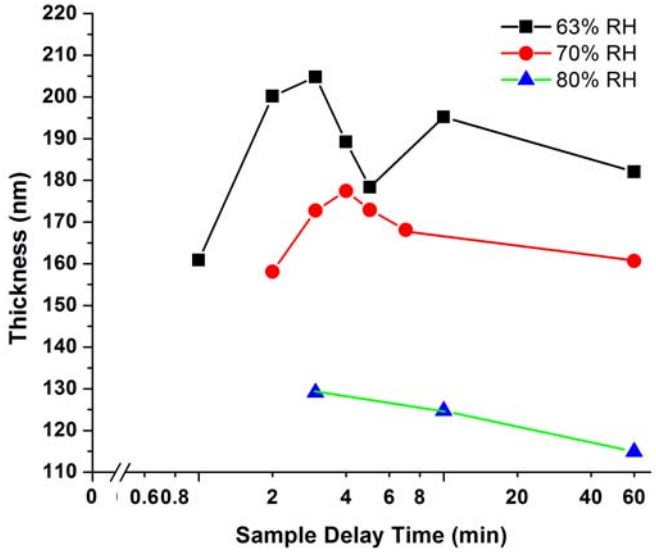

Figure 5.6 Effect of relative humidity (RH) on sample thickness. Three sets of samples prepared under different RH are compared.

affected sample thickness. All water modified thin film samples were prepared in 1 mM R6G aqueous solution. Under 63% RH, which was the most common ambient humidity in our lab, 0 min-delay sample was too thin to produce a reliable estimate, 1 min-delay sample was 161±5 nm, and the rest settled down at 192±10 nm in thickness; under 70 % RH, both 0 min and 1 min-delay samples were too thin to be measured, 2 min-delay sample was 158±1 nm, and the rest were stabilized at 170±6 nm thick; under 80 % RH, 0min, 1min and 2min-delay were all too thin to be measured, the other three samples remained at a thickness of 123±7 nm. It's safe to conclude that the higher the RH, the thinner the sample and the more samples have unmeasurable thickness. This is possibly because higher humidity can keep the nascent alcogel thin films more moisturized and made the stage of fluid-like structure last longer, leading to easier gel loss during preparation. As shown in Figure 5.6, at 3 min-delay time, regardless of RH all samples remained at a measurable thickness and the sample thickness started stabilizing with delay time.

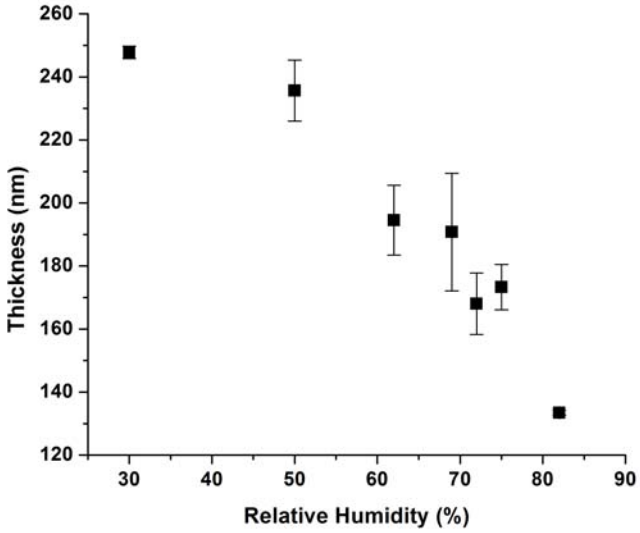

Figure 5.7 Thickness variation of 3 min-delay samples with RH.

To understand further about how exactly humidity affects the sample thickness, we fixed sample delay time at 3 min, a wider RH range from 82 % to 30% was examined. Three min-delay was chosen because that's the point where sample thickness started stabilizing regardless of humidity variation. The thickness of 3 min-delay sample should reflect the rough thickness of the whole set of samples prepared under the same RH. Seven hydrogel-like thin film samples were prepared with 3 min-delay time in 1 mM R6G aqueous solution under the controlled humidity. As shown in Figure 5.7, the thicknesses of them were compared. The sample thickness decreased 46% from 248±2 nm to 134±1 nm when RH increased from 30% to 82%, and the rate of decrease was slow at the beginning and became faster after RH passed 50%. When RH increased from 50% to 72%, which was the ambient humidity range of our lab, the sample thickness dropped from 236±10 nm to 168±10 nm. Since environmental humidity showed a non-negligible effect on sample thickness, all samples were prepared under a controlled humidity hereafter, unless specified individually.

5.3.3.2 Absorption measurements

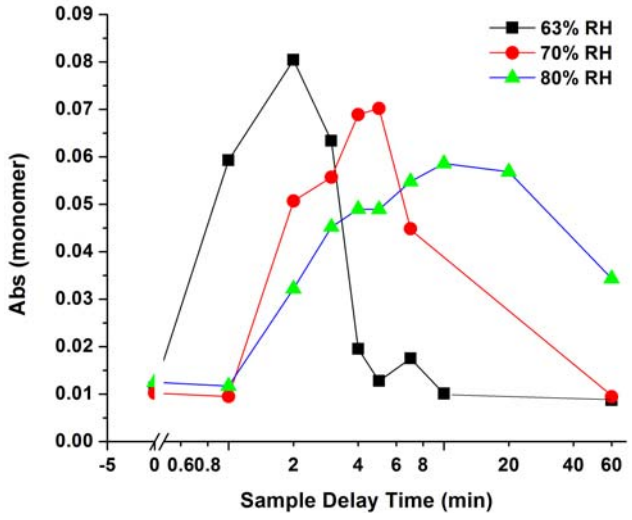

Figure 5.8 Variation of R6G absorbance with RH. Samples prepared under three different RHs are displayed.

Environmental humidity during sample preparation also affected the absorbance of dye doped samples, or precisely the guest loading capacity of samples. As shown in Figure 5.8, the absorbance of three full sets of R6G doped thin film samples is compared. They were the same sets of samples described in Figure 5.6, being prepared under RH of 63%, 70% and 80% separately. Regardless of the humidity, they all showed a similar trend of absorbance variation with sample delay time, that is a rapid increase followed by a slow decrease. As explained in section 5.3.1.2, the initial loss of absorbance intensity was partially caused by gel loss, and the gradual decrease of absorbance intensity after peak-delay-time (see definition in Chapter 2.3.7) was due to passing of the reactive stage. However, both the peak absorbance and the peak-delay-time varied with RH. The peak-delay-time was 2 min under 63% RH, increased to 5 min under 70% RH, and was then extended to 10 min under 80% RH. Extension of peak-delay-time suggested elongated chemically reactive stage of nascent alcogel thin films. As indicated in Figure 5.8, under 63% RH, 5 min-delay sample almost lost its dye loading capacity with a very low absorbance of 0.013; under 70% RH, 5 min-delay sample was the peak-delay-sample with an absorbance of 0.070, even the 7 min-delay sample still showed good dye loading capacity with the absorbance of 0.045; under 80% RH, the 60 min-delay sample still showed a good dye loading capacity with the absorbance of 0.034. When RH increased from 63% to 80%, the chemical reactive stage of nascent alcogel thin films was extended from 5 min to beyond 60 min. The peak absorbance of each set decreased with increased RH, which should be related to the thinner thickness of samples in higher RH. Increasing RH helps to extend the chemical reactive stage of nascent alcogel thin films, but at a price of gel

loss and consequently lower absolute dye loading capacity of the sample. One explanation for this behavior of new gel is that high humidity could maintain the fluid-like state of nascent alcogel thin films longer, thus leading to easier gel loss during preparation.

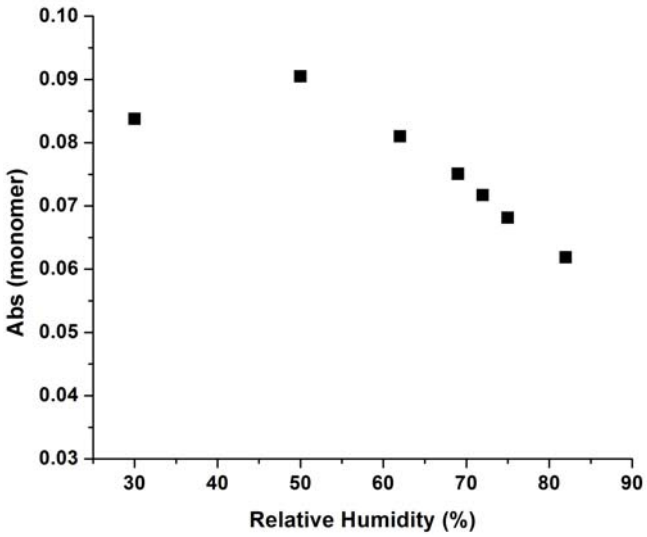

Figure 5.9 Absorbance variation of R6G doped 3 min-delay hydrogel-like thin film samples with RH.

To really quantify the effect of humidity on absorbance and eliminate the effect of sample delay time on absorbance, the same set of 3 min-delay time samples in Figure 5.7 were compared, and RH still ranged from 82 % to 30%. 3 min-delay time was chosen for an additional reason, which is 3 min was the most often appeared peak-delay-time under ambient conditions. Higher absorbance signals would provide a better signal to noise (S/N) ratio. The effect of humidity on sample absorbance is shown in Figure 5.9. The overall trend was that when RH increased, sample absorbance decreased, which should be partially due to the drop of sample thickness. The only exception was the 50% RH sample, which kept a noticeably higher absorbance (0.090) than that of 30% RH sample (0.084). Considering the 7.3% relative experimental error of absorbance measurements (experimental error data is discussed in section 5.3.5.1),

the difference between them could be neglected. Overall, when RH fell to between 30% and 60%, the absorbance of samples barely changed, once it passed 60%, sample absorbance decreased significantly with increased RH.

5.3.3.3 Fluorescence recovery by photobleaching (FRAP)

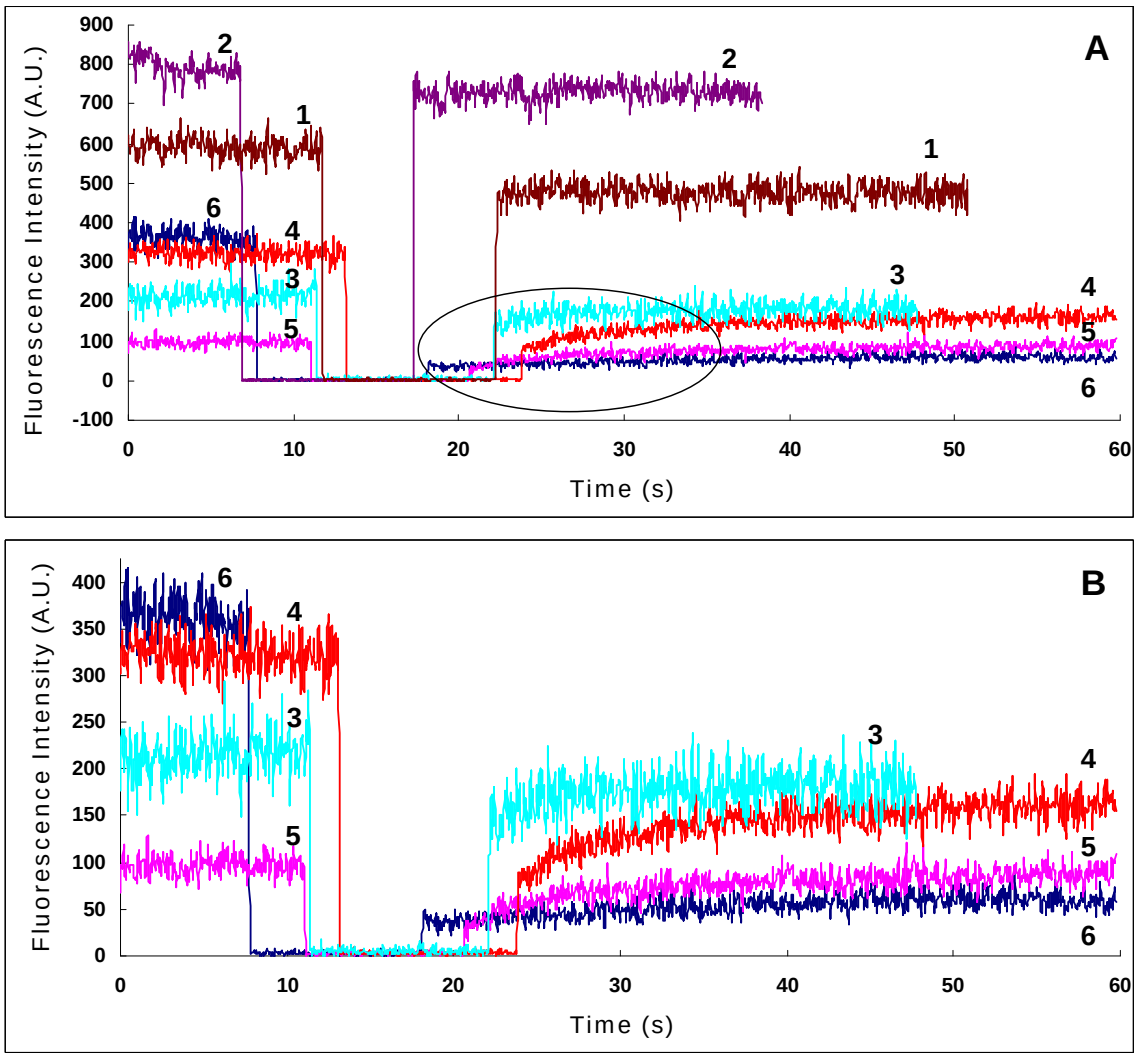

Figure 5.10 (A) FRAP traces from Fl in six 0 min-delay hydrogel-like thin film samples under different humidity, and (B) the expanded view of the four samples circled in (A).

Environmental humidity could affect the diffusion rate of Fl in hydrogel-like thin films. Because of the difficulty to control and measure the exact humidity around the

sample during FRAP experiment, we only did a rough humidity control of examined samples. Briefly, after sample preparation, a cuvet (both sides are open) was glued on the top of a gel sample, and then the sample was stored overnight in a chamber equilibrated with water moisture. When the cuvet-glued sample was taken out of the chamber, rough humidity control of each sample was then realized by sealing the open side of the cuvet after different delay time. Because the humidity in the chamber was higher than ambient humidity, we believe that the longer the delay time, the lower the local humidity would be obtained around the sample. Samples labeled with 1, 2, 3, 4, 5 and 6 in Figure 5.10 represent samples with 1 min-delay, 2 min-delay, 4 min-delay, 5 min-delay, 6 min-delay and 25 min-delay respectively before sealing, corresponding to humidity from high to low.

Qualitatively, the higher the humidity, the faster Fl molecules diffuse in the silica hydrogel-like thin films. As samples 1 and 2 demonstrated in Figure 5.10 (A), when the local humidity of the sample was very high, molecular diffusion in the film was so fast that the fluorescence intensity had completely recovered before we unblocked the detector. And in both traces, the fluorescence after recovery ($I(\infty)$) was about 85~95% of its initial fluorescence before photobleaching ($I(i)$), indicating that very high portion of Fl molecules were mobile. Since local humidity around sample 3 was a little bit lower than sample 1 and 2, Fl molecules diffused relatively slower, and the recovered portion was able to be partially captured after we unblocked the detector. $I(\infty)$ was about 80% of its $I(i)$ in trace 3, indicating most Fl molecules were mobile in sample 3.

In Figure 5.10 (B), as the local humidity went from high to low, sample 4 showed a faster recovery than sample 5, and sample 5 showed a much faster recovery than sample

6. In traces 4 and 5, the fluorescence after recovery ($I(\infty)$) was about 50~80% of its initial fluorescence before photobleaching *(I(i)*), indicating that more than half Fl molecules were still mobile in samples 4 and 5. There was almost no recovery detected from sample 6, since it was delayed too long before being sealed, and it turned into a dry sample. Without much water around, most Fl molecules in sample 6 were immobilized, indicated by the very low $I(\infty)$ (only 10% of its *I(i)*). In summary, humidity can affect molecular diffusion inside silica hydrogel-like thin films. The higher the humidity, the faster guest molecules can diffuse. Low ambient humidity causes fast evaporation from such a thin film, thus lowering the water content of thin film and resulting in very slow or even no mobility of trapped molecules.

5.3.4 The Change of Gel Characteristics with Sol Aging Time

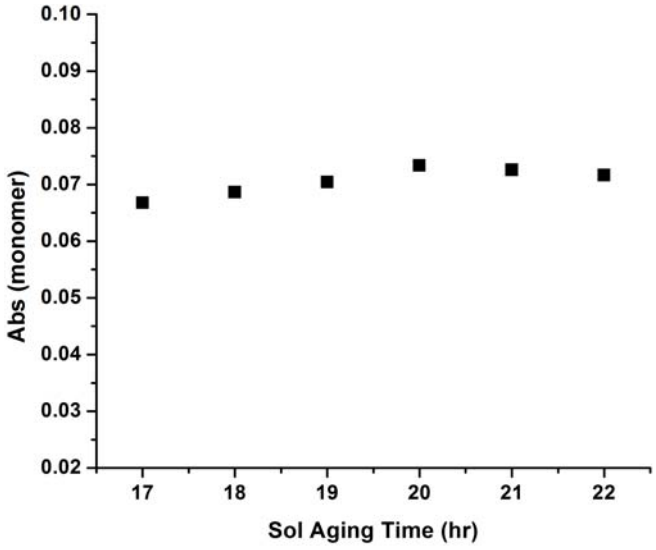

Figure 5.11 Absorbance variation of R6G doped 3min-delay hydrogel-like thin film samples with sol aging time.

We've already demonstrated that sample delay time and environmental humidity are the two major factors to affect the characteristics of produced new gel samples. Since the new hydrogel-like thin film samples were produced from alcogel thin films, any factor affecting the structure of alcogel thin film would affect the structure of

produced hydrogel-like thin films. With the same precursor, the same components of sol and the same spin-rate of gel deposition, the only factor that varied during sample preparation was sol aging time. To examine whether sol aging time could affect the produced new gel thin film, five samples were prepared in 1mM R6G solution with 3 min-delay time under 65% RH, with sol aging time ranged from 17 hr to 22 hr. As shown in Figure 5.11, under a controlled humidity and fixed delay time, the sample absorbance practically didn't change with sol aging time. The absorbance of all R6G doped hydrogel-like thin film samples was scattered around 0.07, with an average of 0.071±0.002. As a result, we believed that sol aging time didn't affect the characteristics of produced new hydrogel-like thin film samples. Usually, silica sols were aged 19 ~20 hr before gel deposition on coverslips.

5.3.5 Reproducibility of Sample preparation

Reproducibility of sample preparations was examined by both absorption and thickness measurements. Hydrogel-like thin film samples under investigations were all prepared in 1 mM R6G solution with a fixed delay time under a controlled RH.

5.3.5.1 Absorption measurements

No.	1	2	3	4	5	6	7	8	Ave
Abs.	**0.073**	**0.077**	**0.077**	**0.066**	**0.077**	**0.078**	**0.073**	**0.064**	**0.073** ±0.005

Table 5.1 R6G absorbance (monomer peak) of eight different 3 min-delay hydrogel-like thin film samples, prepared under 63% RH.

Table 5.1 summarized the absorption measurement data from eight different 3 min-delay samples prepared under 63 % RH on four different days. The absorbance of

these eight R6G doped samples was very close, with an average of 0.073±0.005, which indicates that our preparation protocol is highly repeatable. The relative standard deviation of absorption measurements was 7.3%, we thus assume any absorbance variation falling in the 7.3% range will be considered no change.

5.3.5.2 Profile thickness measurements

To determine the variation of thickness measurements from the profilometer, we scanned the same spot of a hydrogel-like thin film sample ten times and summarized the results in Table 5.2. The standard deviation was 5.7 nm, the relative standard deviation was 3.3%, and they reflect the instrumental error. To examine whether the location of scanning spot on the sample would cause a big fluctuation of thickness measurements, ten different spots were randomly chosen on one sample and scanned, with data summarized in Table 5.3. Compared to the instrumental error, the standard deviation of thicknesses on different spots increased about 3 nm to 8.8 nm, and the relative standard deviation increased to 5.2% from 3.3%. This increase relative to instrumental error is small, suggesting that the variation of sample thickness on different spots is most likely still due to instrumental error, and our hydrogel-like thin film has an even surface.

No.	1	2	3	4	5	6	7	8	9	10	Ave
H (nm)	**163.8**	**177.5**	**183.9**	**175.9**	**176.3**	**177.0**	**168.3**	**174.9**	**170.1**	**177.1**	**174.5** ±5.7

Table 5.2 Ten times thickness measurements of one spot on a sample, prepared in with 4 min-delay time under 70 % RH.

Spot No.	1	2	3	4	5	6	7	8	9	10	Ave
H (nm)	**177.0**	**158.0**	**170.1**	**179.0**	**161.2**	**174.0**	**155.7**	**165.3**	**165.4**	**180.0**	**168.6** ±8.8

Table 5.3 Thickness measurement of ten spots on the same sample in Table 5.2.

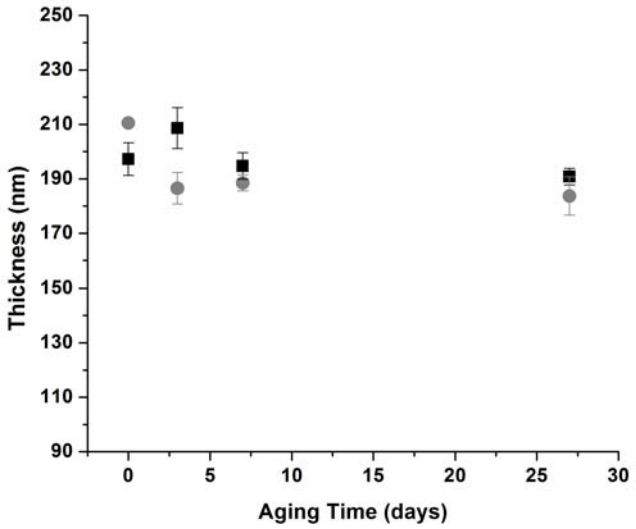

Figure 5.12 Variation of sample thickness with sample aging time. Squares: 2 min-delay hydrogel-like thin film sample prepared under 63% RH; Circles: 10 min-delay sample prepared under 63% RH.

Also, we had been monitoring the thickness of two different samples over a month, and tried to find out whether it is possible to collect reliable thickness data of samples even they have been aged for different days after preparation. Figure 5.12 demonstrated that sample thickness didn't seem to change with its aging time. The 2 min-delay hydrogel-like thin film sample kept a thickness of 200.2±7.4 nm with a relative standard deviation of 3.7%, and the 10 min-delay sample remained 195.2±13.3 nm thick with a 6.8% relative standard deviation. 3.7% and 6.8% are still close to or comparable to the instrumental error and the error due to sampling different spots, we thus believe thickness of hydrogel-like thin films doesn't change within one-month aging.

The reproducibility of sample preparation was also examined by thickness measurements from different samples. Table 5.4 summarized the results from six

different 3 min-delay hydrogel-like thin film samples, which were prepared in 1mM R6G solution under 63% RH on four different days. The standard deviation was 10.7 nm, and the relative standard deviation was 5.4%. By summarizing the results from those thickness tests, we chose the greatest standard deviation to represent the experimental error for thickness measurements, which is 13.3 nm. And the corresponding relative standard deviation was 6.8%. Thus, sample thicknesses varied in 6.8% range will be considered the same.

No.	1	2	3	4	5	6	Ave
H (nm)	**180.2**	**203.0**	**204.8**	**207.1**	**206.1**	**191.6**	**198.8** ±10.7

Table 5.4 Thickness measurement of six different 3 min-delay samples, prepared under 63% RH on different days.

5.3.5.3 Unit absorbance

After the experimental errors of absorption and thickness measurements were determined, we can calculate the error of the unit absorbance of hydrogel-like thin film samples. The unit absorbance of sample is the absorbance per unit height in μm, which will help us to compare the dye loading capacity of each sample by eliminating the thickness influence. Since most of the samples were prepared under 63% RH, and 3 min-delay samples were the most studied ones, data in Table 5.1 and Table 5.4 were used as representative values of absorbance (A) and thickness (H, μm) to calculate the error of unit absorbance (A/H, μm^{-1}). A is 0.073, δA is 0.005, H is 0.1988 μm, and δH is 0.0107 μm. According to Equation 5.2,[30] the error of unit absorbance A/H will be 0.034 μm^{-1}, and the relative error will be 9.1%. The unit absorbance variation of

dye-doped hydrogel-like thin film samples within 9.1% range will be considered no change.

$$\delta(A/H) = \sqrt{(\delta A)^2 (\frac{\partial(A/H)}{\partial A})^2 + (\delta H)^2 (\frac{\partial(A/H)}{\partial H})^2} \qquad \textbf{5.2}$$

5.3.6 Homogeneity of Hydrogel-like Thin Film Samples

Since the new gel film is derived from alcogel, even though it behaved dramatically different from alcogel, such as showing hydrophilic surface and supporting molecular diffusion, we still suspect there might remain some alcogel characteristics and it is actually a hybrid alcogel-hydrogel material. One convenient way to verify if it's a hybrid gel or a homogeneous hydrogel is to examine whether the sample absorbance is linearly proportional to the sample thickness. If the absorbance is linearly related to sample thickness, the new gel thin film is homogeneous hydrogel, if it's not, the gel should be a hybrid alcogel-hydrogel. Homogeneous hydrogel would evenly trap dye molecules (as demonstrated in Figure 5.1 (B2)), displaying a linear relation of absorbance to thickness. Because of the much higher guest loading capacity of hydrogel than that of alcogel (as demonstrated in Figure 5.2 (B)), if the new gel is a hybrid alcogel-hydrogel, hydrogel part would trap a lot more dye molecules than the alcogel part, at the same time, molecules encapsulated in the alcogel part would be unevenly distributed (as demonstrated in Figure 5.1 (B3)), and both should cause non-linear relation of sample absorbance with sample thickness.

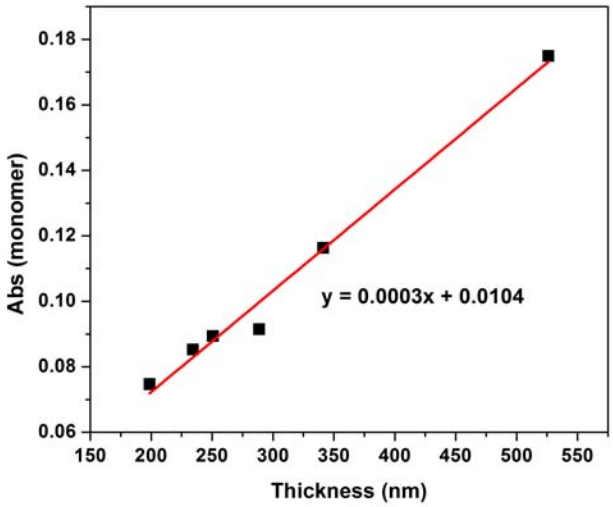

Figure 5.13 Absorbance variation of R6G doped hydrogel-like thin film sample with thickness.

In Figure 5.13, five hydrogel-like thin film samples with different thicknesses ranging from 200 nm to 550 nm were compared. They were all prepared in 1 mM R6G solution with 3 min-delay time under 63% RH, and the thickness variation was realized by changing the spin rate. As demonstrated in Figure 5.13, the absorbance of R6G doped new gel thin film was in a good linear relationship with its thickness, which suggests that the new gel thin film is indeed a piece of homogeneous hydrogel. Cracking of gel sample was observed when the thickness passed 350 nm. To make a piece of stable hydrogel-like thin film using the method we developed, the thickness is suggested to be controlled under 350 nm.

5.3.7 Microstructure of the New Hydrogel-like Thin Films

5.3.7.1 Unit absorbance

According to Figure 5.14, the unit absorbance of samples underwent a gradual increase and then a relatively rapid decrease with sample delay time no matter under which RH. The unit absorbance of samples is calculated by using the absorbance and thickness data from Figure 5.8 and Figure 5.6.

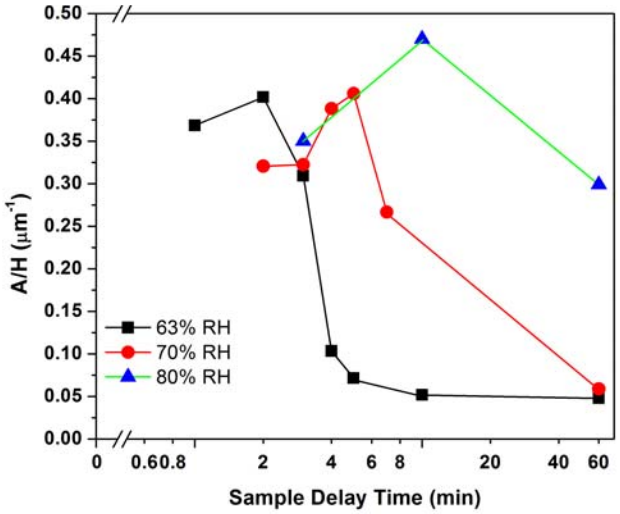

Figure 5.14 Unit absorbance variation of R6G doped thin film samples with sample delay time Samples prepared under three different RHs are displayed.

Under a lower 63% RH, the unit absorbance of 1 min-delay sample (0.368 μm^{-1}), which was the only sample before peak-delay-sample, was pretty close to that of the peak-delay-sample (0.402 μm^{-1}). Considering 9.1% of the relative error of unit absorbance, technically there's no difference between them. When RH increased to 70%, the difference of unit absorbance between the first two samples (~0.32 μm^{-1}) and the peak-delay-sample (~0.41 μm^{-1}) cannot be neglected any more, because the variation is more than 20%, but the one right before peak-delay-sample would be considered to have a comparable unit absorbance as that of peak-delay-sample. When RH increased even higher to 80%, the difference of unit absorbance between the first sample (3 min-delay, 0.350 μm^{-1}) and the peak-delay-sample (0.470 μm^{-1}) was very obvious, more than 25%. Therefore, we can conclude that when RH increased from 63% to 80%, the difference of unit absorbance between samples with delay time shorter than the peak-delay-time and the peak-delay-sample gradually increased, which should be related to the longer reactive stage under higher RH. The longer the reactive stage, the more gradual change of samples could be tracked before peak-delay-time. Once the peak-delay-time was passed, the unit absorbance of samples under 63% RH rapidly

decreased, at 5 min-delay time, the sample almost lost its dye loading capacity. Under 70% RH, 5 min-delay sample was the peak-delay sample, showing maximum dye loading capacity, when delay time increased to 60 min, it showed complete loss of dye loading capacity. Under 80% RH, the 60 min-delay sample stilled remained 70% dye loading capacity compared to the peak-delay sample. Thus, high RH was found to help remaining high dye loading capacity of samples which passing peak-delay-time. It's also worth pointing out that the unit absorbance of peak-delay sample under 80% RH (~0.47 μm^{-1}) was 15% higher than those of the peak-delay samples under 63% and 70% RH (~0.40 μm^{-1}). In summary, higher RH helped to prolong chemical reactive stage of nascent thin film alcogel, which provided enough time to track the gradual change of produced hydrogel-like thin film samples and helped most samples to maintain relatively high dye loading capacity.

5.3.7.2 SEM images

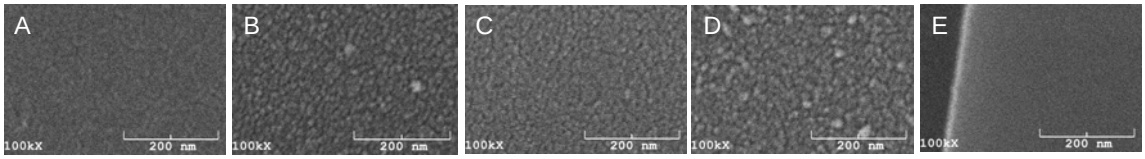

Figure 5.15 SEM images of (A) clean bare coverslip, (B) 0 min-delay gel on coverslip, (C) 0 min-delay gel on coverslip/VWR microscope slide, (D) 0 min-delay gel on VWR microscope slide, and (E) 0 min-delay gel on 900 nm CVD SiO_2/Si.

Unit absorbance of thin film samples varied with sample delay time, suggesting that there must be some difference between the gel structures of different delay-time samples. In Figure 5.15 (B), a 0 min-delay hydrogel-like thin film deposited on a coverslip showed a rough surface with channels and pores distributed everywhere, whereas the surface of a 0 min-delay thin film on 900 nm CVD SiO_2/Si (900 nm-thick

SiO_2 deposited on Si by chemical vapor deposition) shown in Figure 5.15 (E) was very smooth. There are two possible reasons for the difference. One is that, as the substrate for gel deposition, the coverslip (thickness: ~0.15 mm) is a lot thinner than SiO_2/Si (thickness: ~0.60 mm), those channels and pores could be due to the bending of coverslip during spinning; another reason could be the different surface structure between glass coverslip and CVD SiO_2. To find out whether it's due to bending or different surface structure of substrates, SEM images of 0 min-delay samples deposited on different substrates were compared in Figure 5.15. The corresponding substrates are coverslip (size: 25 mm x 25 mm, thickness: 0.13~0.17 mm, Figure 5.15 (B)), the same size of coverslip glued on top of VWR microscope slide (size: 25 mm x 25 mm, thickness: ~1 mm, Figure 5.15 (C)), the same size VWR microscope slide (Figure 5.15 (D)), and 900 nm SiO_2/Si (size: 25 mm x 25 mm, thickness: ~0.6 mm, Figure 5.15 (E)). All the gel samples deposited on glass substrates showed similarly rough surface, no matter the substrate was thick or not, their surface was rougher than a bare coverslip (Figure 5.15 (A)), and the one on SiO_2/Si (Figure 5.15 (E)) was the smoothest. This experiment demonstrated that the rough surface with channels and pores was not due to bending of substrate but different surface structure between regular glass surface and CVD SiO_2. This interpretation was further confirmed by AFM roughness measurements in section 5.3.7.3. Because what we observed from the SEM images of 0 min-delay gel on different substrates was actually the topography of the underneath substrates, CVD SiO_2 is a lot smoother than regular silica glass surfaces, that's why that sample showed the smoothest surface.

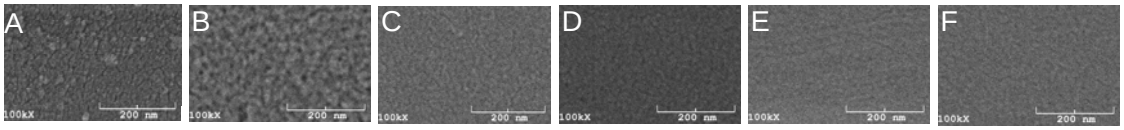

Figure 5.16 SEM images of hydrogel-like thin film samples with delay time of (A) 0 min, (B) 1 min, (C) 2 min, (D) 3 min, (E) 10 min, and (F) Alcogel

When gel samples with various delay-times were prepared on coverslip, different roughness or pore sizes were expected. The 2 min peak-delay-sample was expected to have the roughest surface or largest-size of pores because it showed the highest guest loading capacity. However, as shown in Figure 5.16, 1 min-delay sample was the roughest, the 2 min peak-delay-sample was just as smooth as the other longer-delay-time samples and the alcogel sample. Based on thickness measurement, we know that samples before peak-delay-time were thinner than the others due to gel loss, and some of them were too thin to be measured by profilometer. The rough features shown on 0 min-delay and 1 min-delay samples possibly just reflect the underneath surface features of coverslip substrate instead of the features of gel samples themselves

5.3.7.3 AFM roughness measurements

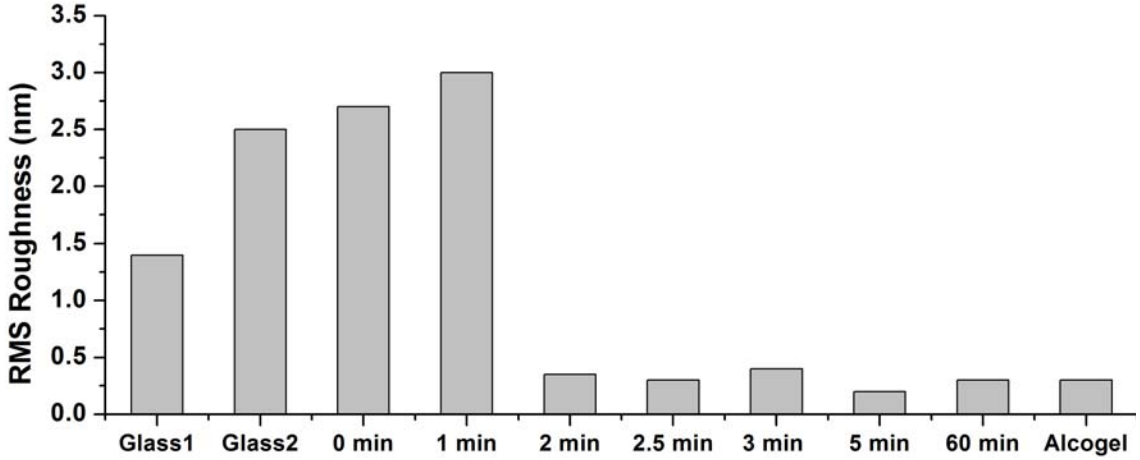

Figure 5.17 AFM RMS roughness of bare coverslips, different delay-time thin films and alcogel thin film.

To examine what caused the roughness change and how exactly sample roughness changes with delay time, two coverslip substrates cleaned by acetone/methanol (5 min sonication in each solvent) and the regular NaOH cleaning procedure (referring to Chapter 2.3.1), and a series of delay samples were prepared. Their AFM images were collected and root-mean-square (RMS) roughnesses were then calculated based on AFM images. Glass 1 in Figure 5.17 represents the acetone/methanol cleaned coverslip, and Glass 2 represents the coverslip cleaned by our regular NaOH procedure. As shown in Figure 5.17, the roughness of acetone/methanol cleaned coverslip was ~1.5 nm, the regularly cleaned coverslip, the 0 min-delay and 1 min-delay samples showed a similar roughness between 2.5 ~ 3 nm, all the other delay samples and the alcogel sample showed a very small roughness ~ 0.3 nm. As reported by Pantano et al.,[31] NaOH cleaning etched glass surface and created a surface with RMS roughness ~ 3 nm, which matched up what we observed from Glass 2. Acetone/methanol could not etch the glass surface and left the surface of Glass 1 smoother. The similarity of roughness between

Glass 2 and 0 min-delay or 1 min-delay hydrogel-like thin film samples indicates that what contributed to the roughness of those two short-delay-time samples was not the gel but the underlying features of glass substrate. When the gel thickness was thin enough, what we observed from the gel samples was indeed the topography of the substrate or the combined topographic features of gel and substrate. As sample delay time increased, sample thickness increased to a thickness much thicker than the 3 nm roughness of glass substrate, and what we observed from those samples would only reflect the real features of deposited gel surface. Those samples with delay time $\geq$ 2 min all showed a surface as smooth as the alcogel thin film sample, with the RMS roughness ~ 0.3 nm , which is the resolution of our AFM instrument.

Even though variation of unit absorbance with sample delay time indicated that there must be some difference inside the structure between samples with different delay-times, with the techniques we used (SEM and AFM), no subtle difference of the gel structure was detected. High-resolution TEM would be helpful to solve the difference of microstructures between them if we can find a way to make the same type of thin film hydrogel on TEM grids.

5.3.8 Improvement of Guest Loading Capacity

5.3.8.1 Improvement of dye loading capacity

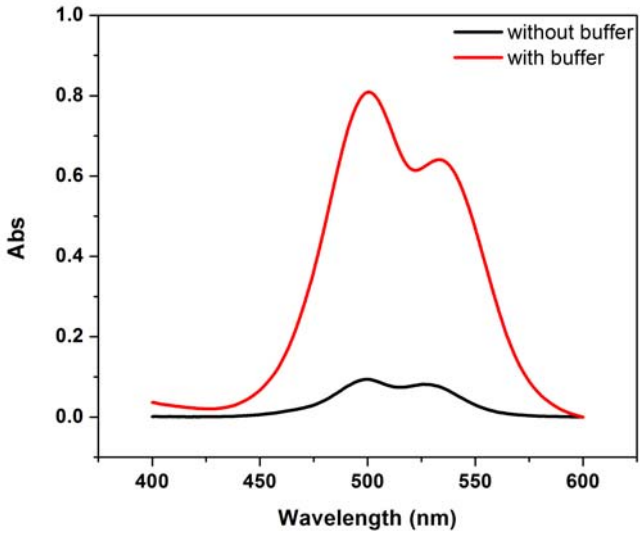

Figure 5.18 Absorption spectra of 2 min-delay hydrogel-like thin film samples prepared in 1 mM R6G aqueous solution (lower), and in 1 mM R6G/10 mM pH 7 PBS (upper) under 63% RH.

Improving guest loading capacity of silica matrix can improve the sensitivity and the shelf-life of silica based sensors. Figure 5.18 showed the significant difference between two R6G doped hydrogel-like thin film samples prepared with or without the existence of 10 mM pH 7 phosphate buffer solution (PBS). Dye loading capacity of the one prepared in R6G/PBS was improved more than ten times as that of the other one prepared in R6G solution only. Both SEM and AFM images were collected from these two types of samples, but no structure difference was detected from SEM images even with magnification as high as 100,000 x, neither any difference was detected from surface RMS roughness. With the limitation of our techniques, we still couldn't find out the reason for this significant improvement of guest loading capacity.

Sample	Thickness	Integrated Abs.	Absolute Conc. (M)
R6G Solution	0.1 **mm**	181.1	**1.0×10^{-3}**
Gel, without buffer	201.8 **nm**	30.1	**0.082**
Gel, with buffer	188.6 **nm**	306.6	**0.90**

Table 5.5 Comparison of R6G-doped hydrogel-like thin film samples with R6G aqueous solution.

In Table 5.5, thickness and the integrated absorbance of the two R6G doped hydrogel-like thin film samples displayed in Figure 5.18 are summarized, and are compared with the data of 1 mM R6G aqueous solution. Absorption spectrum of the 1 mM R6G solution was taken in a 0.1 mm-thick sandwich-structure cell (which was made by stacking two cover glasses together using double-sided tape as a spacer), whereas the spectra of those two gel samples were based on only ~200 nm thickness. Assuming they all contained the same species of R6G molecules, if we use the 1 mM aqueous R6G solution as a reference, based on Beer's law, the absolute concentration of these two samples would be converted to 0.082 M and 0.90 M respectively, which were 82 times and 900 times as that of the saturated R6G aqueous solution (1 mM) prepared at room temperature.

5.3.8.2 The effect of ionic strength on dye loading capacity

Since adding salt greatly improved the dye loading capacity of produced thin film hydrogel samples, to optimize the dye loading capacity of samples, PBS ranging from 0.1 to 100 mM were used to make 0.1 mM R6G solutions. Concentration of 0.1 mM R6G was chosen because it provided better absorbance signals than any lower-concentrated R6G solution, and a wider range of PBS to mix with than the saturated 1 mM R6G solution. The experiment was repeated in two continuous days with ambient RH ~64%, and samples were all 2 min-delay hydrogel-like thin film

samples. As shown in Figure 5.19, when the concentration of PBS was 0.1 mM, the absorbance of monomer peak was 0.046±0.005, which is comparable to that of 2 min-delay sample produced in 10 times more concentrated 1 mM R6G aqueous solution (0.058±0.002, Figure 5.18 (lower)). As the concentration of PBS kept increasing, the sample absorbance rapidly increased to a peak ~ 0.30, and then slowly decreased to ~0.20 with PBS concentration of 100 mM. Considering the 7.3% experimental error of absorbance measurement, we believe that 0.5 mM to 10 mM would be the PBS range to provide maximum dye loading capacity of samples. The latter decreasing trend with PBS concentration was possibly because that salt molecules inside the solution can compete with dye molecules to occupy the sites in pores, thus leading to lesser amount of dye being encapsulated.

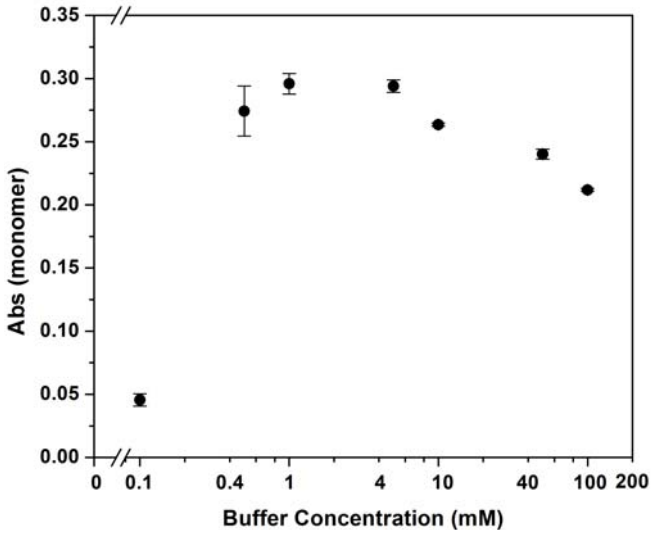

Figure 5.19 Absorbance of R6G doped 2 min-delay hydrogel-like thin film samples prepared in 0.1 mM R6G in variously concentrated pH 7 PBS.

5.3.8.3 Real-time trapping and post-trapping of R6G molecules

To better understand the process of gel formation, two methods were used to trap R6G molecules. In Figure 5.20, "real-time trapping" samples were prepared by dipping 2 min-delay alcogel thin films in variously concentrated R6G (from 0.1 mM to 1 mM) in 10 mM pH 7 PBS, and "post-trapping" samples were prepared by dipping 2 min-delay alcogel thin films in 10 mM pH 7 PBS to form the gel first and then being dipped in variously concentrated R6G aqueous solutions to trap dye molecules afterwards. 10 mM PBS was chosen because it not only falls in the buffer range to provide the maximum loading capacity of sample but also is concentrated enough to eliminate the influence of dye concentration on ionic strength.

Since both sets of samples were prepared from differently concentrated R6G solutions, the change of R6G species along with concentration was studied. R6G absorption spectra were resolved into monomer and dimer peaks by Gaussian fitting (referring to Chapter 2.5.3). Figure 5.20 (left Y axis) demonstrates the change by monitoring R6G dimer/monomer peak ratio with concentration. In aqueous solution, when R6G concentration was equal to or lower than 0.1 mM, dimer/monomer ratio was smaller than 0.5, suggesting that monomers dominated; once the concentration passed 0.1 mM, the ratio increased rapidly and reached 1.4 at 1mM concentration, suggesting more and more R6G dimers formed and then dominated. The relative amount of R6G monomers and dimers in solution affected the absorbance of R6G doped hydrogel-like thin film samples to different extent if prepared by different dye-trapping methods.

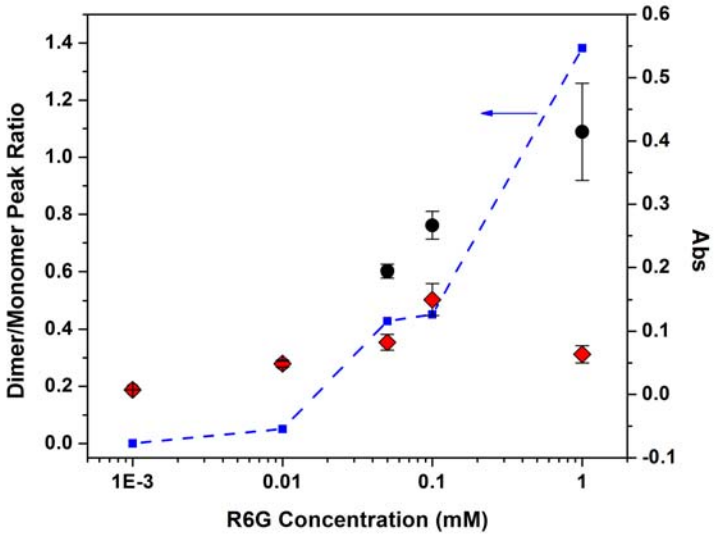

Figure 5.20 (Right Y axis) Absorbance of R6G doped 2 min-delay samples prepared by real-time trapping method (circles), and absorbance of R6G doped 2 min-delay samples prepared by post-trapping method (diamonds). (Left Y axis) R6G dimer/monomer peak ratios of variously concentrated R6G aqueous solutions (dashed line with square marks).

The big difference between those two sets of samples was clearly demonstrated in Figure 5.20 (right Y axis). With real-time trapping method (circles), the absorbance of samples followed a fast-increase relationship with concentration of R6G solution; with post-trapping method (diamonds), the absorbance first slowly increased with R6G concentration, after reached a peak at 0.1 mM concentration, then dropped. In the former case, gel network was forming with R6G molecules around, due to the strong electrostatic attraction between negatively-charged gel surface and positively-charged R6G molecules, R6G molecules would be attracted to the surface and acted as templates to affect the pore sizes and shapes, thus a lot of R6G molecules would be encapsulated inside pores due to attraction; simultaneously, regular diffusion of R6G molecules also helped the encapsulation. Template encapsulation would not be limited by the size of

pores or dye molecules, whereas the diffusion encapsulation would be affected. As the concentration of R6G solution increased, more and more R6G dimers or aggregates existed, if the size of dimers and aggregates was larger than pore sizes, those dye molecules cannot be encapsulated any more, which leads to the amount of encapsulated dye molecules decreasing. In real-time trapping, even though encapsulation by diffusion was weakened, template encapsulation was still ongoing. The overall increase trend of absorbance with R6G concentration by real-time trapping method might suggest that template encapsulation is dominating in this case. On the contrary, if gel structure was formed before dye encapsulation by post-trapping method, encapsulation of dye molecules can only be realized through diffusion. As explained earlier, encapsulation by diffusion was limited by the size of dye molecules. When more and more R6G dimers or aggregates existed in higher concentrated R6G solution, the encapsulation of R6G molecules became harder, which explains why the absorbance of samples dropped at 1 mM concentration compared to 0.1 mM concentration.

It has to be pointed out that, when R6G monomers absolutely dominated in solution (concentration $\leq$ 0.01 mM), there was no difference of absorbance between R6G doped samples prepared by two different methods; as the concentration increased, the absorbance difference between the two sets of samples became larger and larger, once dimers absolutely dominated in solution at 1 mM concentration, the difference between them was huge: the peak absorbance of "real-time trapping" sample was 6.5 times as that of the "post-trapping" sample. It is probably because at very low concentration, R6G monomers dominate, and monomers can be easily encapsulated by either method, at the same time, there are more than enough sites available inside gel

network for such small amount of molecules, so the amount of molecules that could be encapsulated depended on the amount of R6G molecules available in solution, and both methods were concentration-dependent, that's why they showed similar dye loading capacity at very low concentration of R6G solution. When the concentration of R6G solution increased, on one hand, existence of more and more R6G dimers or aggregates would cause the amount of dye being encapsulated by post-trapping method to drop, but would not affect much to the sample prepared by real-time trapping method; on the other hand, the already formed gel has limited sites for dye encapsulation, when the concentration increased to a certain point, the amount of encapsulated dye would be limited by the available sites inside gel, whereas encapsulation during gel formation was not limited by sites. Molecular size and available sites both should contribute to the big difference of dye loading capacity between hydrogel-like thin film samples prepared by these two methods when the concentration of R6G solution increases.

5.3.9 pH Sensor Study

5.3.9.1 Prototype pH sensor development

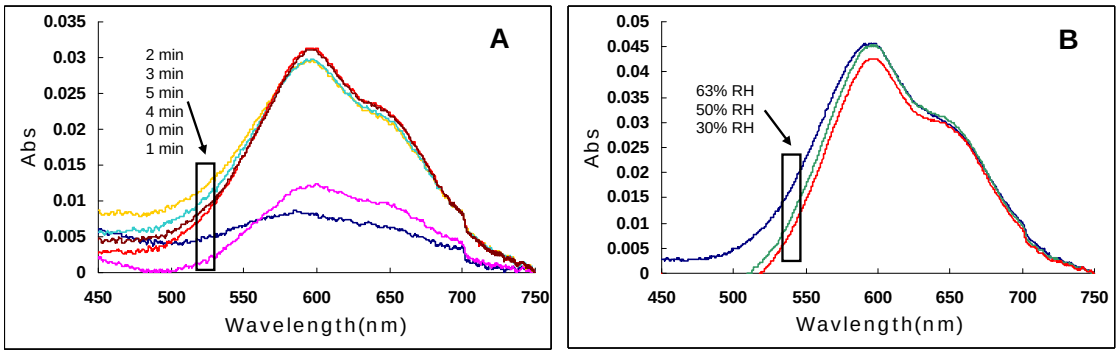

Figure 5.21 (A) Variations of NBC absorbance with sample delay time, with all samples prepared under 63% RH in 0.35 mM NBC aqueous solution. (B) Variations of NBC absorbance

with environmental humidity, with all samples prepared with 3 min delay in 0.35 mM NBC aqueous solution.

Based on the investigations of this new gel material doped with R6G, the development of prototype silica hydrogel-like thin film sensors doped with Nile blue chloride (NBC) was a lot easier. Since both sample delay time and environmental humidity can affect the characteristics of the hydrogel-like thin film, we studied the variation of NBC absorbance with sample delay time and humidity. There are two major peaks in NBC doped silica thin film samples, one peak is close to 596 nm, due to aggregation of NBC, and the other peak is close to 644 nm, which is the monomer peak of NBC.[32] Between them, 596 nm-peak was dominating in our prototype hydrogel-like thin film sensors because of the very high concentration inside.

In Figure 5.21 (A), five NBC doped hydrogel-like thin films were prepared under 63% RH in 0.35 mM NBC aqueous solution, with delay time varied from 0 min to 5 min. Such a small range of delay time was chosen because we know that R6G doped samples have a peak-delay-time close to 3 min if prepared under 63% RH. 0 to 5 min should cover the peak-delay-time of NBC doped samples. As demonstrated in Figure 5.21 (A), only 0 min-delay and 1 min-delay samples show substantial decrease of absorbance due to gel loss, the other four samples with delay time from 2 min to 5 min all stabilized at absorbance ~ 0.03. We then chose 3 min as the standard delay time for preparation of all NBC doped samples. In Figure 5.21 (B), three NBC doped hydrogel-like thin films were prepared in 0.35 mM NBC aqueous solution with 3min-delay time, under 63% RH, 50% RH and 30% RH, respectively. There's a detectable drop of absorbance when RH decreased, however, the difference between

them was so small (< 6%), possibly just due to experimental error. We believe NBC doped samples are not sensitive to environmental humidity if RH ≤ 63%. Hereafter, all NBC doped thin film samples were prepared just under ambient conditions, with humidity monitored at 52 ± 2% RH.

It has been demonstrated in section 5.3.8 that PBS buffer could improve guest loading capacity of hydrogel-like thin film samples, thus we applied the similar real-time trapping protocol to NBC doped thin film samples. As indicated in Figure 5.22, the dye loading capacity of sample was improved 1.6 times when prepared in 5mM PBS buffer. Even though the improvement was not as impressive as that of R6G doped samples, its intensity was good enough for the subsequent investigations.

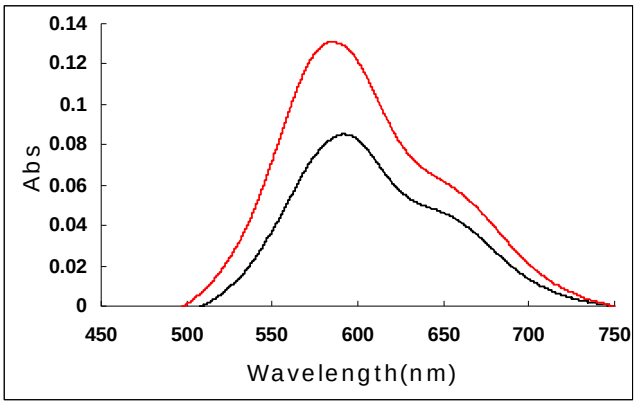

Figure 5.22 Absorption spectra of 3 min-delay samples prepared in 0.025 mM NBC aqueous solution (lower), and in 0.025 mM NBC/5 mM pH 7 PBS (upper) under 52% RH.

5.3.9.2 pH response, leaching and reversibility investigations

Nile blue chloride is a pH indicator that undergoes color change from blue to red in pH range of 10.1 to 11.1. Before the investigation of pH response of NBC in our prototype hydrogel-like thin film sensors, we studied its pH response in aqueous solutions. A series of 0.005 mM ~ 0.01 mM NBC aqueous solutions in different pH

ranged from 0 to 13 were prepared. The collected absorption spectra of them are shown in Figure 5.23. In neutral aqueous solution, NBC shows a major monomer peak at 635 nm, when the solution gets more concentrated, a peak at 596 nm indicates the aggregation of NBC molecules; Under strong acidic condition, it gets protonated and shows an additional peak at 457 nm; Under basic condition, its iminium group gets deprotonated, and it only shows one peak at 522 nm.[32-34]

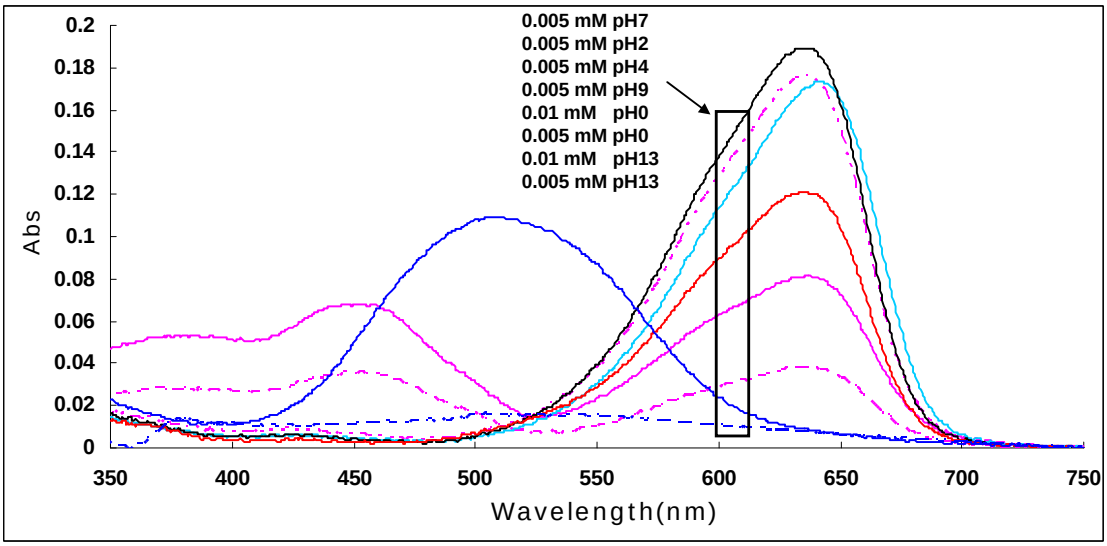

Figure 5.23 NBC absorption spectra in different pH solutions.

As demonstrated in Figure 5.23, with the same low concentration of NBC (0.005 mM), when pH varied from 2 to 7, there's no substantial change of the spectra in terms of both intensity and shape. It did show a detectable drop of the 635 nm-peak intensity at pH 2 and 4 compared to pH 7. When the solution became more acidic to pH 0, with the same 0.005 mM concentration, the 635 nm-peak intensity dropped to one fifth of the pH 7 sample, while a new peak appeared at 457 nm. To confirm this observation of this new peak, we doubled the concentration of NBC to 0.01 mM at pH 0, the two peaks at 635 nm and 457 nm both became more obvious. When the solution became more basic

to pH 13, with the same 0.005 mM concentration, the spectrum turned into almost a flat line. After the concentrated was doubled to 0.01 mM, remaining pH 13, one huge bump appeared at 522 nm. From this experiment, we learned that the molar absorption coefficients of the basic and acidic species of NBC are smaller than its neutral species, and the concentration of NBC should be kept fairly high enough to observe the response of NBC to pH change. These observations match what was reported by Krihak and coworkers.[32]

Prototype hydrogel-like thin film sensors for pH response, leaching and reversibility investigations were all 3 min-delay samples prepared in 0.025 mM NBC/5 mM pH 7 PBS buffer under 52 ± 2% RH. Since in both hydrogel-like thin film sensor and the corresponding alcogel thin film sensor, only one peak dominated during the whole investigations, we monitored the dominated peak (λ_{max}) and the corresponding peak absorption intensity (I_{max}) along with time. During the pH response, leaching and reversibility investigations, NBC doped silica hydrogel-like thin film sensors and alcogel thin film sensors were all blown dry before taken absorption spectra.

NBC undergoes colorimetric change from blue to red around pH 10 ~ 11 range, three sodium hydroxide solutions with pH 11, 11.5 and 12 were used to test the pH response of our prototype thin film sensors. As shown in Figure 5.24 (A), in pH 11 sodium hydroxide solution, the response of the sensor was very slow, after 25 min, λ_{max} only dropped about 15 nm from 585 nm to 570 nm and then settled down, after one more hour it stayed at 570 nm, even after two more days, it still didn't change (data not shown); in pH 11.5 sodium hydroxide solution, the response was much faster, after 25 min, λ_{max} dropped about 25 nm from 585 nm to 560 nm, after one more hour, it dropped

to 520 nm, which is the characteristic peak wavelength of NBC in basic condition; in pH 12 sodium hydroxide solution, the response rate was similar as in pH 11.5, but after 25 min, the silica thin film was completely dissolved in the solution (as indicated by the 0 absorption intensity in Figure 5.24 (B)). It is know that silica dissolves when pH > 10.3.[24,35] Results from Figure 5.24 (A) demonstrate that pH 11 was not basic enough to trigger obvious pH response, pH 12 was too strong for silica type pH sensors, and pH 11.5 was the best solution to reveal the pH response of our hydrogel-like thin film sensor.

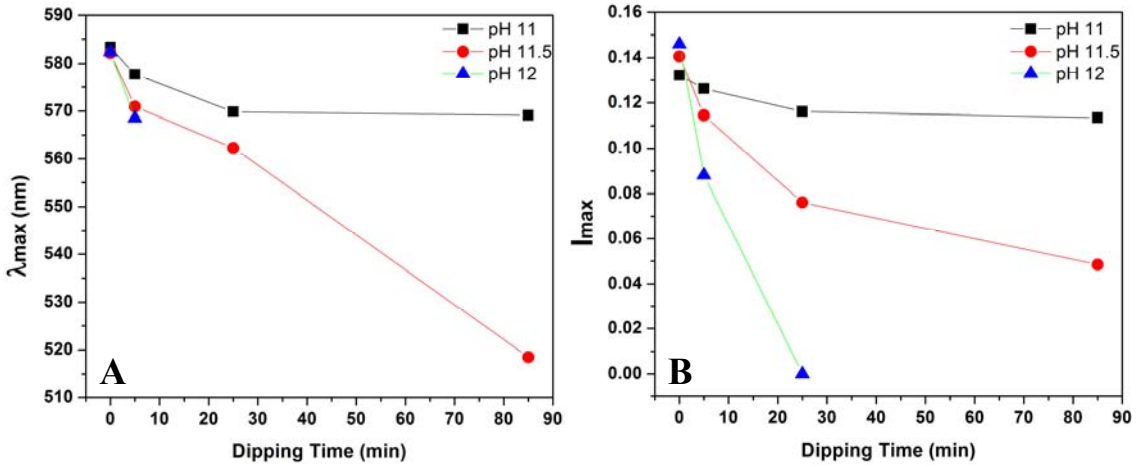

Figure 5.24 pH response and leaching of prototype NBC doped thin film sensors. (A) Peak wavelength (λ_{max}, nm) and (B) peak absorption intensity (I_{max}) change with dipping time in pH 11, pH 11.5 and pH 12 NaOH solutions.

In Figure 5.24 (B), by monitoring the peak intensity of each NBC doped sensor, we could study the leaching rates of them. In pH 11 sodium hydroxide solution, the sensor showed a slow leaching, peak intensity dropped ~15% from 0.13 to 0.11 after 85 min. In pH 11.5 sodium hydroxide solution, the peak intensity dropped faster, after 25 min, it dropped to half of the original intensity, and after one more hour, the intensity dropped

65% to 0.05. Three are three reasons for this faster intensity drop: (1) dissolving of silica thin film, (2) leaching of dye molecules, (3) the change of NBC species. As discussed in NBC solution study, the molar absorption coefficient of the basic species of NBC is smaller than its neutral species. More basic species in the sensor along with dipping time also resulted in a decrease of absorption intensity. Molecule leaching might only contribute a little to the intensity drop, compared to gel dissolving and NBC species change. As demonstrated by the sensor in pH 12 sodium hydroxide solution, the dissolving of silica thin film became dramatic, with the whole thin film completely gone in 25 minute.

We also investigated the reversibility of the prototype sensors by dipping them in pH 11.5 and pH 7 solutions successively, and compared with the corresponding alcogel thin film sensors as well. As shown in Figure 5.25 (A), the new hydrogel-like thin film sensor underwent a significant λ_{max} change from 582 nm to 532 nm in pH 11.5 solution for 65 min and stayed at 530 nm after additional one hour-dipping, which suggests that all NBC molecules turned into basic species. Followed by only 5 min-dipping in low pH 7 PBS buffer, λ_{max} rapidly increased from 530 nm to 576 nm, indicating that all basic NBC species completely turned back to neutral species in 5 min, after another 20 min exposure in pH 7 buffer, λ_{max} showed a slight drop to 570 nm, which might be due to the fluctuation of the measurements caused by very low absorption signals. By contrast, the alcogel thin film sensor barely showed any response to high pH 11.5 exposure for as long as 125 min, with λ_{max} only slowly decreasing from 594 nm to 581 nm, even after 25 min exposure in pH 7 PBS buffer, λ_{max} still remained between 583 nm and 587 nm, which suggests that most NBC molecules were still neutral species. So it's safe to

conclude that during this reversibility investigation, alcogel thin film sensor doped with NBC didn't show sensitivity to pH change, whereas the hydrogel-like thin film sensor was very sensitive. The big difference of the pH response between hydrogel-like thin film sensor and alcogel thin film sensor, demonstrated in Figure 5.25 (A), reflects the totally different internal structures of them, with the former more hydrogel-like and so more highly porous, which makes the encapsulated NBC molecules more accessible to external solvents and thus more sensitive to pH change, whereas the latter was denser and NBC molecules were deeply trapped or caged inside pores, thus much less accessible to surrounding solvent molecules, and caused very low sensitivity to pH change.

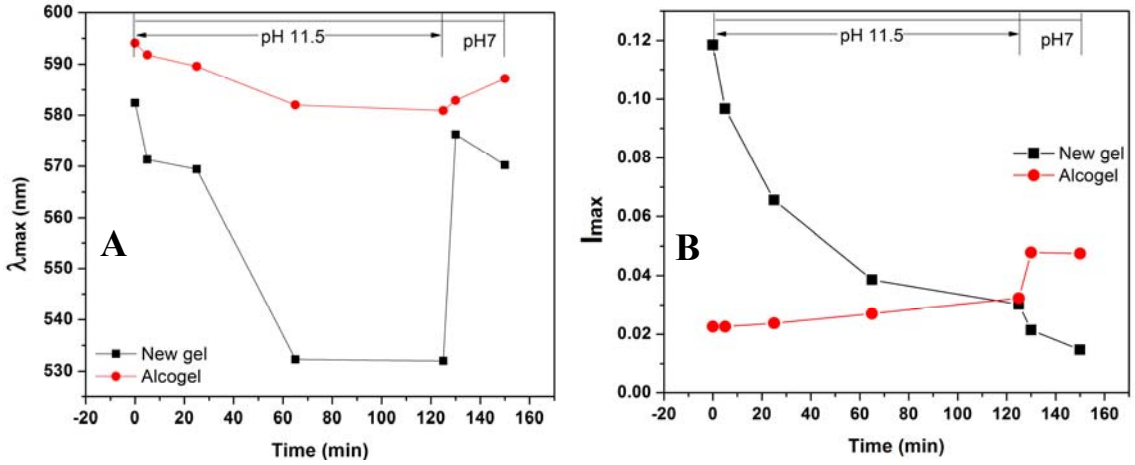

Figure 5.25 Comparisons of prototype NBC doped hydrogel-like (or new gel) thin film sensors and the corresponding alcogel thin film sensors. (A) Peak wavelength (λ_{max}, nm) and (B) peak absorption intensity (I_{max}) change with time by dipping them in pH 11.5 NaOH solution and 5 mM pH 7 PBS buffer successively.

The peak absorption intensity change of them shown in Figure 5.25 (B) also demonstrated the big difference between these two types of pH sensors. It is worth pointing out the difficulty of preparing similarly concentrated NBC doped alcogel thin

film. With an absorption intensity of 0.12 (which is the initial peak intensity of hydrogel-like thin film sensor) at 595 nm in a ~200nm-thick alcogel thin film, the bulk concentration of NBC doped sol would be converted to 0.35 M. It can be prepared by mixing 5 μL of 44.1 M NBC aqueous solution with 630.45 μL sol, or by mixing ~80 mg NBC powder with 630.45 μL sol. Since 44.1 M is far higher than the saturated aqueous NBC (0.35 mM) we could prepare in the lab, it's impossible to prepare the NBC doped sol by adding a small amount of highly concentrated NBC solution. ~80 mg NBC powder was then mixed with 630.45 μL sol, and let it age overnight before spincoating to obtain the corresponding NBC doped alcogel thin film sensor (referring to Chapter 2.3.2). Due to the limited solubility of NBC in sol, there were still a lot of NBC powders existed and suspended in the sol before spincoating. The huge difference of the initial peak absorption intensity between them should be due to the unmatchable NBC concentration in alcogel thin film compared to hydrogel-like thin film. Our hydrogel-like thin film can magically encapsulate 6 times as that amount of NBC molecules in alcogel thin film, or maybe even higher, because suspended NBC powder should also contribute to the absorption intensity.

Figure 5.25 (B) shows that, when the hydrogel-like thin film sensor was exposed in pH 11.5 solution, its peak absorption intensity continuously dropped, and it showed a faster dropping rate in the first one hour with a 67% intensity drop and then slowed down. As explained earlier, the intensity drop in pH 11.5 solution was caused by dissolving of silica thin film, leaching of dye molecules, and the change of NBC species. After the sensor being immersed into pH 7 PBS, its peak intensity continued decreasing, indicating continuous leaching of molecules. Since Figure 5.24 (A) demonstrated that

all basic NBC species completely turned back to neutral species after 5 min-immersion in pH 7 buffer, this nonreversible dropping trend of peak intensity in pH 7 buffer should not be caused by the species change of NBC. Silica gel doesn't dissolve at pH 7. The only possible reason could be that the gel structure became much looser after continuous gel dissolving upon previous 125 min-exposure in pH 11.5 solution, which makes the leaching of molecules easier. For hydrogel-like thin film sensor, the overall nonreversible dropping trend of peak intensity in pH 11.5 and pH 7 solutions should reflect a combined effect of silica gel dissolving, NBC species change and weak leaching.

In Figure 5.25 (B), the peak intensity of the alcogel thin film sensor slowly increased from ~ 0.02 to ~ 0.03 when exposed in pH 11.5 solution for 125 min, and this continuous increase was probably due to improved solubility of NBC upon longer exposure in solution. But because of the limited guest loading capacity of alcogel thin film, the absorption intensity was still very low. When the alcogel thin film sensor was immersed into 5 mM pH 7 PBS buffer, the increase trend became more obvious, and peak intensity increased ~50% from 0.032 to 0.048 in 5 min, which should be resulted from the species change of NBC molecules from basic to neutral. Since in alcogel thin film sensor, most NBC molecules were caged inside pores, which makes them inaccessible to surrounding solvent molecules, the amount of NBC molecules that underwent species change was small. That explains why for another 20 min exposure in pH 7 PBS buffer, the peak intensity of alcogel sensor remained very low at 0.048.

In summary, the prototype pH sensor showed a much faster pH response and much higher guest loading capacity than the corresponding alcogel sensor did. The

nonreversible absorption intensity drop of NBC doped hydrogel-like thin film sensor in pH 11.5 sodium hydroxide solution was mainly due to the dissolving of silica gel matrix.

5.4 CONCLUSIONS

The protocol to prepare stable hydrogel-like silica thin films was developed and optimized. This new film is highly hydrophilic, enables high guest loading capacity, and supports molecular diffusion. Studies on variations of absorbance, contact angle and fluorescence intensity with sample delay time all revealed that nascent alcogel thin films were chemically reactive, the reactive stage lasted ~ 10 min under ambient conditions, and most importantly sample delay time resulted in dramatically different characteristics of produced thin film samples, with shorter-delay-time samples resembling hydrogel and longer-delay-time samples resembling alcogel. It was discovered that hydrogel-like silica thin films produced in pure water easily cracked, and were not as stable as those produced in dye solutions or dye/PBS mixture, because the existence of hydrophobic dye molecules helped relieving surface tension in sol-gel matrix. And, it's also discovered that environmental humidity significantly affected both thickness and dye loading capacity of thin film hydrogel samples. Sample thickness and absorbance both decreased with increased RH. For R6G doped 3 min-delay samples, the sample thickness decreased 46% from 248±2 nm to 134±1 nm, and the absorbance dropped 30% from ~0.09 to ~0.06 when RH increased from 30% to 82%. Higher RH helped to remain the fluid-like structure of nascent alcogel thin film, which leads to easier gel-loss during preparation, thus lower absorbance of dye-doped

sample. FRAP experiments demonstrated that humidity can affect molecular diffusion inside silica hydrogel-like thin films. The higher the humidity, the faster guest molecules can diffuse. Low ambient humidity causes fast evaporation from such a thin film, thus lowering the water content of thin film and resulting in very slow or even no mobility of trapped molecules. However, with a controlled RH and fixed delay-time, we found that sample absorbance was not affected by sol aging time. Usually, sols were aged 19 ~ 20 hr before gel deposition. Our reproducibility tests based on samples prepared under a controlled RH and fixed delay-time revealed that the relative experimental error of absorbance, thickness and unit absorbance were 7.3%, 6.8% and 9.1% respectively. Sample thickness practically didn't change with aging time over a month. Nice linear relationship of sample absorbance with sample thickness demonstrated that this new gel thin film was indeed a piece of homogeneous hydrogel. Since cracking of gel sample was observed when the thickness was close to 350 nm, the thickness is suggested to be controlled no thicker than 350 nm.

Even though the unit absorbance of sample varied with sample delay time, suggesting the possible difference of internal structures between various-delay-time samples, no subtle difference of the gel structure was detected from SEM images and AFM roughness measurement. The unit absorbance comparison of three sets of R6G doped thin film sample prepared under different RH suggested that higher RH not only helped to prolong chemical reactive stage of nascent thin film alcogel, thus providing enough time to track the gradual change of produced thin film hydrogel samples, but also helped to keep the high dye loading capacity of samples.

Dye loading capacity of hydrogel-like thin film samples could be improved more than ten times by preparing samples in dye/PBS instead of dye aqueous solution itself. The reason for this significant improvement of guest loading capacity is still not clear. PBS with concentration ranged from 0.5 mM to 10 mM was found to provide maximum dye loading capacity of samples. Between the two methods of dye encapsulation, real-time trapping was hardly affected by the size of dyes or the available sites inside gel, whereas post-trapping was limited by both.

A prototype hydrogel-like thin film pH sensor doped with NBC showed higher sensitivity and faster response time than the corresponding silica alcogel thin film sensor, and the nonreversible absorbance drop of it in pH 11.5 sodium hydroxide solution was mainly due to the dissolving of silica gel matrix at high pH.

In summary, homogeneous thin film hydrogel-like samples with thickness between 100 nm and 300 nm were produced. This new film is highly hydrophilic, enables high guest loading capacity, and supports molecular diffusion. The reproducibility of sample preparation was greatly improved by controlling environmental humidity, dye loading capacity of samples was improved by using PBS solutions, and the concentration of R6G trapped inside hydrogel-like thin film could reach as high as 900 times of its saturated aqueous solution. Real-time trapping can simply be accomplished by dipping a chemically reactive precursor alcogel film into a dye buffer solution, and provided very high guest loading capacity. Since alcohol exposure can be kept to a minimum during dye encapsulation, this new silica film makes a promising candidate for biomolecule encapsulation and thus biosensor development.

Experimental results in section 5.3.1 have been submitted to Journal of the American Chemical Society in 2010, pending review.

5.5 CHAPTER 5 REFERENCES

(1) Avnir, D.; Levy, D.; Reisfeld, R. *The Journal of Physical Chemistry* **1984**, *88*, 5956.

(2) Kaufman, V. R.; Avnir, D.; Pines-Rojanski, D.; Huppert, D. *J Non-Cryst Solids* **1988**, *99*, 379.

(3) Pouxviel, J. C.; Dunn, B.; Zink, J. I. *The Journal of Physical Chemistry* **1989**, *93*, 2134.

(4) Simon, D. N.; Czolk, R.; Ache, H. J. *Thin Solid Films* **1995**, *260*, 107.

(5) Cerqua, K. A.; Hayden, J. E.; LaCourse, W. C. *J Non-Cryst Solids* **1988**, *100*, 471.

(6) Zusman, R.; Rottman, C.; Ottolenghi, M.; Avnir, D. *J Non-Cryst Solids* **1990**, *122*, 107.

(7) Avnir, D.; Coradin, T.; Lev, O.; Livage, J. *J Mater Chem* **2006**, *16*, 1013.

(8) Gupta, R.; Chaudhury, N. K. *Biosensors and Bioelectronics* **2007**, *22*, 2387.

(9) Jerónimo, P. C. A.; Araújo, A. N.; Conceição B.S.M. Montenegro, M. *Talanta* **2007**, *72*, 13.

(10) Kato, M.; Shoda, N.; Yamamoto, T.; Shiratori, R.; Toyooka, T. *Analyst* **2009**, *134*, 577.

(11) Jin, W.; Brennan, J. D. *Anal Chim Acta* **2002**, *461*, 1.

(12) Craith, B.; Donagh, C.; McEvoy, A.; Butler, T.; O'Keeffe, G.; Murphy, V. *Journal of Sol-Gel Science and Technology* **1997**, *8*, 1053.

(13) Livage, J.; et al. *Journal of Physics: Condensed Matter* **2001**, *13*, R673.

(14) Wolfbeis, O. S.; Oehme, I.; Papkovskaya, N.; Klimant, I. *Biosensors and Bioelectronics* **2000**, *15*, 69.

(15) Dunbar, R. A.; Jordan, J. D.; Bright, F. V. *Analytical Chemistry* **1996**, *68*, 604.

(16) Krupa, I.; Nedelcev, T.; Racko, D.; Lacik, I. *J. Sol-Gel Sci. Technol.* **2010**, *53*, 107.

(17) Wang, B. Q.; Li, B.; Deng, Q.; Dong, S. J. *Anal. Chem.* **1998**, *70*, 3170.

(18) Zareba-Grodz, I.; Mista, W.; Strek, W.; Bukowska, E.; Hermanowicz, K.; Maruszewski, K. *Opt. Mater.* **2004**, *26*, 207.

(19) Bandyopadhyay, A.; De Sarkar, M.; Bhowmick, A. K. *J. Mater. Sci.* **2006**, *41*, 5981.

(20) Gong, J. P.; Katsuyama, Y.; Kurokawa, T.; Osada, Y. *Adv. Mater.* **2003**, *15*, 1155.

(21) Yasuda, K.; Gong, J. P.; Katsuyama, Y.; Nakayama, A.; Tanabe, Y.; Kondo, E.; Ueno, M.; Osada, Y. *Biomaterials* **2005**, *26*, 4468.

(22) Venkateswara Rao, A.; Latthe, S. S.; Nadargi, D. Y.; Hirashima, H.; Ganesan, V. *J Colloid Interf Sci* **2009**, *332*, 484.

(23) Onda, T.; Shibuichi, S.; Satoh, N.; Tsujii, K. *Langmuir* **1996**, *12*, 2125.

(24) Brinker, C. J.; Scherer, G. W. *Sol-Gel Science: the physics and chemistry of sol-gel processing*; Academic press: San Diego, 1990.

(25) Zhou, Y. Y.; Yip, W. T. *J. Phys. Chem. B* **2009**, *113*, 5720.

(26) Furukawa, R.; Arauzlara, J. L.; Ware, B. R. *Macromolecules* **1991**, *24*, 599.

(27) Scherer, G. W. *J Non-Cryst Solids* **1987**, *89*, 217.

(28) Thouless, M. D. *Acta Metallurgica* **1988**, *36*, 3131.

(29) Zarzycki, J.; Prassas, M.; Phalippou, J. *Journal of Materials Science* **1982**, *17*, 3371.

(30) Bevington, P. R. *Data Reduction and Error Analysis for the Physical Sciences*; McGraw-Hill Book Company: New York, 1969.

(31) Mellott, N. P.; Brantley, S. L.; Hamilton, J. P.; Pantano, C. G. *SURFACE AND INTERFACE ANALYSIS* **2001**, *31*, 362.

(32) Krihak, M.; Murtagh, M. T.; Shahriari, M. R. *Journal of Sol-Gel Science and Technology* **1997**, *10*, 153.

(33) Jose, J.; Burgess, K. *Tetrahedron* **2006**, *62*, 11021.

(34) Dunnigan, M. G. *Stain Technology* **1968**, *43*, 243.

(35) Iler, R. K. *The Chemistry of Silica* John Wiley & Sons, Inc.: New York, 1979.

CHAPTER 6 CONCLUSIONS

This dissertation summarizes all the major research works I accomplished during the past six years. The focus of my research is to study different silica gel materials for sensor development. Included are the study of guest-host interactions altered by pore surface modification in silica alcogel and silica hydrogel, and the development of stable silica hydrogel-like thin films for fast sensor matrix. Understanding the molecular interactions between guest molecules and silica gel matrix before and after organosiline modification helps to manipulate the properties of silica gel materials so that gaining control over sensor development.

Post-synthesis grafting protocols to modify pore surfaces in silica alcogel thin film using APTS and MTES were developed, which is potentially applicable to tailoring local environments to manipulate guest-host interactions. Contact angle measurement alone is capable of monitoring chemical modifications on a film surface, but it does not provide any clue on the extent of modification underneath. Post-synthesis grafting beneath the film surface can be monitored by measuring the change in rotational mobility and photostability from single R6G molecules. The fact that R6G experienced a 5-fold increase in the percentage of tumbling molecule in APTS modified samples, but only a slight increase when modified by MTES proves that charge-reversal is a more effective way to modify pore surface than charge-neutralization is. R6G photostability decreased upon both APTS and MTES modifications, which suggests that pore surface grafting induces more R6G dynamic motions that lead to faster photodegradation. In both cases, only a very small change in R6G rotational mobility

was observed after silane modification, and fixed molecule was still the dominate category, which emphasizes that physical confinement is still the major factor that control guest-host interaction in modified alcogel films. Nevertheless, we have demonstrated that photostability measurement is a more sensitive technique to probe guest-host interactions when full scale molecular rotation is disfavored.

For the first time, post-grafting method was successfully applied to modify pore surfaces of highly hydrated silica hydrogel. This study verified the applicability of our post-synthesis grafting protocol, and confirmed the hypothesis that pore surface modification is more effective in hydrogel than that in alcogel. To eliminate the effect of physical confinement on guest molecules and the limited accessibility of modifying reagents to pores, dye must be infused into hydrogel after pore surfaces have been modified. Charge-reversal of pore surfaces by APTS modification showed a greater effect on guest molecules mobility than the hydrophobic capping by MTES modification: APTS caused the anisotropy value of R6G drop ~67%, MTES only caused a ~20% drop. For Fl, APTS modification showed a 6-fold increase of anisotropy value, whereas MTES brought a 2.5-fold increase. However, surface modifications through physical method, that is to increase ionic strength by adding 1.0 M sodium chloride or to neutralize pore surfaces by using pH 2.0 hydrochloric acid, barely affected the mobility of guest molecules. It was discovered that the mobility of encapsulated molecules were affected not only by post-grafting on pore surfaces but also the solvent for organosiliane reagents. The ease of locating dye band to track modification process makes R6G a better probe than Fl to monitor the pore surface modification in hydrogel.

The protocol to prepare stable hydrogel-like silica thin films was developed and optimized. By varying the aging time of nascent silica alcogel thin films before hydrogel induction, silica thin films with different characteristics could be produced, with shorter aging-time samples resembling hydrogel more and longer aging-time samples resembling alcogel more. Environmental humidity significantly affected both thickness and dye loading capacity of thin film hydrogel-like samples, which both decreased with increasing RH. Reproducibility of sample preparations was greatly improved by controlling the aging time and environmental humidity. Nice linear relationship of sample absorbance with sample thickness demonstrated that this new gel thin film was indeed a piece of homogeneous hydrogel. The reactive stage of precursor silica alcogel thin film matrix could be elongated by increasing environmental humidity, and the dye loading capacity of samples could be improved more than ten times by using buffer solutions. Since dye encapsulation is simply accomplished by dipping a chemically reactive alcogel thin film into a dye-doped buffer solution, alcohol exposure can be kept to a minimum during dye encapsulation, which makes this new silica film a promising candidate for biomolecule encapsulation and thus biosensor development. At the end, a prototype silica hydrogel-like thin film pH sensor was also constructed and it showed much faster response than the corresponding alcogel thin film sensor.

APPENDIX

Licenses of copyright permissions

Fwd: copyright permission

Dr. Roland W. Kunz [kunz@oci.uzh.ch]
Sent: Thursday, December 09, 2010 2:02
To: Lei, Qiong

Dear Dr. Lei,

CHIMIA grants you the right to reproduce figure 4 from:
Gallagher, D.; Ring, T. A., *Chimia* **1989**, *43* (10), 298-304
in your PhD dissertation on condition of proper citation and copyright notice.

Best regards
Dr. Roland W. Kunz
CHIMIA Chairman

—

University of Zurich
Dr. Roland W. Kunz
Institute of Organic Chemistry
Winterthurerstrasse 190
CH-8057 Zürich

Tel: +41 44 635 42 35
Fax: +41 44 635 68 12

www.oci.uzh.ch
roland.kunz@oci.uzh.ch

Begin forwarded message:

> **From:** Philippe Renaud <philippe.renaud@chimia.ch>
> **Date:** 25. Oktober 2010 09:29:30 GMT+02:00
> **To:** Roland Kunz <kunz@oci.uzh.ch>
> **Subject: Fwd: copyright permission**
>
> ---
> Philippe Renaud

AMERICAN INSTITUTE OF PHYSICS LICENSE TERMS AND CONDITIONS

Dec 10, 2010

This is a License Agreement between Qiong Lei ("You") and American Institute of Physics ("AIP") provided by Copyright Clearance Center ("CCC"). The license consists of your order details, the terms and conditions provided by American Institute of Physics , and the payment terms and conditions.

All payments must be made in full to CCC. For payment instructions, please see information listed at the bottom of this form.

License Number	2564411279475
License date	Dec 08, 2010
Licensed content publisher	American Institute of Physics
Licensed content publication	Review of Scientific Instruments
Licensed content title	Methods of single-molecule fluorescence spectroscopy and microscopy
Licensed content author	W. E. Moerner, David P. Fromm
Licensed content date	Aug 1, 2003
Volume number	74
Issue number	8
Type of Use	Thesis/Dissertation
Requestor type	Student
Format	Print
Portion	Figure/Table
Number of figures/tables	1
Title of your thesis / dissertation	Study of Silica Sol-Gel Materials for Sensor Development
Expected completion date	Dec 2010
Estimated size (number of pages)	200
Total	0.00 USD
Terms and Conditions	

American Institute of Physics -- Terms and Conditions: Permissions Uses

American Institute of Physics ("AIP") hereby grants to you the non-exclusive right and license to use and/or distribute the Material according to the use specified in your order, on a one-time basis, for the specified term, with a maximum distribution equal to the number that you have ordered. Any links or other content accompanying the Material are not the subject of this license.

1. You agree to include the following copyright and permission notice with the reproduction of the Material: "Reprinted with permission from [FULL CITATION]. Copyright [PUBLICATION YEAR], American Institute of Physics." For an article, the copyright and permission notice must be printed on the first page of the article or book

chapter. For photographs, covers, or tables, the copyright and permission notice may appear with the Material, in a footnote, or in the reference list.

2. If you have licensed reuse of a figure, photograph, cover, or table, it is your responsibility to ensure that the material is original to AIP and does not contain the copyright of another entity, and that the copyright notice of the figure, photograph, cover, or table does not indicate that it was reprinted by AIP, with permission, from another source. Under no circumstances does AIP, purport or intend to grant permission to reuse material to which it does not hold copyright.
3. You may not alter or modify the Material in any manner. You may translate the Material into another language only if you have licensed translation rights. You may not use the Material for promotional purposes. AIP reserves all rights not specifically granted herein.
4. The foregoing license shall not take effect unless and until AIP or its agent, Copyright Clearance Center, receives the Payment in accordance with Copyright Clearance Center Billing and Payment Terms and Conditions, which are incorporated herein by reference.
5. AIP or the Copyright Clearance Center may, within two business days of granting this license, revoke the license for any reason whatsoever, with a full refund payable to you. Should you violate the terms of this license at any time, AIP, American Institute of Physics, or Copyright Clearance Center may revoke the license with no refund to you. Notice of such revocation will be made using the contact information provided by you. Failure to receive such notice will not nullify the revocation.
6. AIP makes no representations or warranties with respect to the Material. You agree to indemnify and hold harmless AIP, American Institute of Physics, and their officers, directors, employees or agents from and against any and all claims arising out of your use of the Material other than as specifically authorized herein.
7. The permission granted herein is personal to you and is not transferable or assignable without the prior written permission of AIP. This license may not be amended except in a writing signed by the party to be charged.
8. If purchase orders, acknowledgments or check endorsements are issued on any forms containing terms and conditions which are inconsistent with these provisions, such inconsistent terms and conditions shall be of no force and effect. This document, including the CCC Billing and Payment Terms and Conditions, shall be the entire agreement between the parties relating to the subject matter hereof.

This Agreement shall be governed by and construed in accordance with the laws of the State of New York. Both parties hereby submit to the jurisdiction of the courts of New York County for purposes of resolving any disputes that may arise hereunder.

Gratis licenses (referencing $0 in the Total field) are free. Please retain this printable license for your reference. No payment is required.

If you would like to pay for this license now, please remit this license along with your payment made payable to "COPYRIGHT CLEARANCE CENTER" otherwise you will be invoiced within 48 hours of the license date. Payment should be in the form of a check or money order referencing your account number and this invoice number RLNK10896835.
Once you receive your invoice for this order, you may pay your invoice by credit card. Please follow instructions provided at that time.

Make Payment To:
Copyright Clearance Center
Dept 001
P.O. Box 843006
Boston, MA 02284-3006

If you find copyrighted material related to this license will not be used and wish to cancel, please contact us referencing this license number 2564411279475 and noting the reason for cancellation.

Questions? customercare@copyright.com or +1-877-622-5543 (toll free in the US) or +1-978-646-2777.

SPRINGER LICENSE
TERMS AND CONDITIONS

Dec 10, 2010

This is a License Agreement between Qiong Lei ("You") and Springer ("Springer") provided by Copyright Clearance Center ("CCC"). The license consists of your order details, the terms and conditions provided by Springer, and the payment terms and conditions.

All payments must be made in full to CCC. For payment instructions, please see information listed at the bottom of this form.

License Number	2564431109535
License date	Dec 08, 2010
Licensed content publisher	Springer
Licensed content publication	Pharmaceutical Research
Licensed content title	Fluorescence Recovery After Photobleaching: A Versatile Tool for Mobility and Interaction Measurements in Pharmaceutical Research
Licensed content author	Tom K. L. Meyvis
Licensed content date	Aug 1, 1999
Volume number	16
Issue number	8
Type of Use	Thesis/Dissertation
Portion	Figures
Author of this Springer article	No
Order reference number	
Title of your thesis / dissertation	Study of Silica Sol-Gel Materials for Sensor Development
Expected completion date	Dec 2010
Estimated size(pages)	200
Total	0.00 USD
Terms and Conditions	

Introduction
The publisher for this copyrighted material is Springer Science + Business Media. By clicking "accept" in connection with completing this licensing transaction, you agree that the following terms and conditions apply to this transaction (along with the Billing and Payment terms and conditions established by Copyright Clearance Center, Inc. ("CCC"), at the time that you opened your Rightslink account and that are available at any time at http://myaccount.copyright.com).

Limited License
With reference to your request to reprint in your thesis material on which Springer Science and Business Media control the copyright, permission is

your use of the licensed material other than as specifically authorized pursuant to this license.

No Transfer of License
This license is personal to you and may not be sublicensed, assigned, or transferred by you to any other person without Springer Science + Business Media's written permission.

No Amendment Except in Writing
This license may not be amended except in a writing signed by both parties (or, in the case of Springer Science + Business Media, by CCC on Springer Science + Business Media's behalf).

Objection to Contrary Terms
Springer Science + Business Media hereby objects to any terms contained in any purchase order, acknowledgment, check endorsement or other writing prepared by you, which terms are inconsistent with these terms and conditions or CCC's Billing and Payment terms and conditions. These terms and conditions, together with CCC's Billing and Payment terms and conditions (which are incorporated herein), comprise the entire agreement between you and Springer Science + Business Media (and CCC) concerning this licensing transaction. In the event of any conflict between your obligations established by these terms and conditions and those established by CCC's Billing and Payment terms and conditions, these terms and conditions shall control.

Jurisdiction
All disputes that may arise in connection with this present License, or the breach thereof, shall be settled exclusively by the country's law in which the work was originally published.

Other terms and conditions:

v1.2

Gratis licenses (referencing $0 in the Total field) are free. Please retain this printable license for your reference. No payment is required.

If you would like to pay for this license now, please remit this license along with your payment made payable to "COPYRIGHT CLEARANCE CENTER" otherwise you will be invoiced within 48 hours of the license date. Payment should be in the form of a check or money order referencing your account number and this invoice number RLNK10896861.
Once you receive your invoice for this order, you may pay your invoice by credit card. Please follow instructions provided at that time.

Make Payment To:
Copyright Clearance Center
Dept 001
P.O. Box 843006
Boston, MA 02284-3006

If you find copyrighted material related to this license will not be used and wish to cancel, please contact us referencing this license number 2564431109535 and noting the reason for cancellation.

Questions? customercare@copyright.com or +1-877-622-5543 (toll free in the US) or +1-978-646-2777.

AMERICAN CHEMICAL SOCIETY LICENSE TERMS AND CONDITIONS

Dec 10, 2010

This is a License Agreement between Qiong Lei ("You") and American Chemical Society ("American Chemical Society") provided by Copyright Clearance Center ("CCC"). The license consists of your order details, the terms and conditions provided by American Chemical Society, and the payment terms and conditions.

All payments must be made in full to CCC. For payment instructions, please see information listed at the bottom of this form.

License Number	2544310907377
License Date	Nov 08, 2010
Licensed content publisher	American Chemical Society
Licensed content publication	The Journal of Physical Chemistry C
Licensed content title	Probing the Effect of Post-Synthesis Grafting on Guest−Host Interactions in Sol−Gel Silica with Single-Molecule Mobility and Photostability
Licensed content author	Qiong Lei et al.
Licensed content date	Dec 1, 2009
Volume number	113
Issue number	50
Type of Use	Thesis/Dissertation
Requestor type	Not specified
Format	Print
Portion	Full article
Author of this ACS article	Yes
Order reference number	
Title of the thesis / dissertation	Study of Silica Sol-Gel Materials for Sensor Development
Expected completion date	Dec 2010
Estimated size(pages)	200
Billing Type	Invoice
Billing Address	402 Wadsack Dr Apt G Norman, OK 73072 United States
Customer reference info	
Total	0.00 USD
Terms and Conditions	

Thesis/Dissertation

ACS / RIGHTSLINK TERMS & CONDITIONS
THESIS/DISSERTATION

INTRODUCTION
The publisher for this copyrighted material is the American Chemical Society. By clicking "accept" in connection with completing this licensing transaction, you agree that the following terms and conditions apply to this transaction (along with the Billing and Payment terms and conditions established by Copyright Clearance Center, Inc. ("CCC"), at the time that you opened your Rightslink account and that are available at any time at <http://myaccount.copyright.com>).

LIMITED LICENSE
Publisher hereby grants to you a non-exclusive license to use this material. Licenses are for one-time use only with a maximum distribution equal to the number that you identified in the licensing process; any form of republication must be completed within 60 days from the date hereof (although copies prepared before then may be distributed thereafter).

GEOGRAPHIC RIGHTS: SCOPE
Licenses may be exercised anywhere in the world.

RESERVATION OF RIGHTS
Publisher reserves all rights not specifically granted in the combination of (i) the license details provided by you and accepted in the course of this licensing transaction, (ii) these terms and conditions and (iii) CCC's Billing and Payment terms and conditions.

PORTION RIGHTS STATEMENT: DISCLAIMER
If you seek to reuse a portion from an ACS publication, it is your responsibility to examine each portion as published to determine whether a credit to, or copyright notice of, a third party owner was published adjacent to the item. You may only obtain permission via Rightslink to use material owned by ACS. Permission to use any material published in an ACS publication, journal, or article which is reprinted with permission of a third party must be obtained from the third party owner. ACS disclaims any responsibility for any use you make of items owned by third parties without their permission.

REVOCATION
The American Chemical Society reserves the right to revoke a license for any reason, including but not limited to advertising and promotional uses of ACS content, third party usage, and incorrect figure source attribution.

LICENSE CONTINGENT ON PAYMENT
While you may exercise the rights licensed immediately upon issuance of the license at the end of the licensing process for the transaction, provided that you have disclosed complete and accurate details of your

proposed use, no license is finally effective unless and until full payment is received from you (by CCC) as provided in CCC's Billing and Payment terms and conditions. If full payment is not received on a timely basis, then any license preliminarily granted shall be deemed automatically revoked and shall be void as if never granted. Further, in the event that you breach any of these terms and conditions or any of CCC's Billing and Payment terms and conditions, the license is automatically revoked and shall be void as if never granted. Use of materials as described in a revoked license, as well as any use of the materials beyond the scope of an unrevoked license, may constitute copyright infringement and publisher reserves the right to take any and all action to protect its copyright in the materials.

COPYRIGHT NOTICE: DISCLAIMER
You must include the following copyright and permission notice in connection with any reproduction of the licensed material: "Reprinted ("Adapted" or "in part") with permission from REFERENCE CITATION. Copyright YEAR American Chemical Society."

WARRANTIES: NONE
Publisher makes no representations or warranties with respect to the licensed material.

INDEMNITY
You hereby indemnify and agree to hold harmless publisher and CCC, and their respective officers, directors, employees and agents, from and against any and all claims arising out of your use of the licensed material other than as specifically authorized pursuant to this license.

NO TRANSFER OF LICENSE
This license is personal to you or your publisher and may not be sublicensed, assigned, or transferred by you to any other person without publisher's written permission.

NO AMENDMENT EXCEPT IN WRITING
This license may not be amended except in a writing signed by both parties (or, in the case of publisher, by CCC on publisher's behalf).

OBJECTION TO CONTRARY TERMS
Publisher hereby objects to any terms contained in any purchase order, acknowledgment, check endorsement or other writing prepared by you, which terms are inconsistent with these terms and conditions or CCC's Billing and Payment terms and conditions. These terms and conditions, together with CCC's Billing and Payment terms and conditions (which are incorporated herein), comprise the entire agreement between you and publisher (and CCC) concerning this licensing transaction. In the event of any conflict between your obligations established by these terms and conditions and those established by CCC's Billing and Payment terms and conditions, these terms and conditions shall control.

JURISDICTION
This license transaction shall be governed by and construed in accordance with the laws of the District of Columbia. You hereby agree to submit to

the jurisdiction of the courts located in the District of Columbia for purposes of resolving any disputes that may arise in connection with this licensing transaction.

THESES/DISSERTATION TERMS
Publishing implications of electronic publication of theses and dissertation material
Students and their mentors should be aware that posting of theses and dissertation material on the Web prior to submission of material from that thesis or dissertation to an ACS journal may affect publication in that journal. Whether Web posting is considered prior publication may be evaluated on a case-by-case basis by the journal's editor. If an ACS journal editor considers Web posting to be "prior publication", the paper will not be accepted for publication in that journal. If you intend to submit your unpublished paper to ACS for publication, check with the appropriate editor prior to posting your manuscript electronically.

If your paper has already been published by ACS and you want to include the text or portions of the text in your thesis/dissertation in **print or microfilm formats**, please print the ACS copyright credit line on the first page of your article: "Reproduced (or 'Reproduced in part') with permission from [FULL REFERENCE CITATION.] Copyright [YEAR] American Chemical Society." Include appropriate information.

Submission to a Dissertation Distributor: If you plan to submit your thesis to UMI or to another dissertation distributor, you should not include the unpublished ACS paper in your thesis if the thesis will be disseminated electronically, until ACS has published your paper. After publication of the paper by ACS, you may release the entire thesis (**not the individual ACS article by itself**) for electronic dissemination through the distributor; ACS's copyright credit line should be printed on the first page of the ACS paper.

Use on an Intranet: The inclusion of your ACS unpublished or published manuscript is permitted in your thesis in print and microfilm formats. If ACS has published your paper you may include the manuscript in your thesis on an intranet that is not publicly available. Your ACS article cannot be posted electronically on a publicly available medium (i.e. one that is not password protected), such as but not limited to, electronic archives, Internet, library server, etc. The only material from your paper that can be posted on a public electronic medium is the article abstract, figures, and tables, and you may link to the article's DOI or post the article's author-directed URL link provided by ACS. This paragraph does not pertain to the dissertation distributor paragraph above.

Other conditions:

v1.1

Gratis licenses (referencing $0 in the Total field) are free. Please retain this printable license for your reference. No payment is required.

If you would like to pay for this license now, please remit this license along with your payment made payable to "COPYRIGHT CLEARANCE CENTER" otherwise you will be invoiced within 48 hours of the license date. Payment should be in the form of a check or money order referencing your account number and this invoice number RLNK10879848.
Once you receive your invoice for this order, you may pay your invoice by credit card. Please follow instructions provided at that time.

Make Payment To:
Copyright Clearance Center
Dept 001
P.O. Box 843006
Boston, MA 02284-3006

If you find copyrighted material related to this license will not be used and wish to cancel, please contact us referencing this license number 2544310907377 and noting the reason for cancellation.

Questions? customercare@copyright.com or +1-877-622-5543 (toll free in the US) or +1-978-646-2777.